UNIVERSITY OF DHAKA

Development of Electrical Control System through Human Brain Signal Analysis

by

Abdullah-Al Amin

A THESIS

SUBMITTED TO THE FACULTY OF SINCE

IN FULFILMENT OF THE REQUIREMENTS FOR THE

DEGREE OF DOCTOR OF PHYLOSOPY

DEPARTMENT OF BIOMEDICAL PHYSICS AND TECNOLOGY

UNIVERSITY OF DHAKA

DHAKA, BANGLADESH

SEPTEMBER, 2017

Abstract

EEG based Brain-Computer Interface (BCI) systems can establish a direct communication channel from the brain to an electronic device. It bypasses conventional motor output pathways of nerves and muscles and can provide effective control over electromechanical devices such as neuro- prosthesis, wheelchair or other communication devices, making it suitable for physically challenged people. Needless to say, the technology is very sophisticated and it is not mature yet in the global scenario. Besides, most such work is done in the economically advanced countries where technological simplicity, low cost, etc., are not of primary concern, while these are important for a low resource country like Bangladesh. The present work was taken up with such a scenario in mind, development of a BCI system, including hardware and software, with a high quality of performance but keeping cost and technological sophistication low.

In the present work a complete BCI system has been developed from scratch, comprising of (i) hardware and software for EEG recording and interfacing to a computer, (ii) software for EEG trace visualization, (iii) signal analysis and processing, (iv) feature extraction algorithm and (v) classification method. The EEG device used is of only two channels which records from the sensorimotor cortex area (C3 and C4) of the human scalp that are responsible for limb movement. The bioelectric amplifier of the device consists of two channels and was designed to meet the requirement of low component count, high power efficiency, low noise and small physical size, suitable for a wearable system. To overcome some challenges of reliable EEG signal recording, several novel designs of hardware modules like AC coupled input stage, Driven Right Leg (DRL) circuit with improved performance, two-wired active electrode were proposed and implemented. These modules resulted in more stable EEG recordings with substantial amount of interference reduction as well as providing reinforced user safety. A skin-electrode contact impedance measurement system was developed which is able to measure the impedances of the ground and reference electrodes as well. A USB based data acquisition system was also developed for the BCI system using a microcontroller. The data acquisition system is useful during training phase and can also be used for standalone signal processing, data classification and control purpose.

To achieve effective control and communication by the BCI system several offline analyses through individual classifiers or a combination of them were performed with motor-imaginary EEG data (EEG data during imagination of movement) of several subjects. This was done to investigate for suitable feature extraction and classification methods for the developed BCI system. For simplicity and reliability, the activities of μ and β rhythms from sensorimotor cortex during Event Related Desynchronization (ERD) were used for classification. As the μ and β rhythms are physiologically meaningful attributes of the EEG signal during ERD it makes the classification more efficient. The suitable methods from offline analyses were applied to a single trial online classification. This online classification consisted of motor-imaginary of two states as Left and Right hand movements. This was tried on three subjects with no previous experience of BCI. This experiment was conducted using the developed EEG hardware (with only two channels) and Software. With one subject the accuracy was only about 60% while it was more than 80% for the other two subjects, indicating a success of the present work.

Acknowledgements

I am very much grateful to my supervisor **Professor Khondkar Siddique-e-Rabbani** and would like to thank him for his kind and constant support throughout this research work. I would also like to thank all the members of Department of Biomedical Physics and Technology, University of Dhaka, for their support on various occasions. I would also like to thank **Abdullah Abu Sied** (Research Assistant, BMPT) and **Md. Moin Uddin Atique** (Research Assistant, BMPT) for their help and support in several tasks. Finally, I am grateful to all the subjects that participated in different experiments during this research.

The author acknowledges the -financial support of the International Science Programme (ISP) of Uppsala University, Sweden, that covered the student fellowship, stipends and other hardware and components cost throughout this Ph.D studies.

Table of Contents

List of Tables

List of Figures and Illustrations

Chapter 1 : Introduction

1.1 Overview of the Research Field

Recognition of human thought pattern electronically for identifying different objects and intended direction of motion or movement has a great demand, especially for the physically challenged people to enable independent activities such as controlling a wheelchair or a neuro-prosthesis. Research in this area is being conducted in several laboratories in the world with reasonable success, but still requires a substantial amount of improvement as there are various challenges and constraints that require to be overcome for practical use. The system which facilitates such process uses the recordings of cerebral electrical activity or electrical signals of human brain activity over time and then classifying the recorded data associated with different thought or movement of body parts or even just imagination of movement of body parts, gives appropriate outputs to achieve some functions or controls. These systems are referred to as Brain Computer Interface (BCI) or Brain Machine Interface (BMI) or Mind Machine Interface or Direct Neural Interface (DNI) and provide a direct communication pathway between human brain and an external electronic device (Krucoff et al., 2016).

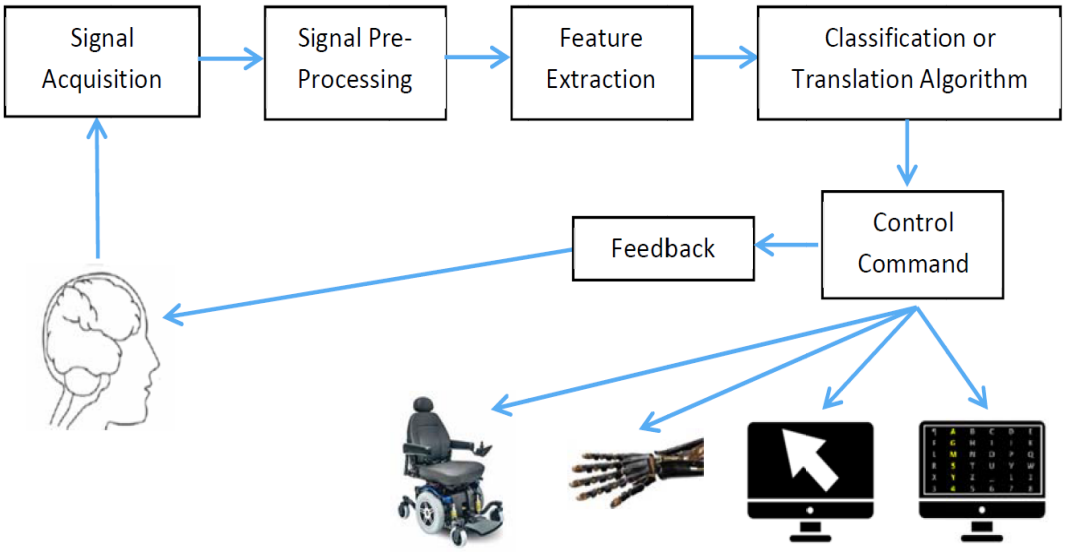

Figure 1.1: Brain-Computer Interface (BCI) System

A Block diagram of a BCI system is shown in Figure 1.1. Basically such a system involves acquisition of brain (cerebral) electrical signals, processing of the signal to eliminate or minimize artefacts, noise and unwanted signals, extracting features from the processed signal that would reveal whether the subject wants to perform any particular task, classification to identify one of a few tasks that the subject wants to perform and then to generate relevant driving signals or command control of a device. There should also be a feedback to the subject to verify whether the performed task is correct or not so that the subject can take corrective actions, if needed.

Primarily there are two types of systems which can record cerebral electrical activity namely, (i) Electroencephalography (EEG) and (ii) Electrocorticography (ECoG). The EEG is non-invasive and recorded from the scalp surface. The signals originate from the neuronal potentials of the brain but are reduced and diffused by the bone, muscle and skin which lie between the recording electrodes and the brain. Since the brain signals are recorded across the scalp in EEG, the signals are of very small amplitude, typically ranging from 10 to 100μV for normal subjects (Wikipedia, 2017, June 22) and increasing to around 300 μV for epileptic subjects (Brown, 1999). Being such a low amplitude signal EEG is highly prone to noise and various artefacts and is therefore one of the most difficult bioelectrical signals to record. Since the EEG signal is diffused by the scalp it has poor spatial resolution. A single EEG electrode gathers information from a brain area with approximately 20 mm diameter and the whole of the brain area is typically covered by many electrodes following a standard 10-20 electrode placement system (Brown, 1999). On the other hand, ECoG system uses electrodes which are placed directly on the cortex by means of surgery; the electrodes are embedded in a thin plastic pad that is placed on the cortex, beneath the dura mater (Serruya et al., 2003). Since the electrodes are placed directly on the cortex, ECoG signals have contribution from smaller localized brain areas, which are not diffused as in EEG, and have higher amplitudes (10 to 20 mV). Being large, ECoG signals do not suffer from the noise and artefacts that affect EEG. Besides, being less diffused, ECoG signals have much better spatial resolution (Wikipedia, 2017, June 22).

ECoG has many advantages over EEG but the only major disadvantage that pushes it back is that it is invasive, requiring surgery and special care which cannot be a routine technique (Brown, 1999). ECoG signals are robust and it requires very little or no training at all for the BCI system

(Yanagisawa, 2011). There are numerous reports on very successful BCI system employing ECoG (Biosignal, 2011) (Schalk et al., 2008) (Yanagisawa, 2011) (Gulati et al., 2015), however, due to the invasive procedure, it is not commonly used for BCI. In spite of low signal quality, low reliability and extensive training requirement using EEG, it is still the most popular choice for BCI or BMI system, simply because it is non-invasive. Besides, it has good temporal resolution, portability, user safety and low device manufacturing and setup cost (Wikipedia, 2017, June 28).

The first BCI system using EEG was reported in 1988, which utilizes alpha rhythm (8 to 14 Hz) to control a mobile robot (Bozinovski et al, 1988 & Bozinovski, 1990). Since then numerous efforts have been made to develop effective BCI systems for various applications. For example, severely paralyzed people were trained to control 'Slow Cortical Potential' to control a computer cursor (Wolpaw et al., 2002) through which they could write on a computer screen, but the process was too slow.

A slightly different technique uses an event related potential (ERP) known as Visual evoked potential (VEP) in which a subject is asked to observe some visual patterns while evoked EEG is recorded from the visual cortex of the brain. For a particular application of VEP in brain control, subjects are asked to select specific letters from a series of randomly appearing letters on a computer screen. This technique uses a particular pattern of the VEP known as the P300 signal which appears involuntarily approximately 300ms after a person recognizes an object that he or she desires to see. This allows BCI systems to classify user intention with high accuracy without prior training (Farwell et al., 1988), (Donchin et al., 2000), (Piccione et al., 2006), (Nijboer et al., 2008). However, it is also slow, approximately 17 character/min was obtained with 95% accuracy (Wikipedia, 2017, June 28).

For typical BCI, EEG signal from sensorimotor cortex is used to classify a subject's movement, or imagination of movement of various body parts. Since imagination of movement is more appropriate for paralyzed patients the latter has been extensively examined and is commonly known as Motor-Imaginary BCI (Pfurtscheller, 2000). Motor-Imaginary BCI (MI-BCI) mainly focuses on changes in the human μ rhythm, which is an EEG oscillation recorded in the 8-13 Hz

range from the central region of the scalp overlying the sensorimotor cortices (Pfurtscheller, 1989). The first MI-BCI with high accuracy, using imagination of left and right hand movement was reported in 1998 by Christoph Guger (Guger et al., 2000). In this study, three subjects were used to perform a real time (online) classification. This experiment was conducted to verify the usefulness of a feature extraction method called 'Common Special Pattern' (CSP). The study used 'Linear Discriminant Analysis' (LDA) classification method for classification and resulted in 98%, 94% and 86% of accuracy for the three subjects respectively. Since then advanced machine learning techniques have been developed and used for MI BCI. Similar motor imaginary EEG data of left and right hand movement was online classified using the 'Welch power spectrum' as feature with three different classifiers. In this study the 'Mahalanobis distance' classifier obtained the highest accuracy of 90%, Gaussian Classifier had accuracy of 80% and 'Hidden Markov Model' resulted in 65% of accuracy (Cincotti et al., 2003). Another online classification of three class motor imaginary EEG data was reported to use imagination of left hand, right hand and foot movement. This study used only 'Band Power' as features and LDA as classifiers and obtained 95% of accuracy (Scherer et al., 2004).

1.2 Motivation

BCI system can improve the quality of life of millions of physically challenged people around the world. In combination with recent immense development of electronic computational power, efficient electromechanical prosthesis and hand held smart communication devices; it is a promising technology that can facilitate functionality, mobility and communication abilities of people with disabilities. To benefit the common people around the world, a practical BCI system should be inexpensive and affordable, should consume low power to run for a long enough time on battery power, should be small in size and light weight, and should be repairable in the low resource countries. However, systems are mostly developed in industrially and economically advanced countries which do not satisfy the requirements mentioned above for a low resource country. They usually target their own population who have high levels of income and have easy access to technical repairing facilities. Therefore, unless such systems are developed indigenously in the low resource countries by the scientists and engineers of these countries, the benefits of BCI cannot be taken to the common people in these countries, which constitute above 80% of the global population. This was the motivation behind taking up the present work.

1.3 Aims and objectives

The primary aim is to develop an appropriate BCI system for the common people of the low resource countries, particularly with the aim of controlling a wheel chair or a limb prosthesis using brain signals. The developed system should have all the attributes mentioned above, i.e., low cost, light weight and portable, low power consumption, amenable to repair in a low resource country. The last requirement specifies that it should be as simple as possible with low component count, and the electronic components should be available widely, i.e., the technology should not depend on expensive and less easily available customized ICs and other components.

Therefore, this work presents a formidable challenge in redesigning of almost all the electronic hardware of existing EEG system, since this forms the backbone of a BCI system.

The cost of reproducing feature extraction and classification techniques, being software based, would be zero once these are developed to mature state, and there would be virtually no requirement for any maintenance and repair. However, any software which has been developed by the rich industrial countries are very expensive to procure because of strict intellectual property rights. Therefore, developing the software also forms part of the objectives of the present work. The technological challenge of developing such algorithm is formidable and the present thesis takes up this challenge as well.

The objectives of the present work may be specifically listed as follows.

1. The efficiency of a BCI system mostly depends on the quality of the EEG data, as the data classification methods are useless if corrupted EEG is analyzed. Since EEG is a very small signal and is easily affected by noise and artefacts, being probably the most difficult bioelectric signal to record, every care should be taken to eliminate or reduce interference noise and artefacts (Brown, 1999). Therefore, understanding sources of interference noise and artefact, how they affect the EEG recording amplifier circuit, investigating how to reduce them and then designing and developing an optimised EEG amplifier system is one of the objectives of this research work. Since the system is intended to be portable for controlling electromechanical prosthesis, making the finished

device with low component count to make it lightweight and portable needs also be integrated with the objective mentioned above.

2. In view of the reported work mentioned earlier, Motor-Imaginary BCI was chosen for the present study. Therefore, developing a BCI system through an analysis of recorded EEG data in real time is another objective of this research work. This would involve finding an appropriate, better and efficient EEG data classification method. For this, sophisticated mathematical analysis of recorded EEG signals would have to be carried out through development of appropriate computer algorithm.

3. Finally, due to limitations of accuracy of purely BCI systems, a combination with a separate signal, such as Electrooculogram (EOG) obtained from the eye muscles will be tried.

The above objectives are summarized in Figure 1.2

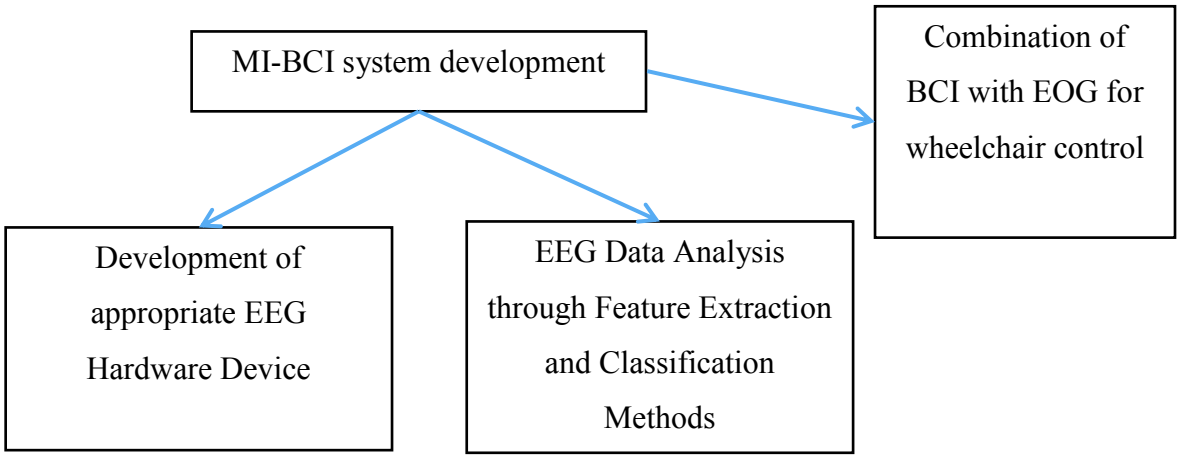

Figure 1.2: Visualization of the main objectives of the present thesis

Further details of the objectives are given below, separating them out into sections of Hardware, Analysis, and a combination of BCI and EOG

Hardware:

The development of appropriate EEG hardware involves several areas which will be tackled in the present thesis through innovation and improvisation and these are visualized through a simplified block diagram as shown in Figure 1.3. The blocks which are to be specifically targeted in the hardware development part of the present work are the following:

1. Analog Front End Instrumentation Amplifier and Filters: The heart of the EEG device is the bioelectric amplifier. Development of an optimized bioelectric amplifier with its amplification and gain stages with the desired properties and parameters as mentioned before forms challenge which will be solved first.

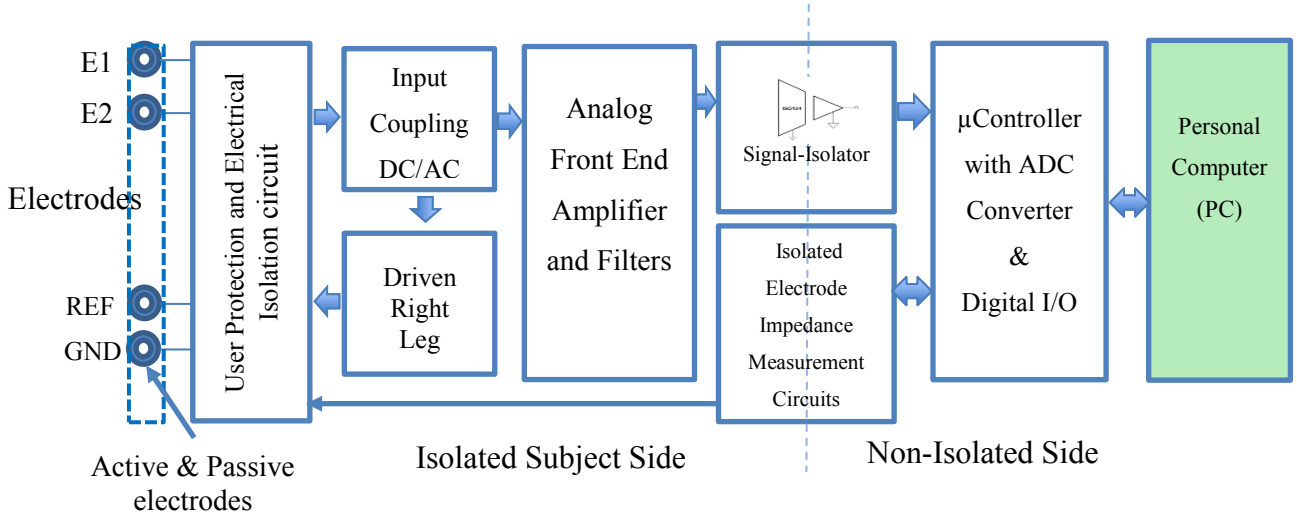

Figure 1.3: The Proposed Design Block Diagram of the EEG Hardware

2. Input Coupling (DC/AC): For patient safety, ac coupling through a capacitor is essential, but such coupling reduces the Common Mode Rejection Ratio (CMRR) significantly in traditional designs of front end amplifiers, compared to that for DC coupling, which gives the highest CMRR. The present work, through an innovative circuit design, will try to obtain high CMRR with AC coupling.
3. Driven Right Leg (DRL): In order to improve CMRR, DRL is an option in many traditional designs, but it needs manual adjustments in each individual measurement to make it effective. The present work will try to design a circuit with automatic compensation so that no manual intervention is necessary, which will contribute to an improved DRL design, if successful.

4. Active Electrode system: A buffer amplifier mounted physically on the EEG electrodes on the scalp can reduce the noise pick up by long lead wires significantly; the configuration being termed as 'active electrodes'. Standard designs of active electrodes need three wires, two for power and one for signal, which increases the bulk of the connecting leads, often not practical for EEG measurements. Two wire designs have been tried but these have still some problems which prevents their use in routine work. The present work will try to develop an improved two wire active electrode design which will remove the above weaknesses.
5. Electrode Impedance measurement system: This is done in many devices to assess the connections of the electrodes before or during an EEG measurement. The present work will try to develop an indigenous design which should be simple and robust.
6. USB interface to a PC: This has also standard designs of various kinds. The present work will develop its own to achieve a cost effective design.

Analysis of EEG data:

The second major objective of the present work involves analysis of EEG Data to extract reliable commands for the BCI system, to operate electromechanical systems such as prosthetics, electric wheelchairs etc., and also for human machine interaction and communication. This would be mainly focused on offline and online analysis of EEG data through feature extraction and classification of EEG signals, specifically for motor movement or intent of movement or imaginary movements. These data classification techniques will be improved selecting more effective features of the data and combination of more than one technique. Then the results will be evaluated to propose an effective wearable BCI system.

Combination of BCI and EOG to improve accuracy:

The third objective of the present work is to investigate the improvement in accuracy through a combination of BCI and EOG, the latter obtained from muscles around the eye for pre-selected eye movements.

1.4 Structure of this Thesis

This thesis is primarily divided into three parts following the overview given in Figure 1.2. The first part covers the hardware development of an improved and cost effective EEG device. The development of the individual design aspects as outlined in the section on objectives above are presented as individual chapters (Chapter 2 to 7). Each chapter deals with background study, present challenges and their proposed solutions, design description, simulations and experimentation. The results and novelty i.e. innovation to solve specific problem are also presented in each chapter.

The second part deals with the analysis of EEG Data through Feature Extraction techniques and Classification Methods, and is dealt with in chapters 8 to 10. Chapter 8 and 9 conducts offline analysis (analysis on recorded EEG data) for BCI purposes and Chapter 10 demonstrates online analysis (real time EEG data analysis) using the developed EEG device and software.

The third part gives the results of a feasibility test of combination EOG signals to that obtained from BCI to achieve better results of controlling electromechanical devices and is presented in Chapter 11.

Chapter 2 to 11 can be regarded as methods section of the thesis, each with individual subdivisions into introduction, methods, results and discussions.

Finally, overall conclusion is presented in Chapter 12.

Chapter 2 : Design of Optimum Bioelectric Amplifier (Analog Front End) for EEG

2.1 Background

To record EEG signal for BCI application, a bioelectric amplifier is essential. Although, design information and theory for bioelectric amplifier is well established, commonly available and there are numerous design notes and excellent books are present (Brown, 1999 & Webster,1998), but every system has its own set of criterion which presents practical challenges that is not usually treated in the text books. These challenges need to be addressed. In this chapter, development of a two channel EEG amplifier is discussed, then the following chapters describes various proposed innovative methods which overcomes different challenges and improves the overall bioelectric signal recording, then eventually development of an optimum bioelectric amplifier for EEG and other electro-physiological signals. This bioelectric amplifier in conjunction with data acquisition system is used for BCI research.

2.2 Design Considerations

As it is mentioned before, EEG is extremely small signal of minimum amplitude of 10 μV, where background noise of about 2 μV p–p is expected even if the very best bioelectric amplifier is used (Brown, 1999). For instance, if we ignore the other source of interfering noise and artefact, only the thermally generated noise form the components is high enough to corrupt the EEG signal as the signal to noise ratio is 5:1 and is very much significant. Therefore, to reduce noise, the amplifier is required to have low parts count, which is also a requirement for low cost and small size wearable feature. It needs to have a narrow bandwidth with sharp cut-off frequency as noise voltage is a function of frequency and sums up to the total thermal noise by a factor of $\sqrt{f}$, i.e, reducing bandwidth by a factor of 5 will reduce noise voltage by a factor of $\sqrt{5}$ (Brown, 1999). The amplifier needs to have at least of 100 dB of gain to be able to record the lowest amplitude EEG signal of 10 μV peak to peak, after amplification the output will then become 1volt peak to peak. On the other hand for a nominal 100 μV peak to peak signal the output will be 10 V peak to peak which is nominal dynamic range of the input of the data acquisition system that is preliminarily used for evaluation of the system. The amplifier is

required to have a Common Mode Rejection ratio of 100 dB. Assuming the average interfering common mode voltage to be of amplitude 100 mV, and the average EEG signal to be 100 μV, this will reduce the common mode voltage to 1% of the output signal voltage. The clinical EEG has the bandwidth of 0.5 to 40 Hz (Brown, 1999), on the other hand some BCI research requires the upper band frequency as high as 200 Hz (Blankertz et al., 2003). Therefore, to have future compatibility, the desired amplifier band width is 0.5 to 200 Hz.

Besides, for diagnosis or for BCI, multichannel EEG is usually required. Normally each would require a differential amplifier with two inputs while all of them can have a common neutral (or ground). However, this would require complex connections when one desires to have EEG from multiple localized points. Therefore, in any EEG system all differential amplifiers should have only the non-inverting inputs as the active electrodes while all the inverting inputs should be connected together to another common electrode. The reference or the common neutral of all the INAs are also connected together. This calls for additional complexity in design which needs to be addressed carefully.

Another problem common with any bioelectric amplifier is the presence of a DC contact potential at the electrodes. Even if these are eliminated using AC capacitor coupling at the input, some slowly varying DC is encountered due to movement of ions in the body beneath the electrodes and due to slight movement of electrodes on the skin, leading to very low frequency noise. Again the first INA stage itself may contribute to a DC offset voltage. Therefore appropriate circuits are needed to eliminate such DC potentials from the output, which otherwise may saturate the whole amplifier system rendering it useless.

2.3 Method

2.3.1 Design

The main component of the bioelectric amplifier is the special form of difference amplifier called Instrumentation Amplifier (INA), it has very high input impedance (~ Giga ohm), and very high Common Mode Rejection Ratio (CMRR, ~ Minimum of 80 dB), followed by a few stages of filters – both high pass and low pass, to provide the desired pass band. Since description, theory of operation and documentation of instrumentation amplifier is widely available, it is not

discussed here, but it can be safely said that it is an essential part of bioelectric amplifier because of its unique attributes mentioned above. There are several ways to configure a multichannel bioelectric amplifier using INA's, the most reliable way is to connect all the inverting input terminals as a common electrode connection and connecting the INA reference pin to the circuit ground or to a Driven Right Leg (DRL) circuit (Discussed in Chapter 4). This connection serves as reference electrode for difference potential measurement. Then, the non-inverting inputs are treated as individual electrode connection, therefore, individual channels. Figure 2.1 shows the general amplifier configuration used for two channel bioelectric amplifier. The number of channel can be increased by this configuration just by adding more INA`s in similar fashion.

Although the reference point is shown in the figure as the ground terminal, in a typical EEG amplifier, this is known as the common neutral point since such patient connected segments are electrically isolated from the main circuit having another ground terminal which is connected to the ac power mains.

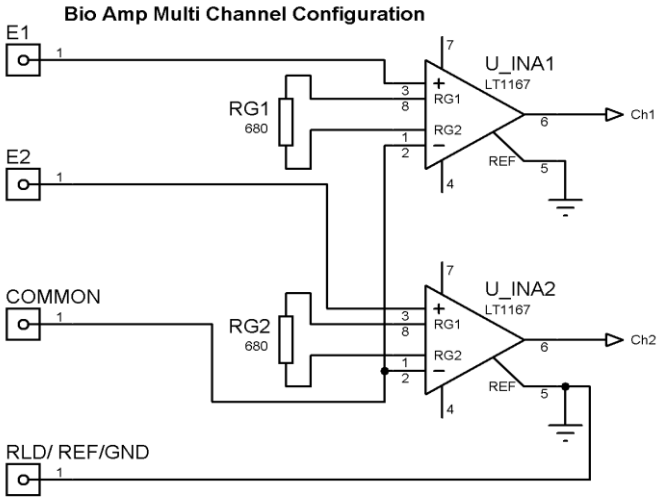

Figure 2.1: Selected Multichannel bioelectric Amplifier configuration

To achieve 100 dB of gain, which equals 100,000 in linear gain, the amplifier was designed to have four gain stages; the first gain stage is obviously the INA, which should have a gain of about 75. This gain value was chosen from the fact that there are three filter stages later which

were designed to have gains of 11 at each stage making a total gain of the filter stages as 1331. Therefore, to have 100,000 of total gain, the first INA stage gain has to be 75.13 (=100,000/1331). In the present work the INA circuitry was designed to have a precise gain of 75.2, making the total gain slightly greater than 100,000, the variation being negligible.

The three filter stages used are of Sallen–Key configuration (Sallen, R. P., 1955) with second order filter topology.

2.3.1.1 Instrumentation Amplifier segment with DC Restoration Circuit

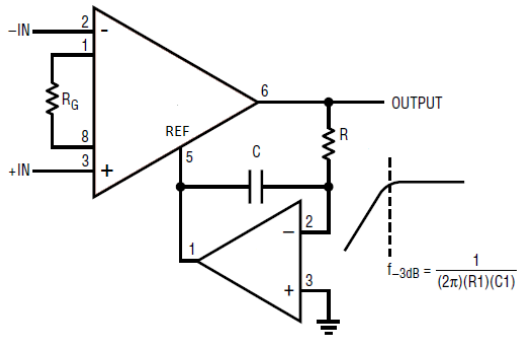

Figure 2.2: DC restoration circuit with the 1st stage INA

As mentioned before, there may be some small DC voltage or very low frequency noise voltage at the output of the INA stage. The typical approach would be to have a high pass filter right after the first INA stage. However, since the cut-off frequency has to be very low (< 0.1 Hz) this calls for reasonably large values of capacitor and resistor to have a large time constant. When a DC voltage suddenly changes at the input the output may become saturated momentarily which would charge up the capacitor. The capacitor may become charged and take a long time to discharge so that measurable signals are available again. To remove this problem, a DC restoration circuit as shown in Figure 2.2 was used. It uses a low pass inverting op-amp filter to extract and invert the very low frequency and DC components of the output of the INA stage which are then fed back to the reference terminal of the INA. The combined INA stage and the inverted low pass feedback essentially produces a high pass filter with much better performance, eliminating the problem of saturation mentioned above.

The low-pass pole translates into a high-pass function as referred to the input with –3dB cut off frequency,

$$f_c = \frac{A}{2\pi RC} \tag{2.1}$$

Where, A refers to the differential gain from input to output of the INA and is given by (according to data sheet of LT1167, the INA used),

$$A = \frac{49.4k\Omega}{R_G} + 1 \tag{2.2}$$

To have gain of 75.2, R_G was chosen to be 665 Ω. Since a resistor of this value is not commercially available it was made up of a 680Ω resistor in parallel to a series combination of two 15 kΩ resistor i.e. 30 kΩ. The midpoint of this series combination also provided a common signal point for Right Leg Drive Circuit described later. To achive cutoff frequency (f_c) of 0.03 Hz the DC restoration highpass filter, the R and C were chosen to be 5.6 MΩ and 1μF respectively.

2.3.1.2 Low-pass filter using second order Sallen-Key topology

Sallen-Key is a second order (i.e., 40 dB/decade attenuation) active filter as shown in Figure 2.3, particularly valued for its simple, low parts count design with excellent performance. This filter topology can be cascaded to obtain higher order.

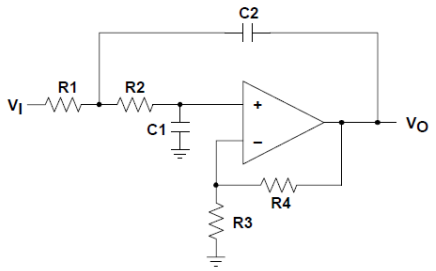

Figure 2.3: Single Stage of Sallen-Key low-pass filter

The transfer function for ideal low-pass Sallen-Key filter is given by,

$$\frac{V_o}{V_I} = \frac{A}{s^2(R_1R_2C_1C_2)+s\big(R_1C_1+R_2C_1+R_1C_2(1-A)\big)+1} \tag{2.3}$$

Where, $s = j2\pi f$. The cut-off frequency is given by,

$$f_c = \frac{1}{2\pi\sqrt{R_1R_2C_1C_2}} \tag{2.4}$$

The Quality factor is expressed as,

$$Q = \frac{\sqrt{R_1R_2C_1C_2}}{R_1C_1+R_2C_1+R_1C_2(1-A)} \tag{2.5}$$

It needs to be mentioned that a high Q-value indicates a large hump on the filter characteristics near the cut off frequency, which is undesirable. To have a desired maximally flat filter response, the Q-factor should be as low as possible (Kugelstadt, 2008).

2.3.1.3 High-pass filter using second order Sallen-Key topology

The high-pass Sallen-Key filter is obtained by interchanging R and C components. Figure 2.4 shows the construction of this filter. The transfer function for ideal low-pass Sallen-Key filter is given by,

$$\frac{V_o}{V_I} = \frac{A(s^2(R_1R_2C_1C_2))}{s^2(R_1R_2C_1C_2)+s\big(R_2C_2+R_2C_1+R_1C_2(1-A)\big)+1} \tag{2.6}$$

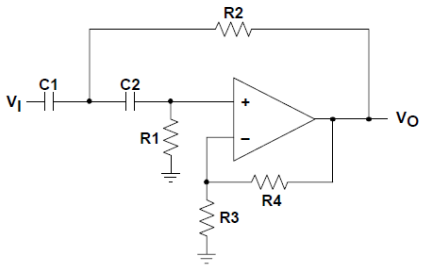

Figure 2.4: Single Stage of Sallen-Key high-pass filter

Similarly, $s = j2\pi f$, also the cut-off frequency is given by Eq. (2.4)

And the Quality factor is given by,

$$Q = \frac{\sqrt{R_1 R_2 C_1 C_2}}{R_2 C_2 + R_2 C_1 + R_1 C_2 (1-A)} \quad (2.7)$$

We used 3 stages of Sallen-Key filter, one high-pass and two low-pass filters, which are all second order filters. Along with input AC coupling (which is a first order high pass filter, discussed in detail in a later chapter) and the DC restoration circuit (which is also a first order high pass filter, discussed before) and the Sallen-Key second order high-pass filter, the overall high-pass filtering of the bioelectric amplifier has an order of 4. Also two second order Sallen-Key low pass filters produces 4th order filtering.

According to the requirements stated above, these filters are designed and simulated first, then the circuits are built and practical analysis is conducted.

2.3.2 Simulation and Schematics

Each filter and Amplifier stages are simulated separately for frequency and gain response, then the final aggregated circuits are simulated. All the simulation, schematic design and PCB layout were performed using a software package called Proteus.

2.3.2.1 Instrumentation Amplifier segment with DC Restoration Circuit

The instrumentation amplifier used in the present work is an INA IC, LT1167, which has excellent CMRR, high input impedance and non-variant gain response in the desired frequency band. Besides, LT1167 has low input bias current due to its FET biased input stage which results in low noise. As there is no simulation model in the Proteus, a three operational amplifier version of INA was constructed and used for simulation based on TL074, a quad op-amp with JFET input. Figure 2.5 shows the schematics of the Instrumentation Amplifier with DC Restoration Circuit.

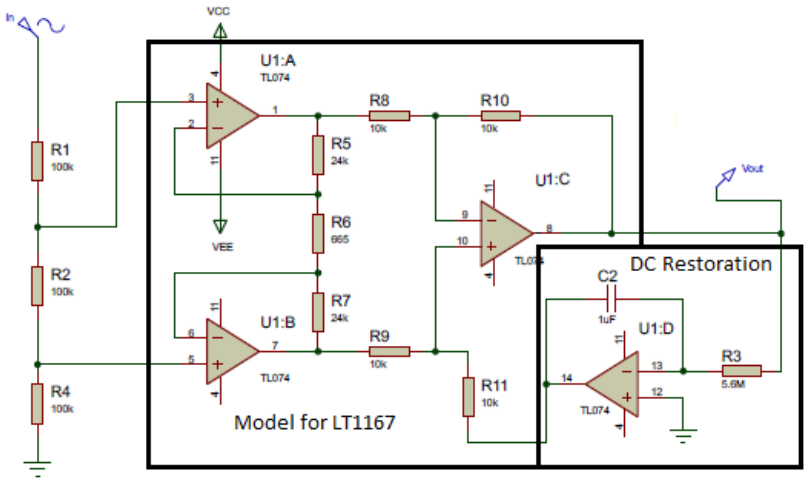

Figure 2.5: Simulation schematics of DC restoration circuit and INA

The resistor network of R1, R2 and R3 provides a differential input signal for the instrumentation amplifier applying a voltage signal at the top of R1. U1:D, C2 and R3 constructs the DC restoration circuit. The rest of the circuitry is part of constructed INA.

2.3.2.2 Sallen-Key Low-pass filter

The single stage Sallen-Key low-pass filter components values are calculated and selected from standard components with minor variations. The schematic used for practical use and simulation is shown in Figure 2.6.

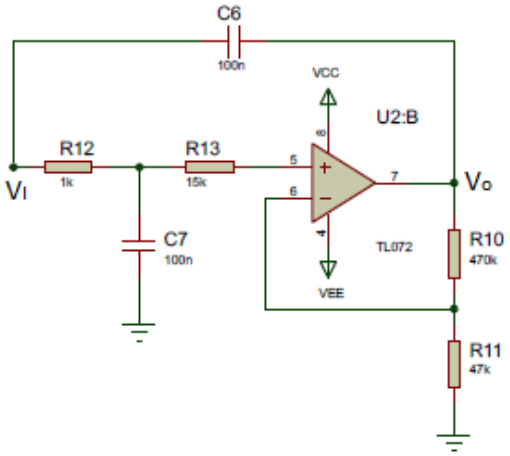

Figure 2.6: Sallen-Key Low-pass filter

2.3.2.3 Sallen-Key High-pass filter

Similar schematic design for simulation and actual circuit of a Sallen-Key high pass filter is shown in Figure 2.7

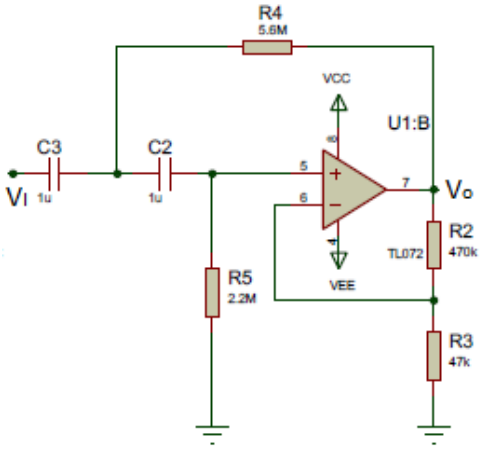

Figure 2.7: Sallen-Key High-pass filter

2.3.2.4 Aggregated amplifiers and filters

The final combined circuit is just adding the stages one after another and since those circuits are presented before, the schematics of combined circuitry is not shown here. The complete circuit schematic are given in Appendix-1.

The simulation and actual circuitry were arranged as follows:

(i) First order RC high-pass input stage for AC input coupling →

(ii) DC restoration and INA (Gain = 75.2) →

(iii) Second order Sallen-Key low-pass filter (Gain = 11) →

(iv) Second order Sallen-Key high-pass filter (Gain = 11) →

(v) Second order Sallen-Key low-pass filter (Gain = 11).

It is to be noted that, (i) and (ii) belongs to the first stage with INA and taken together, constructs one second order high-pass filter. Every input connecting the Electrode has a user protection

circuitry. The detailed circuit diagram for a single channel bioelectric amplifier is given in Appendix-1. Each user and input protection circuit is connected to the INA by means of a switchable jumper, so it is possible to combine the inputs and as well as the Driven Right Leg (DRL, detail description is presented in chapter 4) circuit in different combinations for different amplifier configurations. For a two channel EEG recording amplifier, two single channel circuit boards are combined.

For mains connected PC based data acquisition and analysis, the user and amplifier circuit is isolated by isolation amplifier IC (ISO124) and associated circuitry. The isolated split power supply is achieved by medical grade DC to DC converter (BB722BG).

2.4 Results and Observations

The frequency responses, for simulated and practical measurements of each stage and also of the combined bioelectric amplifier are presented in this section. Figure 2.8 and 2.9 show frequency responses of the INA stage with DC restoration circuit for both simulated and measured cases respectively. Figure 2.10 shows the frequency response of the measured CMRR of the differential amplifier stage i.e. INA stage. It is to be noted that the simulations were performed from 0.01Hz (10mHz) to 10kHz while the practical measurements were performed between 0.1Hz and 10kHz.

The frequency response of the Sallen-Key low-pass filter is shown in Figure 2.11 (Simulated) and in Figure 2.12 (Measured).

The frequency responses of Sallen-Key high-pass filter is shown in Figure 2.13 (Simulated) and 2.14 (Measured).

The frequency response of combined bioelectric amplifier and filters is shown in Figure 2.15 (Simulated) and 2.16 (Measured).

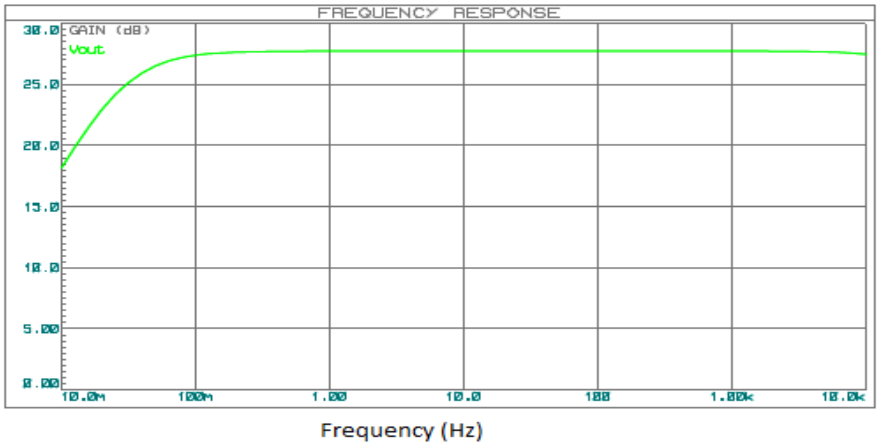

Figure 2.8: Simulated Frequency Response of the INA stage with DC restoration circuit

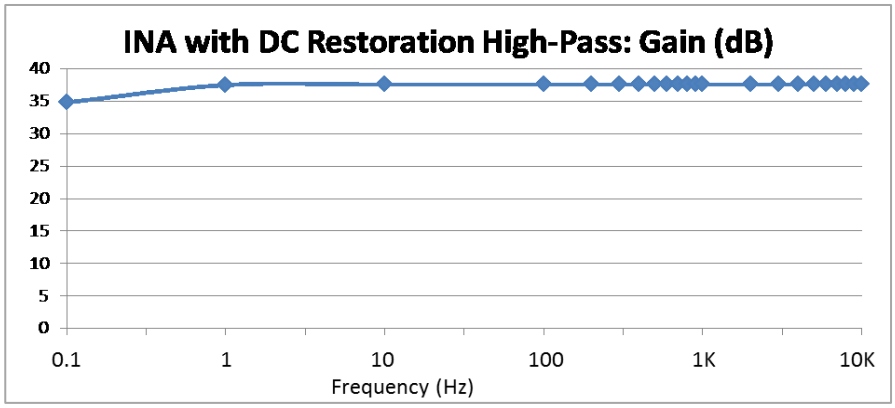

Figure 2.9: Measured Frequency Response of the INA stage with DC restoration circuit

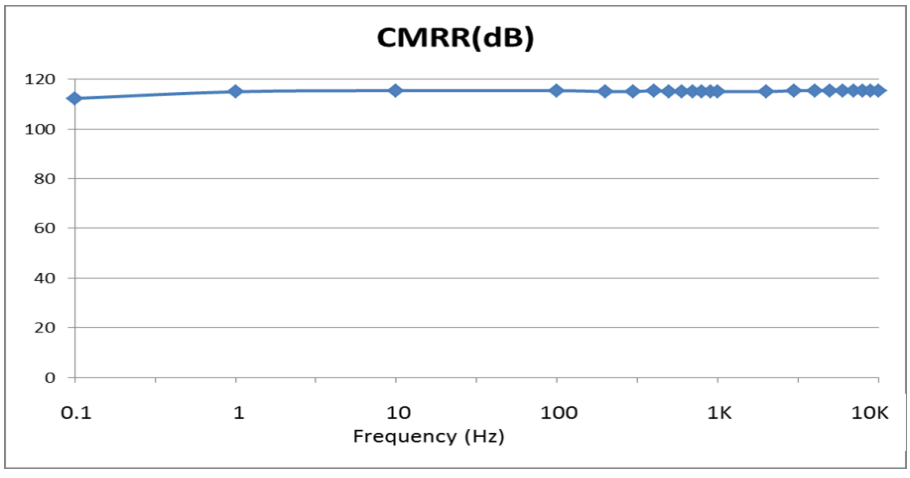

Figure 2.10: Measured CMRR of the Differential Amplifier stage i.e. INA stage

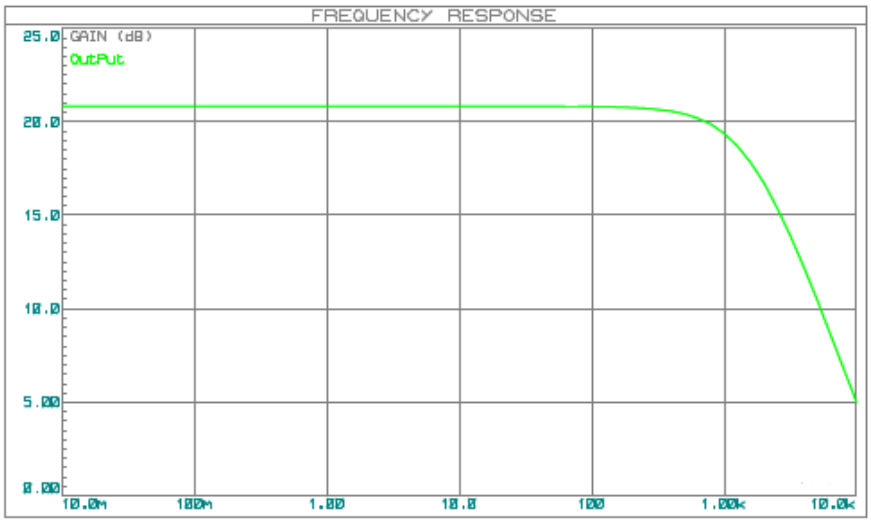

Figure 2.11: Simulated Sallen-Key low-pass filter frequency response

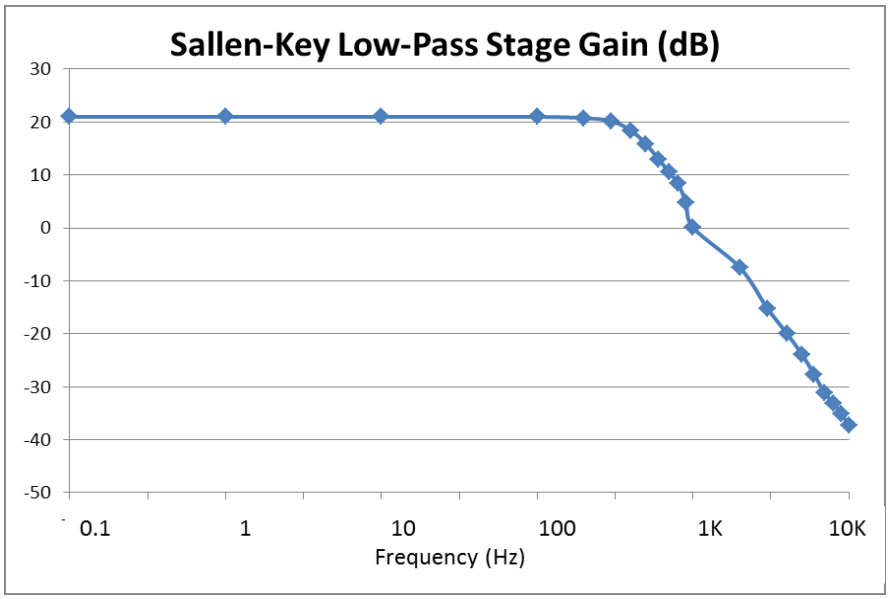

Figure 2.12: Measured Sallen-Key low-pass filter frequency response

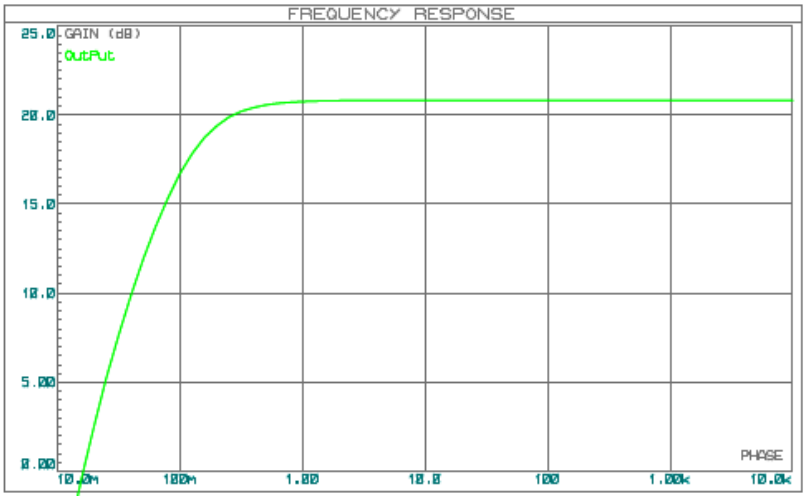

Figure 2.13:Simulated Sallen-Key high-pass filter frequency response

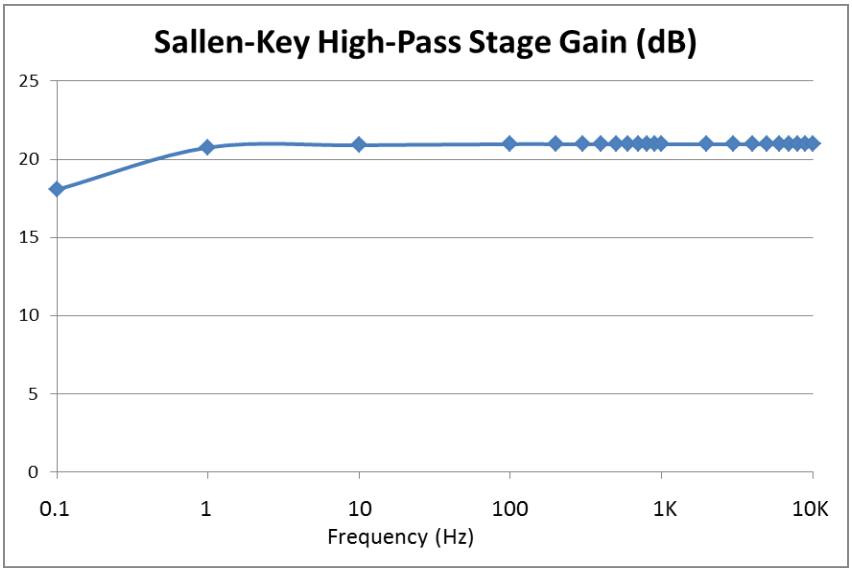

Figure 2.14: Measured Sallen-Key high-pass filter frequency response

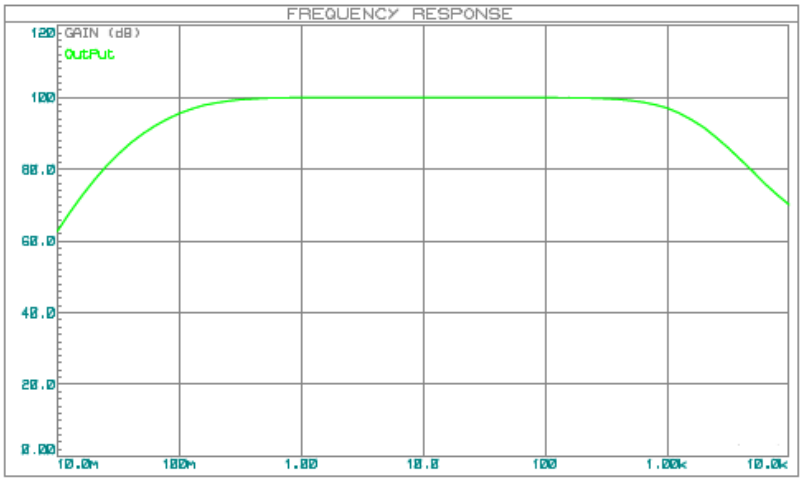

Figure 2.15: Simulated Final bioelectric amplifier frequency response

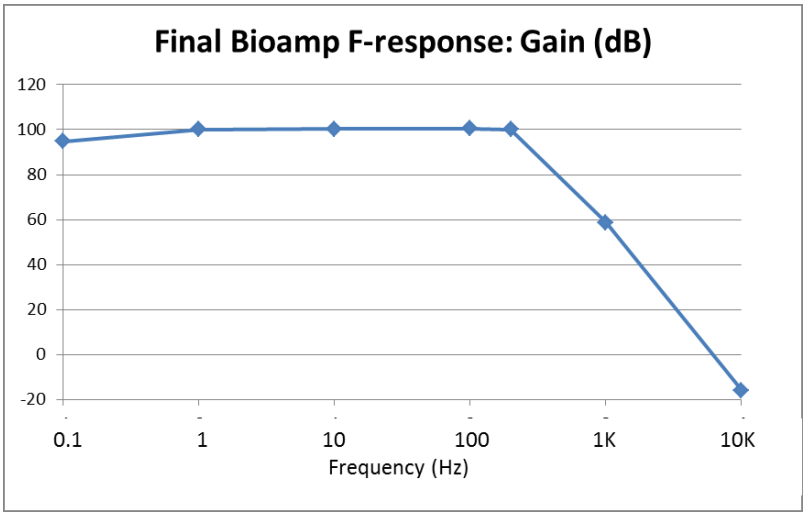

Figure 2.16: Measured Final bioelectric amplifier frequency response

The cutoff frequency of the INA stage with DC restoration circuit is at about 40mHz (0.04Hz) for the simulated circuit (Fig. 2.8) and at slightly less than 100mHz (0.1Hz) for the practical circuit (Fig. 2.9) while the high frequency gains are about 28dB and 37dB for the simulated and practical circuits respectively. The measured CMRR is about 115 dB throughout the frequency range shown (Fig. 2.10) which is expected for an INA with DC coupling, as used for these measurements.

For the Sallen-Key low pass filter circuit, the cutoff frequencies are slightly above 1kHz for the simulated circuit (Fig. 2.11) and about 200Hz for the practical circuit (Fig. 2.12). The gains agree closely for both, which should be about 21dB for the chosen gain of 11. However, the rolling off is sharper for the practical circuit than the simulated one. At 10kHz, the simulated gain is about 5dB while that for the measured one is about -40dB.

For the Sallen-Key high pass filter circuit, the cutoff frequencies are about 0.2Hz for the simulated circuit (Fig. 2.13) and about 0.1Hz for the practical circuit (Fig. 2.14). The gains again, agree closely for both, about 21dB. The rolling off could not be compared since practical measurements below 0.1Hz were not taken.

For the combined amplifier and filters, the gains match very closely, 100dB for both at mid-band. However, the frequency cut-off differs slightly, besides because of the large intervals in measurement frequencies, the precise values of the cutoff frequencies cannot be determined from Fig. 2.16. However, the cutoff frequency of 200Hz shown for the practical low pass filter circuit given in Fig. 2.12 suggests that when two such modules are combined, the cutoff frequency will be slightly less than 200Hz.

The reasons for the differences observed above may be due to the following factors:

i. Tolerances of values of components
ii. Lack of matching between components where required
iii. The INA was simulated using three TL074 op-amps while LT1167 was used for the real circuit. Obviously parameters will differ for the two constructions.

The measured frequency response data from the final bioelectric amplifier, which is aggregation of all stages, confirms that the overall gain is precisely 100 dB and has almost a non-varying gain response over the intended frequency band of 1Hz to about 200 Hz. Fig. 2.16 indicates that there is 40dB attenuation from slightly less than 200 Hz to 1000 Hz, which is very much desirable. The CMRR of the bioelectric amplifier is almost 115 dB, which is well suited for the desired operation of the amplifier.

2.5 Novelty

The main aspect of this bioelectric amplifier is its capability of producing such a high gain (100 dB) with only four amplification stages, with excellent frequency response and stability.

As the first INA stage of the amplifier would be AC coupled to user electrodes by special RC network (to be discussed later) which are expected to degrade the effective CMRR, therefore a very high CMRR (115dB) with the DC coupled input configuration will provide a reasonable margin to achieve the desired 100dB CMRR.

This circuit also used a large differential gain (75.2 or 37.5 dB) at the first INA stage which helps in getting high CMRR.

The stability of the Sallen-Key filter amplifier depends largely on the quality or Q-factor, the higher the Q, the amplifier is more unstable (Kugelstadt, 2008), which means high Q can result in self-ringing or self-oscillation of the amplifier. Therefore extreme care has been taken at the design phase to ensure low Q-factor. The result from the measured data of Sallen-Key filters (both low and high pass) and as well as the total amplifier system, shows there is no abrupt kink in the cut-off region, which implies that the system has low Q and is stable.

Fewer stages of amplifier and filters results in low part count, which makes the device low noise, power efficient and miniature in size, all of these are suitable for the proposed wearable BCI system.

Chapter 3 : Modified Input AC Coupling to Produce Improved CMRR and High Input Impedance

3.1 Background

AC coupling at the front end i.e. in-between body electrode and input of the instrumentation amplifier is very much desirable for recording of bioelectric potentials. Since, the DC skin-electrode contact potential can reach several hundred millivolts and the difference between electrodes can be as high as ±300 mV (Brown, 1999), it limits the admissible gain of the first stage amplifier. The first differential input stage of instrumentation amplifier amplifies the differential signals where the common mode signal is passed with unity gain. The later difference amplifier stage has unity gain and only cancels out the common mode signal. Therefore, larger gain of the INA results in higher Common Mode Rejection Ratio (CMRR) (Pallás et al., 1991). Furthermore, this large skin-electrode contact potential requires large power supply rails to achieve operating dynamic range of the output of the amplifier for desired signal without being saturated. This is problematic, particularly for battery operated wearable devices.

On the other hand, direct coupling of the input of INA can result in flow of DC current through body that could cause in electrolysis and result in tissue necrosis. Thus, DC coupling can introduce potential health hazard to the user who is connected to the amplifier system.

There are several ways to configure AC coupling of the input of INA. The most common AC coupling configuration is the differential RC high pass filter (Pallas et al., 1999) and shown in Figure 3.1.

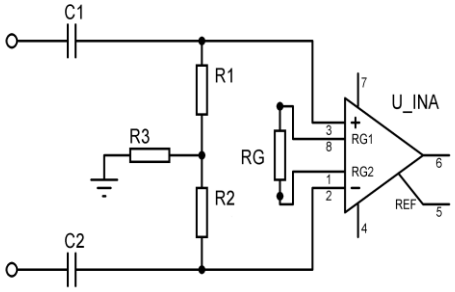

Figure 3.1: Conventional AC coupling with differential RC high pass filter

3.2 Problem Statement

The RC high pass AC coupling circuit shown in Figure 3.1 effectively removes any level of DC potential, but it severely degrades the common mode rejection ratio (CMRR) of the instrumentation amplifier. The reason for this is firstly the tolerance of RC components, i.e. any mismatch between the each high-pass filter components (R1C1 and R2C2) will result in common to differential mode conversion of common mode signal due to potential divider effect (Huhta et al., 1973). Secondly, the input impedance of the INA is no longer high and reduced by the input resistors R1, R2 and R3. Furthermore the impedances of the capacitors adds up to the source impedance.

The CMRR of the system can be improved by lowering the cut-off frequency of the high pass filter by substantial amount, to a point far lower than the required low frequency cut-off. This allows the signals in the pass band to proceed without changes in gain or phase, i.e., these remain unaltered. Therefore, the voltage divider effect of the resistors R1, R2 and R3 will be reduced. But this requires high value of RC components to make the time constant high. Any abrupt change in the signal due to motion and other artefacts, which may saturate the output of the amplifier, will require very long time to restore.

The input impedance and the CMRR of the system can be improved by increasing the value of resistor R3, but it cannot be very high as purpose of this resistor is to provide a path to input bias currents to system ground.

Therefore, the challenge is to design an AC coupling input system for the front end of the bioelectric amplifier with high CMRR and input impedance, using capacitive isolation in the signal path to ensure user safety.

3.3 Method

The proposed system replaces the resistor R3 of the schematic shown in Figure 3.1, by a unity gain buffer driven by the common mode voltage obtained from the resistor network R4 and R5 as shown in Figure 3.2.

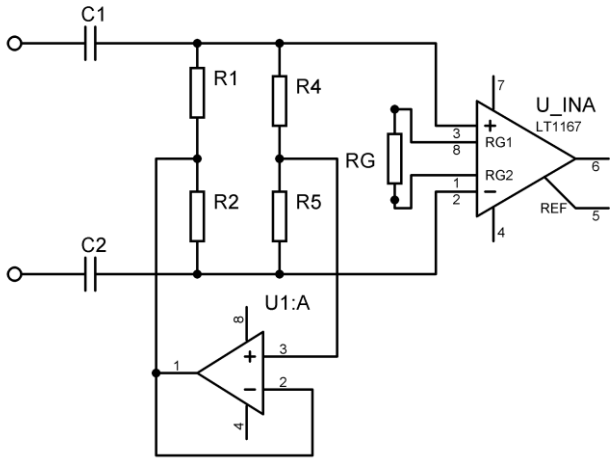

Figure 3.2: AC coupling with proposed RC high pass filter

Since the input impedance of the operational amplifier U1:A is very high, the current path through resistor R4 and R5 faces very high impedance. Also, as the output impedance of U1:A is driven to the common mode voltage potential it reduces any common mode current flow through R1 and R2. Therefore, providing high impedance for the common mode signal and thus increasing CMRR.

On the other hand, the output impedance of the buffer amplifier U1:A is very low for the differential signal, therefore, it provides bias current return path form the instrumentation amplifier inputs effectively, maintaining proper differential gain of the bioelectric amplifier.

The proposed system is simulated to analyse its DC blocking high-pass filtering response as well as its differential gain characteristics. The simulation is carried out using the software Proteus, and the simulated schematic is shown in figure 3.3. For the simulation, the differential input signal is obtained through the series resistor network R16, R2 and R17.

To evaluate the performance of the proposed system, practical measurement is carried out in three phases; firstly, the CMRR of the instrumentation amplifier is measured as function of frequency (from 1 to 200 Hz), without any passive components connected to its input, i.e., with DC coupling, which gives the highest CMRR by the INA circuit. This would act as a reference for the circuit variations at the input.

Then a conventional differential RC high-pass filter is connected to the input and same measurement is carried out. For this measurement, two RC networks were constructed to have less than 1% mismatch. This matching procedure is carried out by constructing a bridge network and minimizing the voltage difference across R1 and R2 (Figure 3.1) by means of continually changing one component until the best balance of the bridge circuit is obtained.

Finally, the proposed system is studied.

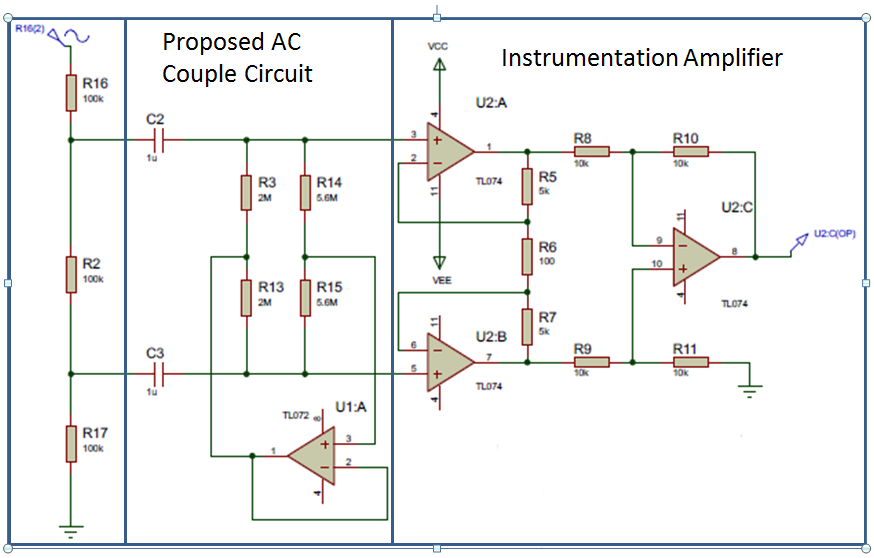

Figure 3.3: Simulation schematic of proposed AC coupling system for the front end of the bioelectric amplifier

3.4 Result and Observations

The simulated result for the proposed circuit with modified AC input coupling is shown in Figure 3.4. It exhibits the desired DC blocking high-pass characteristics with non-variant gain response in the desired frequency band. Experimental result for frequency response of

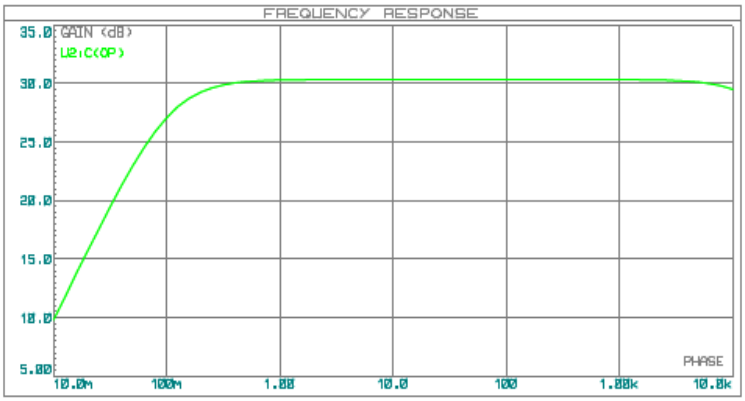

Figure 3.4: Simulated frequency response of Proposed AC coupling system

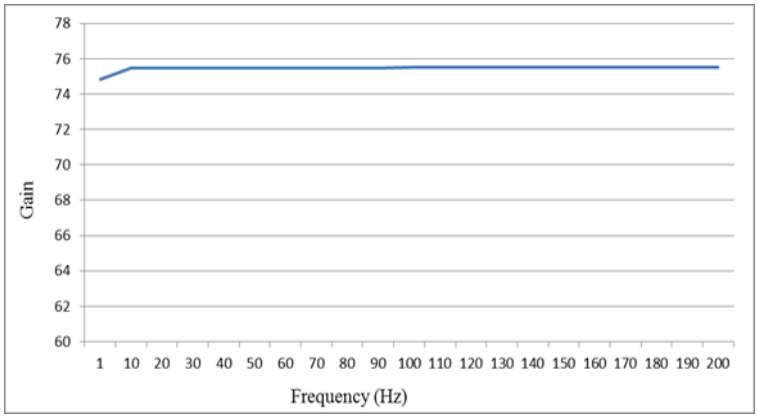

Figure 3.5: Measured frequency response of conventional AC coupling system

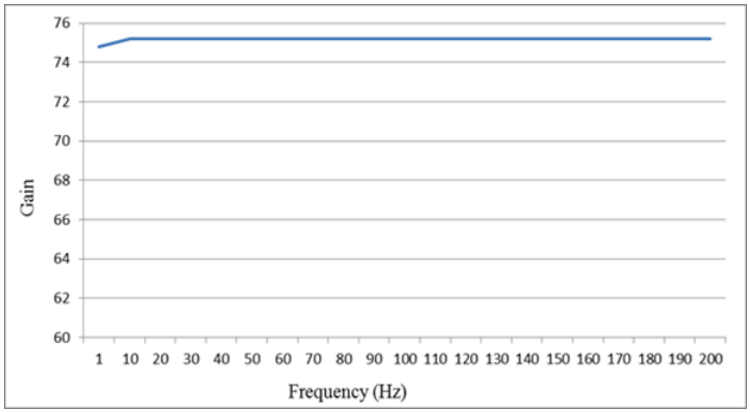

Figure 3.6: Measured frequency response of Proposed AC coupling system

differential gain is shown in Figure 3.5 and 3.6. These two results are consistent and give evidence of unaltered differential gain of the proposed AC coupling system with the conventional one. It is to be noted that Figures 3.5 and 3.6 shows the gain in linear scale. The measured gains shown corresponds to about 38dB which is slightly greater than the simulated value. Again, practical use of LT1167 as the INA as against the TL074 op-amp mostly contributed to this mismatch, which does not say anything against the developed system.

Since the differential voltage gain of the instrumentation amplifier for the first measurement (where no input RC component is used and directly coupled to the measuring signal) is frequency independent at range of our interested band, its graphical result is not shown. Only the CMRR as a function of frequency is given in the Figure 3.7 for comparison.

The CMRR of the directly coupled (DC coupled) instrumentation amplifier (LT1167) is found to be 115 dB. The measured CMRR of conventional RC based AC coupled system and the modified AC coupled system proposed in this work are shown in Figure 3.8 and 3.9 respectively. The former confirms the degradation of CMRR due to passive RC component connected at the input of the INA. From Figure 3.9, it is evident that the CMRR of the proposed system has increased a substantial amount from its conventional counterpart. The CMRR of this proposed system is about 110.5 dB which is very close to the directly coupled INA.

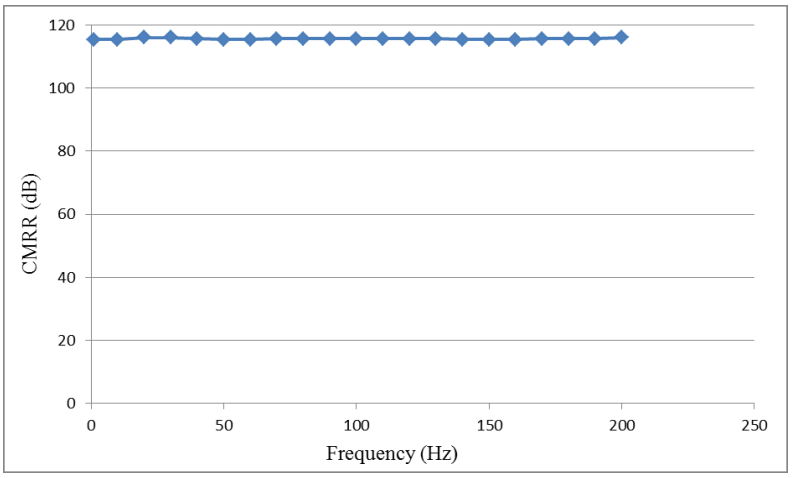

Figure 3.7: Measured CMRR vs. Frequency of Direct coupled INA, for reference

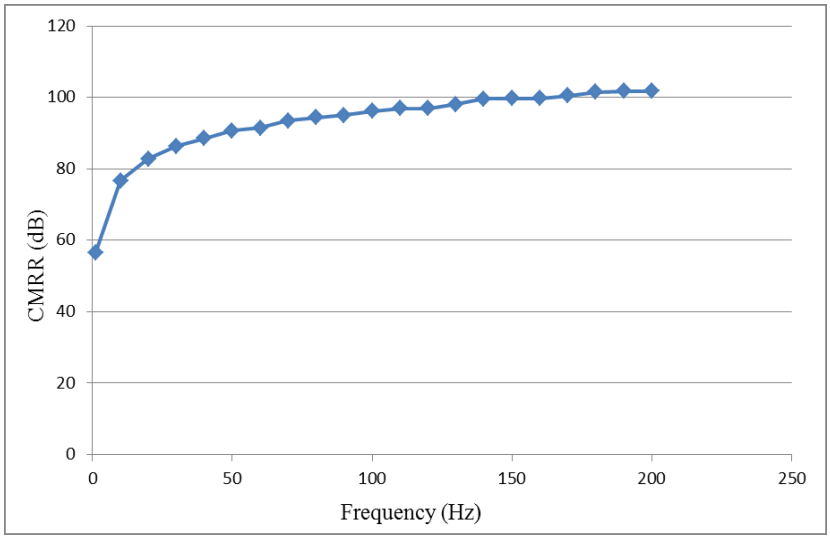

Figure 3.8: Measured CMRR vs. Frequency of Conventional AC Coupled INA

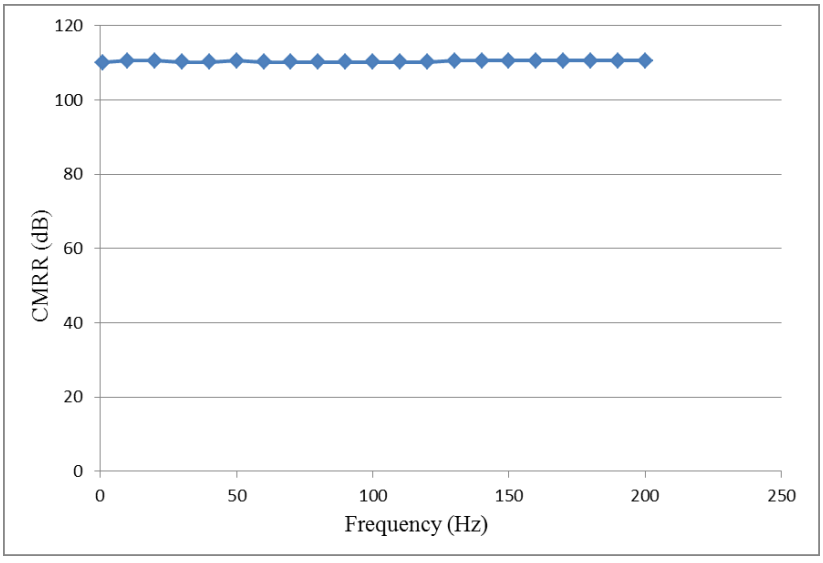

Figure 3.9: Measured CMRR vs. Frequency of the Modified AC Coupled INA

3.5 Novelty

Apart from the DC restoration circuit described in chapter 2.3.1.1, there are several proposed systems which provide AC coupling to the input of instrumentation amplifier with high CMRR and high input impedance that does not depend on the input DC potential difference (Spinelli et al., 2003& 2000), (Pallas et al., 1990, 1993), (Dobrev et al., 2008). But these systems do not ensure fully capacitive coupling with the user body and thus still has the problem of tissue burning hazard of the skin. Also, some of these topologies requires component placement at the feedback path of differential gain stage of three operational amplifier instrumentation amplifier system, which is not possible for integrated instrumentation amplifier circuit (IC INA).

Since the EEG system requires very low skin electrode contact impedance, a DC current blocking front end is crucial for user safety, the proposed system achieves that requirement very efficiently. Moreover, compared to the other topologies, the system uses fewer components and therefore will have low noise. Besides, it will have a small footprint for the overall bioelectric amplifier, making it ideal for a wearable system. Up to the time of writing this thesis and to the author`s best knowledge, the proposed system is a genuine innovation, no other system has reported to have similar performance and functionality.

Chapter 4 : A Stable Driven Right Leg (DRL) Circuit with Improved Performance

4.1 Background

The Common Mode Rejection Ratio (CMRR) of a bioelectric amplifier can be greatly degraded by the use of conventional Driven Right Leg (DRL) system. The common mode signal appears between the reference electrode and the circuit ground due to interfering current flowing into the human body connected to the bioelectric amplifier. The interfering current mainly originates form the mains power supply (50/60 Hz power line) and flows through human body by various capacitive paths as shown in the Figure 4.1. The interfering current that flows through the skin-electrode contact impedance Z_{rl}, then to amplifier ground to Earth ground potential (i.e. through C_{pow}, C_{ca}, C_{cb}, Z_{rl}, and C_{iso}), induces the common mode voltage across Z_{rl} as V_{cm}. This common voltage then appears at the signal measuring electrodes in addition to the differential bioelectric potentials.

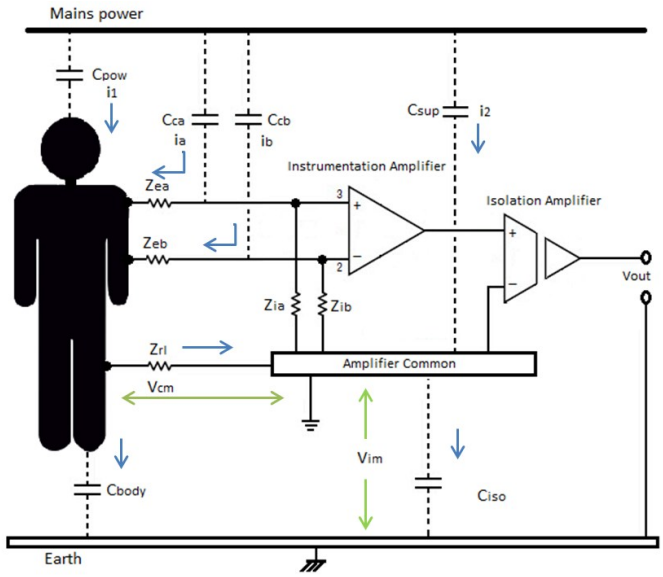

Figure 4.1: Sources of interference at the bioelectric amplifier system

Since, no differential amplifier is ideal and some of the common mode signal will pass through or transformed by the amplifier into an interfering differential signal, it is greatly desirable to

reduce the common mode voltage as much as possible (Winter et al., 1983). One way to do so is to minimise C_{pow}, C_{ca}, C_{cb} and C_{iso} in Figure 4.1 to reduce i_{cm}. Also Z_{rl} can be minimised to reduce voltage across it and thus the overall V_{cm}. But in practice it is not always possible and largely variable. Furthermore, poor electrode contact may present up to 100 k Ω of Z_{rl} (Winter et al., 1983). In some cases the common mode voltage can reach as high as 100 mV (Brown, 1999) to 200 mV peak to peak (Van Rijn et al., 1990), which is enormously large compared to the bioelectric signals and requires other measure to reduce it.

The Driven Right Leg (DRL) system as shown in figure 4.2, serves that purpose effectively. The DRL circuit reduces the common mode voltage by a negative feedback (Winter et al., 1983).

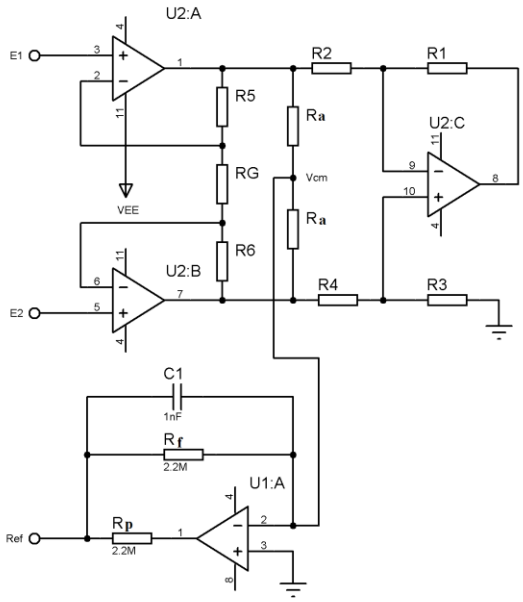

Figure 4.2: Conventional DRL Circuit

This circuit works by sensing the V_{cm}, from the averaging resistors R_a `s. Then, it injects a small amount of current of opposite phase to the subject's body using an inverting amplifier. This opposing current is equal to the displacement current flowing into the body. Therefore, the body acts as a summing junction in a feedback loop and negative feedback drives the common mode voltage to a lower value by making the effective resistance of Z_{rl} much lower. The reduced

amount of Z_{rl} is proportional to the gain of the inverting amplifier. It can be shown that the effective resistance of Z_{rl} can be expressed as,

$$R_{eff} = Z_{rl} \cdot \left(\frac{1}{1+\frac{2R_F}{R_a}}\right) \tag{4.1}$$

It can be shown that the DRL circuit can improve CMRR of the bioelectric amplifier by,

$$CMRR_{DRL} = CMRR_{org} + 20\log(1 + A_d(1 + \frac{2R_F}{R_a})) \tag{4.3}$$

The common mode voltage V_{cm} generated from the mains power-line can be reduced by a factor of 300, resulting in an increase of the CMRR by about 50 dB at 50 Hz (Van Rijn et al., 1990).

The circuit also helps to minimize abnormal high current that is hazardous to subject, by the protection and feedback resistor R_p and R_f. Since any abnormal high current saturates the inverting amplifier and only current path to the circuit ground exists is through these two resistors which are of the order of several MΩ. Equivalent resistance for this case is given by,

$$R_{eq} = R_{RL} + R_f \parallel R_p \tag{4.2}$$

For example if the INA gets faulty and the supply voltage appears any of the inputs of the INA, then the inverting amplifier of DRL is out of its normal operation and saturates. If the supply voltage is 10 V and resistors are 2.2 MΩ, then the current through the body is ~10μA, which is well within safety limit.

Though it seems very attractive to use DRL circuit, there are practical issues which make the DRL circuit very difficult to implement.

4.2 Problem Statement

The first problem of DRL circuit is possible saturation; a saturated DRL amplifier is useless (Hann, 2010). Saturation makes the circuit non-operational and distorted noise can be induced to the signal output rather than 50 Hz sine wave noise. Since the effective resistance of the reference skin-electrode interface Z_{rl} is inversely proportional of the gain of the inverting amplifier, a very high gain is desirable for the DRL circuit. This makes the DRL circuit prone to saturation of the output; mainly due to electrode offset potential, mismatched offset voltage of the first stage amplifiers of the instrumentation amplifier itself (Hann, 2010) and mismatch of the common mode voltage averaging resistors$s$ R_a's. Most of the texts dealing with DRL do not address this problem and some of them suggest a potentiometer for fine adjustment of the R_a's. Since manually adjusting the R_a's is inconvenient and may require readjustments, a DRL circuit with no adjustment would be preferred and has been attempted in the present work.

Since the DRL circuit operates in a closed loop amplifier system with -180° phase shift and additional phase shift of -180° is introduced by the RC network formed by different body stray capacitance and contact impedances, it produces the necessary conditions for oscillation (Winter, et al., 1983). Therefore, this phase shift of the common mode voltage can result in self-oscillation of the DRL amplifier and it is common to have unwanted high frequency noise at the output of the bioelectric amplifier. So, the stability of the overall system is a major concern for the system that uses the DRL circuit and compensation for the phase shift should be applied.

4.3 Method

To solve the saturation problem, a high-pass filter is proposed after the averaging resistors R_a`s to block any DC offset voltage that might saturate the inverting amplifier of DRL circuit (Figure 4.2). Since any abnormal voltage at the input still faces the same criteria stated before, the safety operation of the DRL circuit is not affected by this. A unity gain buffer is placed in between the R_as and the high-pass filter (Figures 4.2 and 4.3) in order to avoid loading of the gain of the INA. This buffer amplifier is commonly used for driving the shield of circuits and other cable shielding.

To have a stable amplifier system it is common to put a capacitor across the feedback resistor R_f. This introduces a phase lag in the system which in turn reduces the self-oscillation; this has been reported earlier (Winter et al, 1983). In this study, we proposed to connect another capacitor across the protection resistor R_p, which shows better stability along with the capacitor across R_f. This configuration results in an active low pass filter which attenuates high frequency signals in a two pole manner. This low pass operation helps reducing the gain requirement for self-oscillation at higher frequencies in more effective way.

The improved DRL circuit that has been proposed in the present work is shown in Figure 4.3. It needs to be noted that the DRL circuit is mainly used to reduce 50Hz mains borne noise, and therefore, its frequency response need to be considered around this frequency. The DRL circuit itself should have a high gain at 50Hz, so that it can reduce it with negative feedback to the body of the patient.

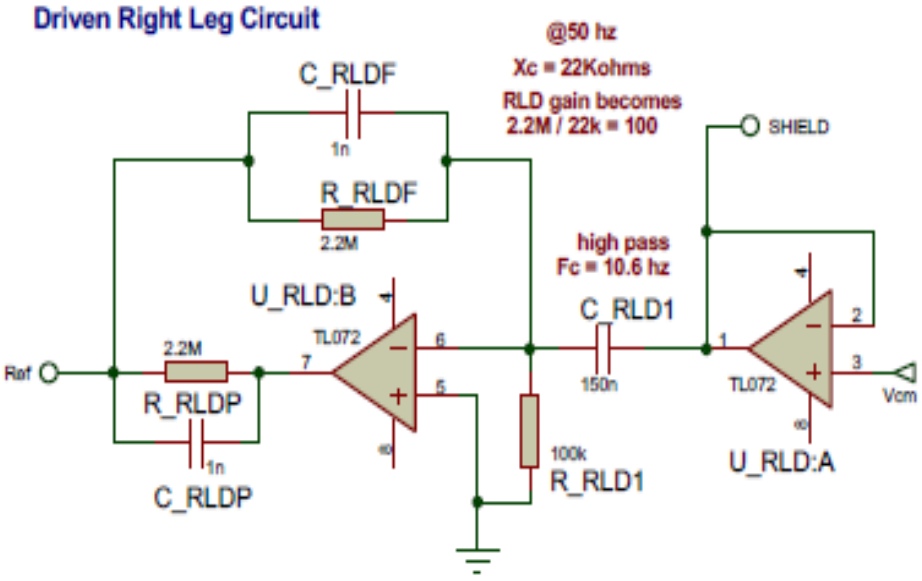

Figure 4.3: Proposed DRL Circuit

This DRL circuit has been designed to have a pass band gain of 100, within the frequency band of 10 to 1KHz. The schematic of the proposed circuit is also simulated for frequency response by the software Proteus. A practical measurement of noise figure in ECG signal was conducted on a volunteer. An experimental comparison was carried out between a very closely matched potentiometer adjusted DRL circuit and the proposed improved DRL circuit, which does not need such manual matching procedure. The bioelectric amplifier used in this study is the developed one described in chapter 2, with the only difference of having a low gain setting.

4.4 Result and Observations

Figure 4.4 shows the simulated frequency response of the propose DRL circuit, which has a high gain at 50Hz. However, through adjustment of component values, it can be improved further.

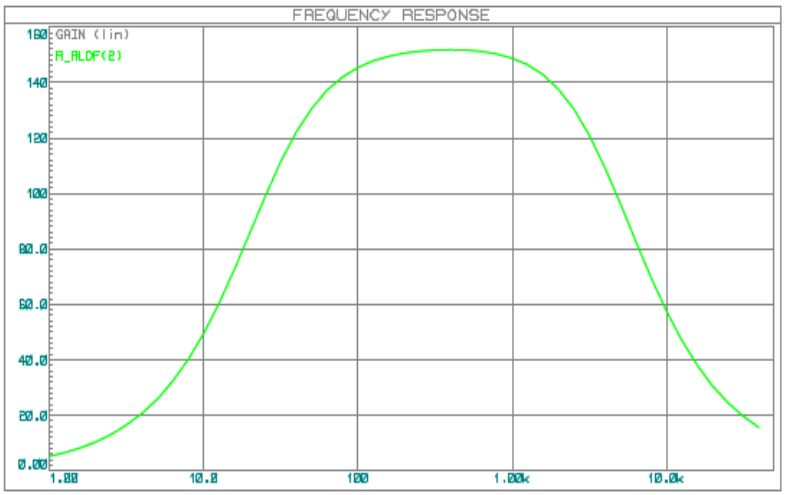

Figure 4.4: Simulated Frequency response of Proposed DRL Circuit

The output at the *Ref* electrode of the DRL circuit (Figure 4.3) have been measured both for the conventional DRL circuit with adjustment using a multi-turn potentiometer (Figure 4.5) and for the proposed DRL circuit without any manual adjustment (Figure 4.6).

These show that the 50 Hz interfering signal is fed-back to the body as a square wave. Figure 4.5 has a DC offset in spite of attempts to minimise it through a careful matching of the resistor R_a during signal acquisition. On the other hand in Figure 4.6 obtained from the proposed circuit, there is no DC offset.

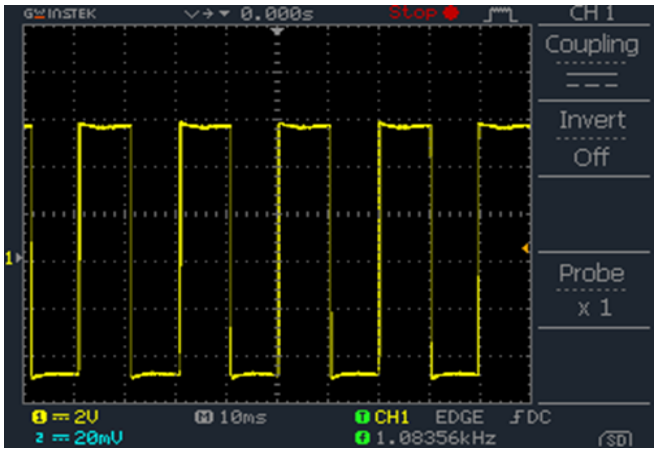

Figure 4.5: DRL amplifier output after potentiometer adjusted

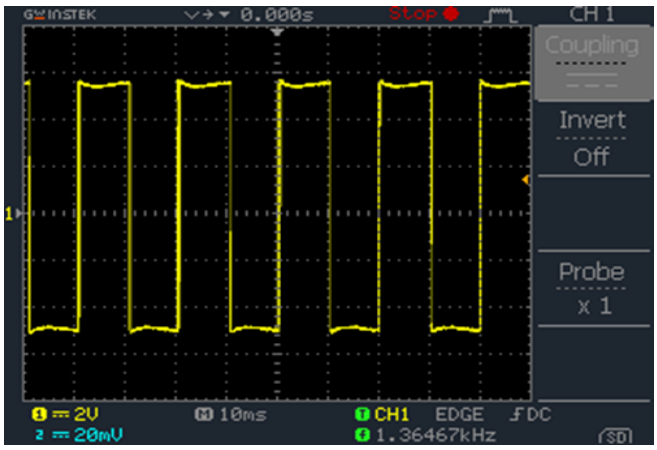

Figure 4.6: DRL amplifier output of the proposed circuit

The ECG recorded from a volunteer using the two DRL circuits are shown in Figure 4.7 and 4.8 respectively, the former using the conventional one and the latter suing the proposed circuit. These have two different vertical scales which need to be considered for a comparison. Besides, gain of the amplifier was changed slightly between the measurements so that the ECG signals do not appear to have the same value. However, the main issue of concern was the signal to noise ratio (SNR). The measured SNR of potentiometer adjusted conventional DRL circuit was 7.6 while that of the proposed DRL circuit was 9.2, thus giving a small improvement. However, the major improvement was that the proposed circuit did not require any manual adjustment, it was fully autonomous.

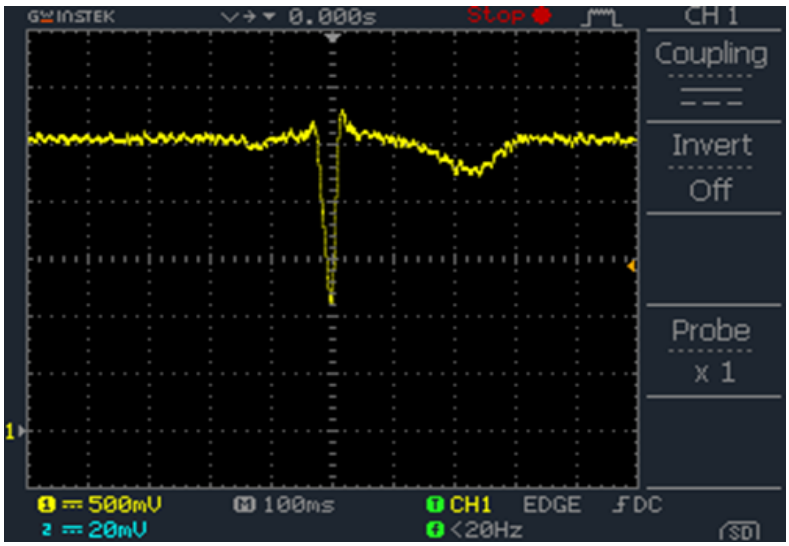

Figure 4.7: ECG trace from the amplifier using conventional DRL circuit

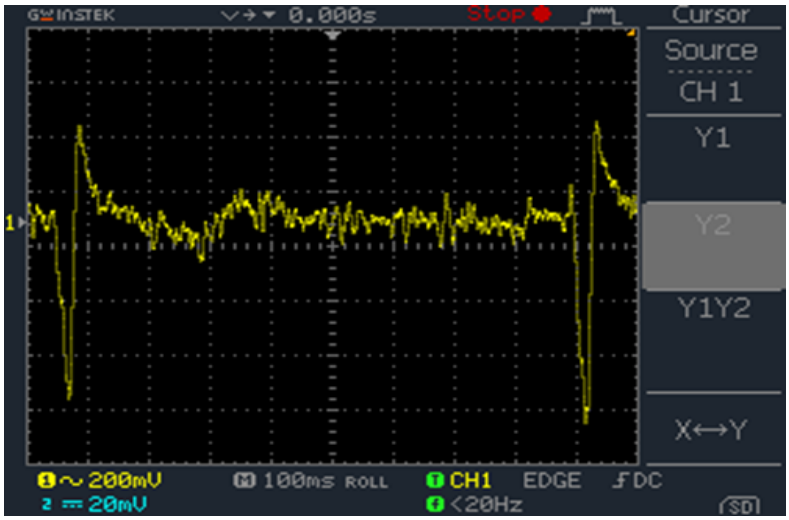

Figure 4.8: ECG trace from the amplifier using proposed DRL circuit at a magnified scale

4.5 Novelty

A simple solution has been proposed to overcome the major problem of DRL amplifier saturation. This proposed DRL is easy to implement i.e. requires no adjustment, which is the major achievement. The measured SNR has also improved a little. The added capacitor across the protection resistor at the output of the DRL circuitry has given further stability. Combining these two low pass filters the proposed DRL circuit has a comparatively narrow pass band frequency, which reduces the chance of self-oscillation and therefore, increases the stability of the overall bioelectric amplifier. Up to the time of writing this thesis, no other design of DRL has been reported to give performances as good as the proposed one developed in the present work.

Chapter 5 : Development of a Novel Self-Biased Low-Noise Two-Wired Active Electrode

5.1 Background

One of the major interference sources in a bioelectric amplifier system is the common mode to differential mode conversion of noise. This interference originates mainly from the capacitive coupling of the cables connected to the electrode with the mains power lines carrying 50Hz alternating currents (Van Rijn et al., 1990). With reference to Figure 4.1 of chapter 4, the input impedances (Z_{ia} & Z_{ib}) of the INA is very high, therefore the currents i_a, i_b, from the capacitive coupling of the cable through C_{ca}, C_{cb}, passes through the skin-electrode contact impedances Z_{ea} & Z_{eb}, then through Z_{rl} to system ground. A skin-electrode contact has a typical impedance of about 20 kΩ at 50 Hz. These impedances are rarely equal for individual electrodes and can differ by almost 50% (Almasi et al., 1970; Grimnes, 1983; Geddes, 1972). So, the 50Hz noise voltage dropped across these two impedances will not be equal and this will give rise to a differential voltage originating from the 50Hz mains noise. This mechanism of conversion of noise voltage which is supposed to be a common mode voltage to a differential input voltage is often called 'Potential Divider Effect' (Huhta et al., 1973; Pacela, 1967). The magnitude of this differential voltage can be expressed as,

$$V_{ab\_diff} = V_{cm}\left(\frac{Z_{ia}}{Z_{ia}+Z_{ea}} - \frac{Z_{ib}}{Z_{ib}+Z_{eb}}\right) \tag{5.1}$$

Also the parasitic capacitances of the cables are usually different, therefore the interfering currents i_a, i_b are different, which contributes to the common mode to differential mode conversion as,

$$V_{ab\_diff} = i_a Z_{ea} - i_b Z_{eb} \tag{5.2}$$

It is evident form Equation 5.2, that there will be common mode to differential mode conversion of the interfering signal due to different i_a, i_b even if the skin-electrode impedances are equal.

It can be shown that, in a typical situation, where the mean interfering current in cable and skin-electrode contact impedances are 10 nA and 20 kΩ respectively, having a relative difference of 50 % can induce a high level of interference of 200 μV peak to peak, which is unacceptable.

One way to reduce this interference is to use shielded cable to connect the electrodes (Horst et al., 1998). But this makes the cables bulky and not practical for EEG, as cable becomes too heavy to keep the electrodes attached to the surface. Also in EEG large number of electrode placement is required in a small region like human scalp, which makes it impractical. However, shielding cable introduces input capacitance to the inputs instrumentation amplifier to the ground, which in turn reduces the input impedance of the amplifier (Van Rijn et al., 1991a) which in not desired.

Another way to reduce this potential divider effect is to reduce the skin-electrode contact impedance. But to reduce it to significant amount, it requires extensive preparation of the skin, which is time consuming and uncomfortable for the subject (Searle et al., 2000). Alternative to these solutions, an active electrode system can be used. It is been shown in several publication that the use of active electrode can reduce power line interference (Fernandez et al., 1997; Ko, 1998; Nishimura et al., 1992, Metting et al., 1996). Since the output impedance of an active electrode is low, the current in the electrode wire due to interface finds a low impedance path to ground. Therefore, the induced common mode voltages and as well as their difference are reduced. In other words, this buffered active electrode system transfers the high skin-electrode impedances (Z_{ea} & Z_{eb}) to low impedances. But most of the active electrode system requires at least three wires per electrode and thus making the cable system bulky, stiff with large connector and additional noise for the amplifier, therefore not practical (Degen et al., 2006).

The number of wires of an active electrode can be reduced to two; there is one commercial system (BioSemi, 2011) meeting the criteria. However, their design is not disclosed to public. Some publications described two wired buffer electrode, one of which uses custom made operational amplifier based integrated circuit (Padmadinata et al., 1990), but the electrode has the restriction of requiring the input potential to be the lowest in the circuit. There is no method provided in the publication showing how this requirement might be met in the case of bioelectric

recordings. Another publication (Degen et al, 2007) also reported a two-wire system but the system requires injecting a small amount of DC current by the DRL amplifier, to bias the gate of the active element which was a PMOS-FET. The skin-electrode contact potential can be as large as ±300 mV (Brown, 1999) and this is also affected by the contact impedance of the reference electrode, which is largely changeable. Therefore, the bias voltage of the MOSFET could be unstable. Thus the operating point of the MOSFET can easily switch from active state to cut-off state, making the signal buffering non-functional.

The most common and reliable electrode material used for bioelectrical measurements is silver-silver-chloride (Ag-AgCl). Ag-AgCl is used in most bioelectric measurement as this material has very low skin-electrode contact impedance and low contact potential, making it suitable for the purpose. However, with usage, Ag-AgCl degrades over time because of its ion-exchange reaction in the electrode-electrolyte interface (Brown, 1999). It also requires thorough cleaning and maintenance. Other electrode materials like Gold plated silver, Aluminium and Tin alloys, Carbon etc., are also used mainly for their inert properties. The metal type electrodes should not be used for long time as the corrosion of the material can give rise to unpleasant skin irritation. These materials mentioned above have moderate skin-electrode contact impedance and contact potential. These materials are comparatively expensive except for the Carbon; it is a suitable choice for electrode material as it is inert, cheap, can easily be shaped, and long lasting. The only drawback of Carbon is that it has relatively large skin-electrode contact impedance. The use of Carbon material is possible if the electrode is active, that is the high impedance of the carbon electrode can be overcome with all the advantaged stated above.

5.2 Problem Statement

The skin-electrode impedance often varies in an unpredictable way; not only as a function of the electrode material, but due to physiological changes in the subject. An active electrode system is required to reduce interface caused by the 'potential divider effect' by transferring the high skin-electrode impedance to low impedance. It also minimizes the impedance mismatch. This electrode system needs to be long time wearable, causing less irritation to the skin and requiring low maintenance.

This active electrode system should have reduced number of wire (Two-wired) with the ability to overcome all of the problems described before. The present work tried to solve this problem developing a new circuit, described in the following section.

5.3 Method

Two self-biasing buffered electrodes using p-type MOSFET and an n-channel JFET is designed, constructed and tested. These proposed systems constitute two wired buffer amplifier with a constant current source biasing. The active element of the system and the biasing passive components (R and C `s) resides at the top of electrode material. The current source and voltage output are placed in the bioelectric amplifier section. A circular Carbon rod of 8 mm and height of 5 mm is used as electrode material, which is connected to the Gate of the MOSFET / JFET through a capacitor and the Gate biasing resistors. The following sections describe the design of these two-wired buffer circuits as well as the simulation and test procedure.

5.3.1 Two-wired Buffer Amplifier Using P-MOSFET

A p-channel enhanced mode MOSFET (BSS84P) is configured as voltage follower or source follower with proposed modification for two-wired interface and Gate biasing. Figure 5.1 shows the circuit schematic. Vin is the input from the electrode on which this circuit is mounted. The current source shown is within the main amplifier circuit from which only two wires need to connect to the S and D nodes shown in this circuit corresponding to the source and drain respectively of the MOSFET.

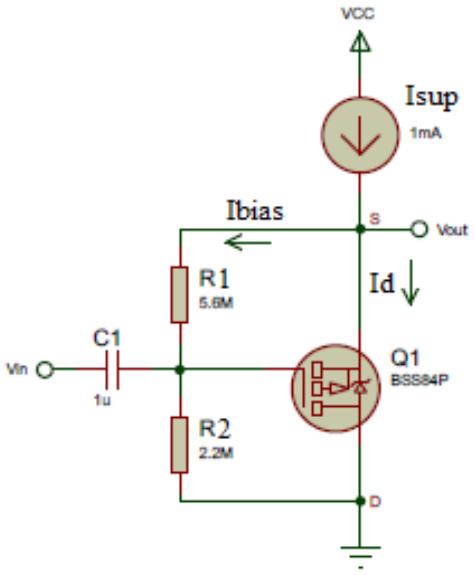

Figure 5.1: Self-biased Two wired buffer circuit using P-channel MOSFET

The proposed system differs from the usual P-MOSFET source follower that it omits the source resistor between the node *S* and Source of MOSFET, as this resistor does not permit for a two wire configuration. The proposed system uses a current source instead, which is a major innovation of the proposed circuit.

In the proposed circuit (Figure 5.1) the current I_{sup}, about 1mA, is divided into the two branches according to the resistances of parallel circuits formed by $R1; R2$ and Source to Drain of the MOSFET (KCL) i.e., $I_{sup} = I_{bias} + I_{SD}$. The branch current I_{bias} develops the biasing voltage of the Gate and I_{SD} determines the operating point (Q_{point}) of the MOSFET. Here, the values of the bias resistors are high, in the Mega ohms range; therefore, I_{bias} will be a few µA while I_{SD} will have almost all of the I_{sup}, which will be of the order of a mA. Therefore, I_{SD} will be almost equal to I_{sup} and may be assumed constant for all practical purposes. When there is no input signal, I_{bias} is also constant, therefore, the Gate bias voltage (V_G) is constant. It only varies when there is an input signal. On the other hand I_{SD} is constant, i.e. it cannot change, so the Source to Drain voltage V_{SD} changes with the varying voltage V_G with a unity gain.

The MOSFET needs to operate in the Saturation or Active region. The criteria for reach the saturation region are,

$$V_{SG} > |V_T| \text{ and } V_{SD} > V_{SG} - |V_T| \tag{5.3}$$

The Drain current of the enhanced P-Channel MOSFET can be expressed as,

$$I_{SD} = \frac{1}{2}\mu_p C_{ox} \frac{W}{L}(V_{SG} - |V_T|)^2 \tag{5.4}$$

Where, V_t is the Gate threshold voltage, μ_p , C_{ox} are charge-carrier effective mobility and gate oxide capacitance per unit area respectively and W, L are gate width and length. In the equation 5.4 the term containing channel-length modulation parameter λ is ignored as it is very close to zero and the I_{SD} does not need to be precise for this application.

Though current source is used, the supply voltage is finite, and therefore the output bias voltage is required to set approximately halfway between the V_{CC} and *Ground*, to obtain the maximum output dynamic range. The maximum output voltage is $V_{CC} - V_{SDsat}$.

As the circuit is a voltage follower, the bias voltage can be expressed as,

$$V_G = V_{SG} + V_{out} \tag{5.5}$$

The Q point I_{SD} can be chosen by the half of its maximum allowed range and with the help of equations 5.3, 5.4 & 5.5 a suitable operating point and component selection can be obtained.

From the small signal analysis, it can be shown that the gain of the source follower can be expressed as,

$$A = \frac{V_{out}}{V_{in}} = \frac{g_m(r_{oc}||r_o)}{1+g_m(r_{oc}||r_o)} \approx 1 \tag{5.6}$$

As $g_m(r_{oc}||r_o) \gg 1$, r_{oc} is the output impedance of the current source, and the trans-conductance g_m, is given by,

$$g_m = \frac{2I_{SD}}{V_{SG}-|V_T|} \tag{5.7}$$

The Drain Source output impedance of the MOSFET r_o is given by,

$$r_o = \frac{1+\lambda V_{SD}}{\lambda I_{SD}} \tag{5.8}$$

The input impedance of the buffer circuit is just the parallel combination of R1 and R2, i.e.,

$$R_i = \frac{R1R2}{R1+R2} \tag{5.9}$$

And the output impedance is,

$$R_o = \frac{1}{g_m}(r_{oc}||r_o) \approx \frac{1}{g_m} \tag{5.10}$$

The r_o is very small compared to the large trans-conductance g_m, and $g_m$increases with the Source to Drain current I_{SD}(Eqn. 5.7). Therefore, the output impedance decreases with increased I_{SD}(by Eqn. 5.7 and 5.10). To have output close to unity and with low impedance, it is desirable to set I_{SD} as large as possible.

It is good to note that the operating output bias voltage is non zero, and as this voltage is almost same for both the active electrode circuit connected to differential inputs, it is cancelled out. If there is a mismatch between these potentials, the AC coupling method by the DC restoration circuit (as described in Chapter 2) of bioelectric amplifier should be suffice to overcome this.

5.3.2 Two-wired Buffer Amplifier Using N-Channel JFET

The circuit configuration and working principle of the proposed n-channel JFET voltage follower for two-wired active electrode is similar to that of P-Channel MOSFET described in section 5.3.1. The necessary biasing is achieved by the Gate resistor R_G and Source resistor R_S, as shown in Figure 5.2. In this design, a small source resistor is used only for the purpose of producing higher potential at the Source than the Gate of JFET, which is necessary for biasing and selecting an appropriate operating point of the active component. The output is taken from the current source node *S* rather than the conventional method of to take it from Source of JFET. Again, it is a major innovation of the proposed circuit. It is assumed that the V_{out} will be less affected by this small resistance of R_S as the output resistance of the current source is very high. Furthermore, the

Gate impedance of the JFET is very high. Therefore, it is also assumed that a very small and negligible DC biasing current would be flowing through R_G compared to the Drain to Source current I_{DS} in a similar manner described in section 5.3.1.

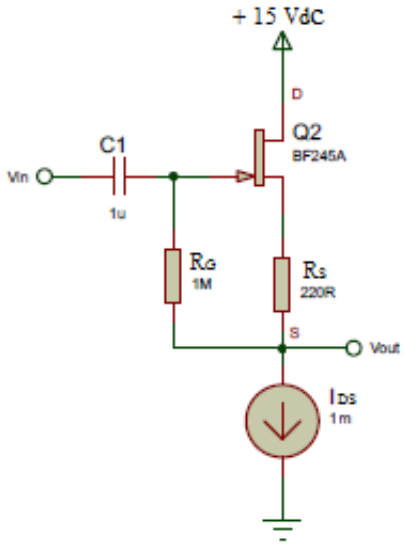

Figure 5.2: Self-biased Two wired buffer circuit using N-channel JFET

The biasing voltage is given by,

$$V_{GS} = V_G - V_S \rightarrow V_{GS} = V_G - I_{DS}R_s \tag{5.11}$$

Since, current through R_G is very small, only arising due to leakage of Drain to Gate current, the voltage across R_G is considered to be zero. As the voltage across both the resistors R_G and R_S is referenced to the common node *S*, the gate to source voltage can be written as,

$$V_{GS} = -I_{DS}R_s \tag{5.12}$$

This equation provides the operating bias condition. Also, the drain to source current is given by,

$$I_{DS} = I_{DSS}(1 - \frac{V_{GS}}{V_C})^2 \tag{5.12}$$

Where, I_{DSS} is the Drain to Source saturation current when $V_{GS} = 0$, and $V_C$is the pinch-off voltage. The transconductance is given by,

$$g_m = -2\frac{I_{DSS}}{V_C}(1 - \frac{V_{GS}}{V_C})^2 \quad (5.12)$$

From small signal model, it can be shown that the gain of the buffer circuit is,

$$A = \frac{g_m(r_{oc}||R_S)}{1+g_m(r_{oc}||R_S)} \approx 1 \quad (5.13)$$

Assuming that $g_m(r_{oc}||R_s) \gg 1$, where r_{oc} is the impedance of the current source, which is very large compared to R_s and provides almost unity feedback to the lower end of the R_G(which supports the idea of taking voltage output V_{out} at the node *S*), creating an increased input impedance as,

$$R_i = R_G + r_{oc} \quad (5.14)$$

And the output impedance can be expressed as,

$$R_o = \frac{r_{oc}||R_S}{1+g_m(r_{oc}||R_S)} \approx \frac{1}{g_m} \quad (5.16)$$

Which is very small, again assuming that, $g_m(r_{oc}||R_s) \gg 1$.

Using the above equations, the JFET can be biased to an optimum operating point, where R_s is minimized and g_m is maximized, and thus constructing a unity gain voltage follower with very low output and very high input impedance.

Similar to the MOSFET voltage follower circuit, this JFET based circuit also has an operating DC bias voltage at the output as well, and it is ineffective at the bioelectric amplifier as mentioned in section 5.3.1.

5.3.3 Constant Current Source and Sink Using MOSFET

The proposed voltage follower buffers circuits that are described in section 5.3.1 and 5.3.2 requires constant current sink and source for desired operation. These two constant current circuits are constructed using conventional dual MOSFET methods as shown in Figure 5.3. These constant current topologies are simple to implement and produces excellent stable DC constant current.

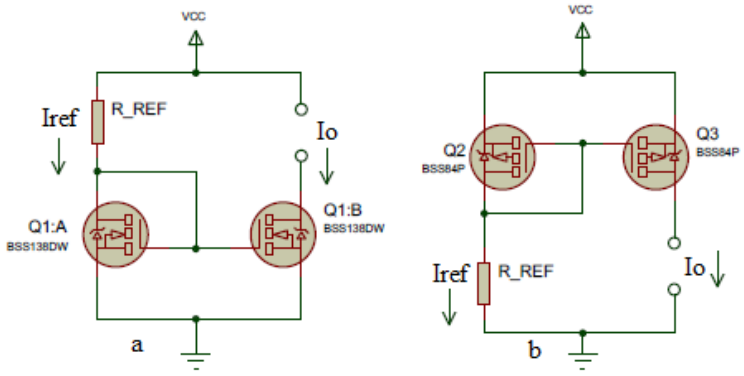

Figure 5.3: Constant Current Sink (a) and Source (b) circuit using N and P-channel MOSFET

Considering current sink circuit in Figure 5.3a, similar to Eqn. 5.4, assuming λ to be zero, the Drain to source current of Q1:A is given by,

$$I_{ref} = \frac{1}{2}\mu_p C_{ox}\frac{W}{L}(V_{GS} - V_T)^2 \tag{5.17}$$

Then the Gate to Source voltage is,

$$V_{GS} = Vcc - R_{REF}I_{ref} \tag{5.18}$$

This Gate to Source voltage is same for Q1:B. Therefore, if the two transistors (Q1:A and Q1:B) have identical physical parameters i.e. $\mu_p C_{ox}\frac{W}{L}$ and V_T are equal, then using Eqn. 5.17, the output current can be expressed as,

$$I_o \approx I_{ref} \tag{5.19}$$

For the current source circuit using P-channel MOSFET as shown in Figure 5.3b, similar analysis can be done with the same result.

5.3.4 Experimental Procedure

Each circuit, including the constant current source and sink is first designed and simulated using the simulation and design software Proteus. Then these circuits are practically constructed and tested.

For testing purpose, at first, the constructed buffer circuits are tested as single ended input /output formation using just a signal generator and an oscilloscope. Then a network of three series resistors of 10 kΩ is connected to a signal generator as shown in Figure 5.4. The differential input of a single channel bioelectric amplifier (described in chapter 2) is connected across $R2$ using (i) 10 cm wire, and then (ii) 1 meter long commercially available EEG cable with Ag-AgCl cup electrode. The cup of the electrodes was connected using crocodile clips. These connections are configurable as with and without the proposed active electrode circuits by means of two manual switches as shown in Figure 5.4. This configuration provides the comparison of output from the bioelectric amplifier produced by employing and not employing the proposed active electrodes in practical situation. The purpose of the varying length of connecting cable was to study the effect of interfering current on the cable length as well. It is expected that the longer cable will induce more capacitance and therefore will result in more interfering currents as described in section 5.1.

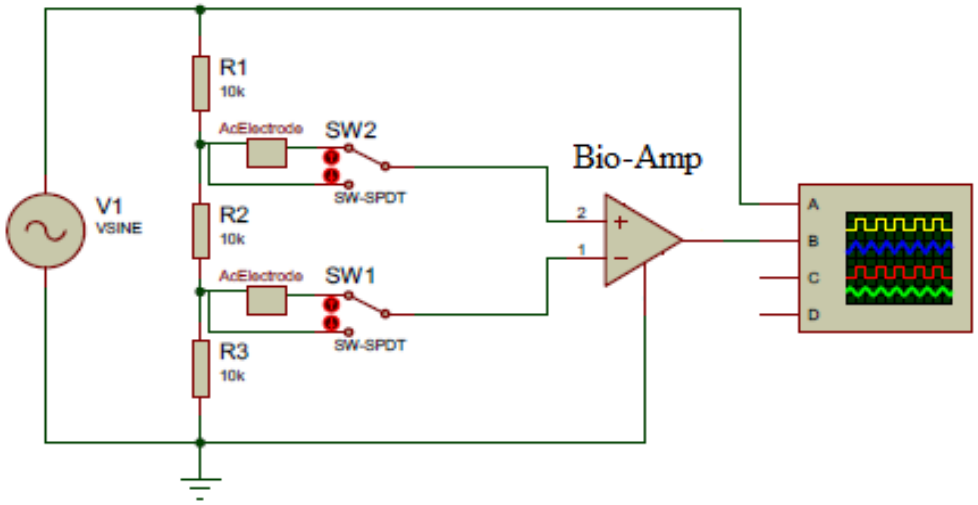

Figure 5.4: Experimental Setup to Evaluate the Performances of Active Electrodes

The signal from the signal generator was approximately 2.5 mV peak to peak and the frequency was 10 Hz. The 2.5 mV peak to peak input signal was the least signal output that can be measured directly by the oscilloscope used. The values of the resistor network were chosen to be of the order of normal skin-electrode contact impedance in practical situation. This creates an input signal to the bioelectric amplifier with much larger amplitude (833 μV) than the maximum input signal that can be amplified by the all four stages (linear gain of 100000 x 833 μV = 83.3 V). So, output of the bioelectric amplifier was taken from the third stage. This third stage output of the bioelectric amplifier produces a linear gain of 9099 which will produce 7.58 volts peak to peak at the output. This gain is selected to meet the output dynamic range of the amplifier (10 V p-p) corresponding to the input signal that is produced by the resistor network along with the signal generator. The interference of 50 Hz power line was left to the measuring environment.

Finally, output from the amplifier is observed and signal to noise ratio is measured for with and without the two active voltage follower circuits, which are connected closely to the two ends of $R2$.

5.4 Result and Observations

The simulated and measured results of the both P-Channel MOSFET and N-Channel JFET were identical; therefore, results of the simulated part of the MOSFET, and experimental part of the JFET are presented here.

Figure 5.5 shows the simulated input and output of the proposed MOSFET source follower (the one to be used in the active electrode circuit), showing the result of the buffering action and Figure 5.6 shows the frequency response over a range of frequencies, 0.01 Hz to 10 kHz. The amplitude of input and output voltage is same with 300 μV peak. The frequency response is well within the expected characteristics, which shows 10 dB attenuation at 0.01 Hz and a flat 0 dB output for 1 to 10 kHz, the cutoff frequency (-3dB) being about 0.04Hz.

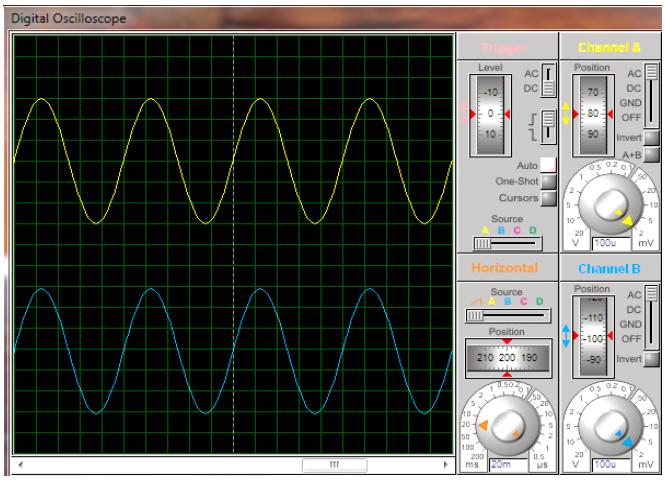

Figure 5.5: Simulated Input(Bottom) Output(Top) of P-Channel MOSFET Active Electrode

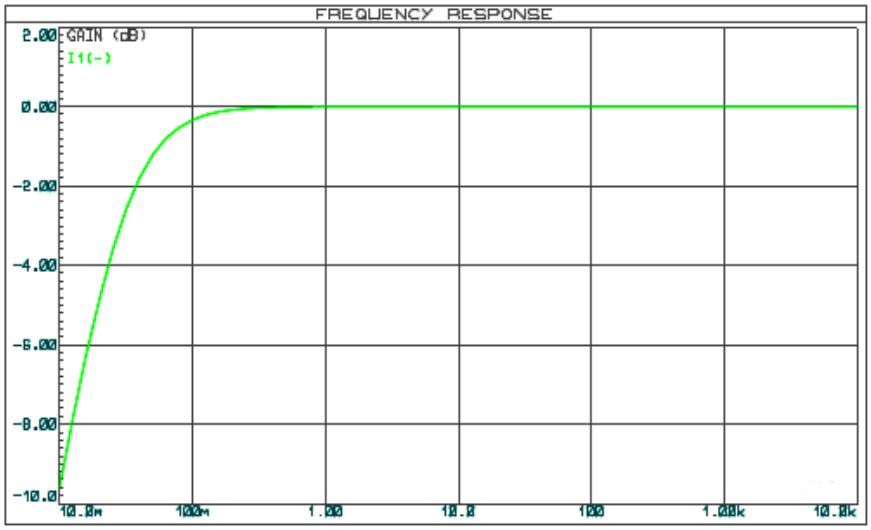

Figure 5.6: Simulated Frequency Response of P-Channel MOSFET Active Electrode

Figure 5.7, shows the voltage input and output of N-Channel JFET source follower circuit in practical measurement. The applied input voltage is 400 mV with a 10 Hz signal (bottom trace), whereas the output voltage is 388 mV peak to peak (top trace). This indicates a decent voltage follower with output being 97 % of the input voltage.

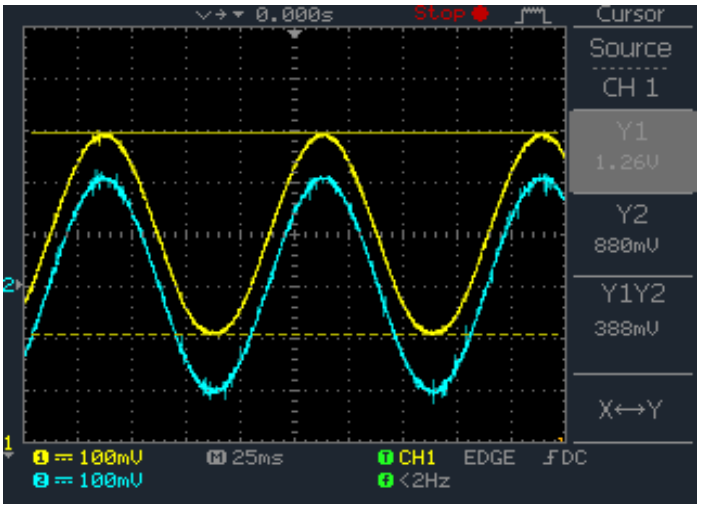

Figure 5.7: Experimental Result of Input (Bottom) Output (Top) of N-Channel JFET Active Electrode

It is interesting to observe that the output signal has less noise compared to the input signal; this is not the action of the high-pass RC input filter as the noise seems to be of high frequency. Probable cause of this high noise at the input is the high input impedance characteristics of the buffer, the noise being induced from the oscilloscope probe. On the other hand the output of the buffer has low impedance. So noised induced by the oscilloscope probe was low.

Figure 5.8 shows the signal of amplitude ~ 2.5 mV peak to peak, that is applied to the two ends of the resistor network by the signal generator as described in Figure 5.4. The differential input

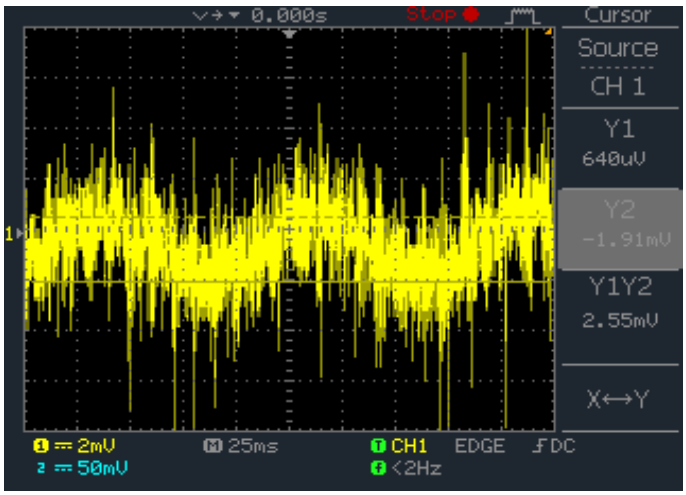

Figure 5.8: Experimental View of the Input Signal of Resistor Network from the Experimental Setup

to the bioelectric amplifier is the potential that is dropped across the central resistor, R_2, with the ground as shown, at the other end of R_3. With 2.5mV across the whole resistor chain, the differential input would be one third of this, i.e., 833.33µV since all the three resistors have the same value (10k). The output of the bioelectric amplifier, with a gain of 9099, was observed and measured using a digital oscilloscope. The inputs to the bioelectric amplifier were obtained first without any buffers at the input (i.e., inputs taken right across R_2 of the chain) but connected with 10cm long unshielded wires each. The corresponding output is shown in Figure 5.9. With the amplifier gain as mentioned above, and with the 833.33 µV peak to peak differential input voltage, the output was expected to be 7.58 volts peak to peak. However, the measured output was 7.03 volt, which is less than the calculated value. This is probably due to the tolerance of the resistors in the network and error in input voltage measurement as it is very noisy.

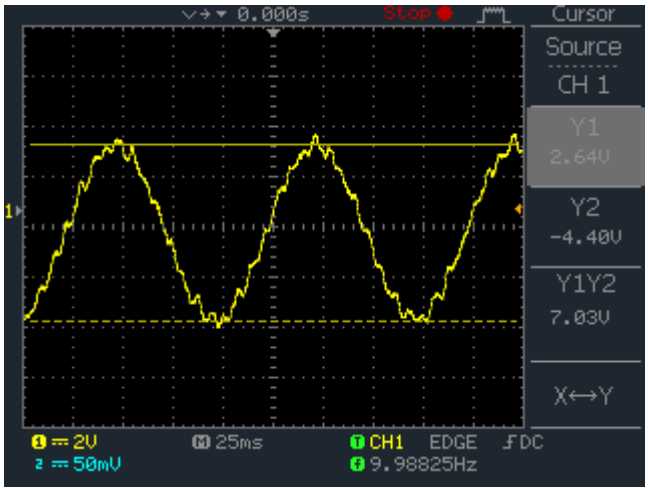

Figure 5.9: Experimental Result of Output Signal of Bioelectric Amplifier with 10cm Connecting Wire and no Buffer Used

From Figure 5.9, the measured noise figure is ~ 0.8 volts peak to peak which results in a Signal to Noise Ratio (SNR) of 8.75. The output obtained with the buffers connected at the inputs (simulating active electrodes) is shown in Figure 5.10. The output of the buffer amplifiers were connected to the respective inputs of the bioelectric amplifier as before, using 10 cm long wires each. The output is very similar to Figure 5.9 but with slightly improved noise figure of ~ 0.64 volts, which results in an SNR of 10.8.

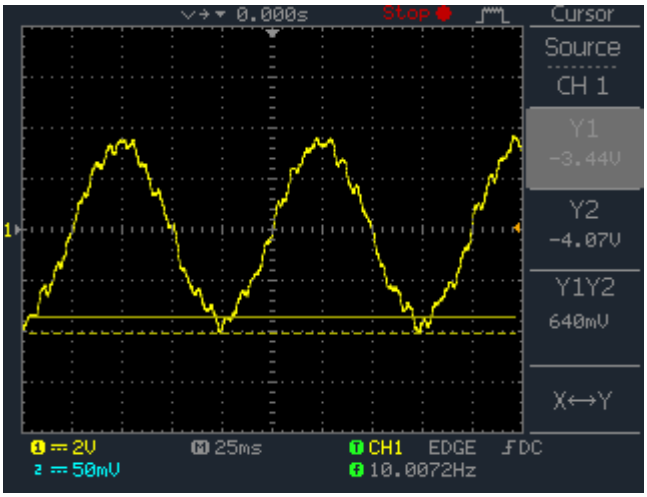

Figure 5.10: Experimental Result of Output Signal of Bioelectric Amplifier with 10cm connecting wire at the inputs connected to the outputs of the respective Buffer Circuits simulating active electrodes.

Figure 5.11 shows the case when a pair of one meter long standard EEG cables was used to connect the inputs of the bioelectric amplifier to the points across R_2 in Figure 5.4, without the buffer circuits. As expected, the 50 Hz line interference is very large, approximately 6.3 volt peak to peak. This results in an SNR of 1.12 (which was the worst case of all the measurements, therefore the experiment was conducted several time).

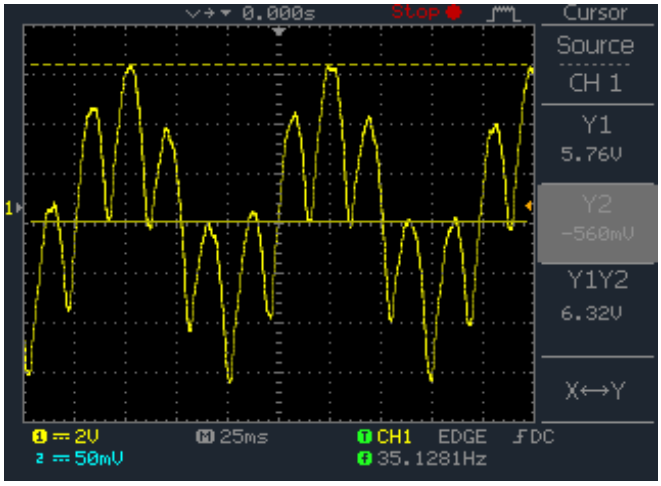

Figure 5.11: Experimental Result of Output Signal of Bioelectric Amplifier with 1 m Standard EEG Cable and with NO Buffer Connected

Finally, Figure 5.12 shows the case when the one meter standard EEG cables were connected to the outputs of the JFET buffer circuits. The result shows that there is a substantial amount of noise reduction. The measured noise figure is ~ 0.72 volts peak to peak, which makes the SNR to be 9.76, very close to the 10 cm wire with buffer connected case.

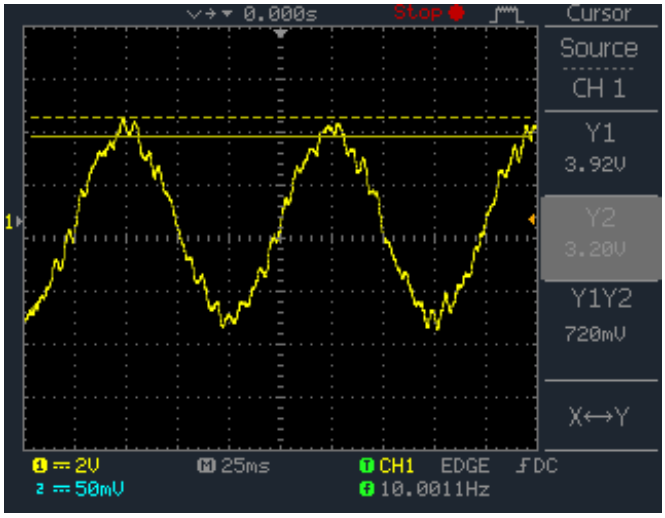

Figure 5.12: Experimental Result of Output Signal of Bioelectric Amplifier with Buffer Circuits and 1 m long standard EEG Cable Connected at input

A length of cable that connects the inputs of the bioelectric amplifier to the differential outputs produced by the resistor chain in Figure 5.4 forms a stray capacitance with the adjacent mains 50Hz lines. This allows a 50Hz current to flow through this capacitor and the appropriate segment of the resistor chain to the ground. Since the other side of the lead is connected to a high impedance input of the bioelectric amplifier, virtually no current flows through this side. The current through the resistor chain to the ground produces an interfering voltage across the segment of the resistor chain. In this case, the current through the lead at the non-inverting input goes through R_2 and R_3, a total of 20kΩ, while that through the lead at the inverting input goes only through R_3, a value of 10kΩ. Typically, the reactance of the capacitor at 50Hz is much larger than 10kΩ. Therefore, the interfering currents produced in the leads are approximately equal if the leads are of the same length and are close to each other and a differential voltage at 50Hz is produced because of the voltage dropped across R_2 only. Again, a longer cable has

larger capacitance and induces more interfering currents. This produced the high interfering noise at 50Hz for the 1m leads when there was no buffer at input, while it was much less with the 10cm leads.

With the buffer circuits placed close to the two inputs across R_2, the outputs of these buffers are connected to the inputs of the bioelectric amplifier through the leads (10cm and 1m). Now the 50Hz currents passing through the capacitances formed by these leads pass through the low output impedances of the buffer circuits to the ground and therefore the potential dropped across the resistors are very small. Therefore, the effective differential input due to 50Hz is very small, which gives the resulting improvement. Therefore, with the buffer circuits in place, the noise with the 10cm leads and the 1m leads were not much different, while without the buffer circuits, the difference was huge.

When connected to the human body, the situation would be slightly different. The differential signal to be measured originates inside the body and the internal impedance of the body is very low compared to the skin-electrode contact impedances. Therefore, the high impedance of concern will be these contact impedances. Because of the lead wire capacitance, the current through the skin-contact impedances will contribute to a differential contribution of the 50Hz noise if the contact impedances are not equal. In practice, these contact impedances may vary widely, by about 10kΩ as mentioned before, and a large noise is experienced frequently in practice. Use of the buffer amplifiers very close to the electrodes will reduce the effect of the capacitive 50Hz current as in the experimental case mentioned above.

There will also be a large capacitance between the 50Hz line and the human body and a 50Hz current will flow through the skin-contact impedance of the contact impedance of the ground electrode. This will contribute to a large common mode voltage and due to limited CMRR of the bioelectric amplifier there will be some 50Hz noise at the output too. This will be the same in both the cases, with or without on-electrode buffer circuits, and therefore, care has to be taken to ensure a low skin-electrode impedance of the ground electrode through careful cleaning and the use of a large electrode.

5.5 Novelty

The designed two-wired active electrode circuits are self-biased; therefore it has more stability. The proposed biasing is not affected by the skin-electrode contact potential and requires no average body potential biasing technique. Also it is usable in any bioelectric amplifier with or without Driven Right Leg (DRL) circuits. The DRL circuit is mandatory for other designs of two wired buffered electrode system for biasing purpose, while it is not so in the present design. The JFET model of the active electrode has very high input impedance as the unity gain feedback is provided at the gate resistor lower end, resulting in a very satisfactory performance.

The inputs of active electrodes are AC coupled by an RC network. The capacitor at the input establishes electrical isolation of the subject and therefore safety as well. Also, as the input of the buffer electrode is AC coupled by this RC circuit, the skin-electrode contact potential is not transferred to the output of the buffer. This allows the bioelectric amplifiers to have large gain at the differential stage for the system which does not uses RC high pass at the input of instrumentation amplifier. Furthermore, the capacitance of the electrode circuit (situated on top of the electrode material) and the mains power line is very small. Therefore, interfering current that passes this RC network is almost nullified, so, the RC components are not required to be matched very closely to minimize the 'Potential Divider Effect'.

The development of this 'self-biased low-noise two-wired active buffer electrode' is an original research contribution. Up to the time of writing this thesis and to the author`s best knowledge, no other system has reported to have similar performance and functionality.

Chapter 6 : A Individual Skin-Electrode Contact Impedance Measurement System

6.1 Background

The interfering noise in a bioelectric signal measurement system extensively depends on the skin-electrode impedance. The contact impedance of common or circuit ground electrode Z_{rl} gives rise to the total common mode voltage (as shown in Figure 4.1 in chapter 4). Also, if there is a contact impedance mismatch between two measuring electrodes that are connected to the inverting and non-inverting input of an instrumentation amplifier, the mismatch converts the common mode voltage to differential voltage by the effect known as 'Potential divider effect' as described in chapter 5 and also illustrated in Figure 4.1. This mismatch is very common and difficult to avoid. The interfering currents flowing to impedance Z_{rl} induces common mode voltage and larger value of this contact impedance means larger interference. Moreover, large value of contact impedance of measuring electrodes produces larger mismatch resulting increased conversion of common mode voltage to differential voltage and increased interference. The reduction of common mode voltage is essential; therefore it is desirable to reduce these skin-electrode contact impedances as much as possible.

The skin-electrode contact impedances can be reduced by proper cleaning and preparation of the skin at the electrode attachment location. It is, therefore necessary to measure and monitor the skin-electrode contact impedance to reduce it as much as possible and to achieve a viable bioelectric signal recording. For example it can be shown that, for an EEG recording system, considering other interference reduction measures are taken, the contact impedance of the electrodes needs to be less than 10 kΩ in order to have an acceptable Signal to Noise Ratio (SNR) in the EEG trace (Brown, 1999).

There are many existing proposed methods to measure and monitor the skin-electrode impedance. One of these methods injects a small amount of current through the reference electrode and measures the individual contact impedances of the other electrodes (Hamilton et al., 2000; & Devlin et al, 1984). These measurement techniques are two electrodes impedance measurement system and actually always measure the reference electrode impedance in series

with the measuring electrode. Another method uses the DRL circuit to superimpose a known voltage and then measures the mismatch between two electrodes (Degen et al., 2008). This method also claims that it can be used simultaneously with bioelectric signal measurement. However, this method does not address the requirement of measuring contact impedance of individual electrodes and the impedance of the common or circuit ground electrode. There are other methods like utilizing the mains power line interfering current to measure the contact impedance, one of which measures the mismatch between two electrodes (Spinelli et al., 2006), but it effectively reduces the input impedance of the bioelectric amplifier and therefore degrades the CMRR. Also, in this method it is unclear how the system would work in a multi-channel amplifier. Another similar method measures individual contact impedances by power line interference current but requires an additional electrode to inject a small DC current to measure voltage across measuring electrode (Grimbergen et al., 1992). In this method, it would be convenient to use the common or circuit ground electrode as the current injecting electrode, so no additional electrode is required, but in that case, the impedance measurement of the common electrode is not possible. In fact, all the above and other similar methods do not discuss the matter of measuring contact impedance of the common electrode, but it is very important to lower the contact impedance of the common or circuit ground electrode Z_{rl}, as it is the major contributor of the common mode voltage.

6.2 Problem Statement

Since, the skin-electrode contact impedance is a major factor of power line interference that impacts the quality of bio-signal output of bioelectric amplifier, it is necessary to measure and monitor it. Though, the common or circuit ground electrode contact impedance Z_{rl} can be greatly reduced by Driven Right Leg (DRL) system (chapter 4), it is desirable to reduce it at the source to avoid unpredictable and unstable behaviour of the DRL system. Although it is possible to make the impedance mismatch of the measuring electrodes ineffective using active electrode, it is always preferable to reduce the contact impedance, as noise generated in the skin-electrode interface increases with the impedance which can be unacceptable in cases like EEG recordings (Brown, 1999). Furthermore, as this impedance appears as the source impedance for bioelectric signals, reducing it makes the signal more robust.

The contact impedance measurement system can indicate an unattached electrode as well. This is necessary for a BCI system that is intended to work for long time. Also to overcome the problems as discussed above, it is desirable to develop a skin-electrode contact impedance measurement system for a multichannel bioelectric amplifier, which is capable of effectively measure contact impedance of each electrode individually including the common or circuit ground electrode. Due to required wearable feature of the overall system, the impedance measurement circuit needs to be constructed of low parts count for low power and small size. The following sections describe the development of such a skin-electrode contact impedance measurement system.

6.3 Method

The proposed system employs a three electrode contact impedance measurement method (Spach et al., 1966) as shown in Figure 6.1 to measure a single electrode`s contact impedance. A very small known sinusoidal current of constant peak amplitude is passed to the subject's body through electrode *A* and *B*, and a high impedance differential amplifier is used to measure the potential between *B* and *C*.

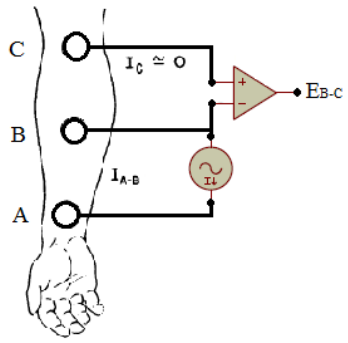

Figure 6.1: Three Electrode Contact Impedance Measurement Method

Here, the impedance to be measured is that of electrode *B*. Since, electrode *C* is connected to the amplifier with a high input impedance; there is no current passing through it and its contact impedance does not affect the measurement (potential across this contact impedance is almost zero). Since the bulk of the body has a very low impedance (usually a few hundred ohms) in comparison to the skin-electrode impedance (a few kilo ohms), the measured potential

essentially represents the potential dropped across the contact impedance at electrode *B* due to the constant current passing through it. From the values of the constant current and the gain of the amplifier, it is easy to calculate the skin-electrode impedance at B.

In the proposed system, the instrumentation amplifiers (INA) of the Analog Front End (AFE) is used as the high input impedance amplifier and the gain of the amplifiers are accounted for the calculation of impedance measurement. This technique results in a reduced part count where only an additional analog switch and a sinusoidal current source is required to construct and integrate the system with bio-electric amplifier. This is the core feature of the proposed contact impedance measurement system along with individual electrode impedance measurement capability. The analog switch (two quad bilateral switches, 4066) is used to configure the current injection and voltage measurement arrangements of the system. Specific arrangements or configuration of these switches allows to measure each electrode`s contact impedance individually. The control of these analog switches will be achieved by the digital control of the data acquisition system (described in the next chapter). Figure 6.2 shows the individual skin-electrode measurement circuit where the INA`s belongs to the bioelectric amplifier circuit.

The sinusoidal current source generates a current of constant amplitude 10 nA with a frequency of 33 Hz. This peak current amplitude is selected to ensure subject safety and to effectively measuring impedance of 1kΩ to 100 kΩ as well. Though, the interested frequency of measurement would be power line frequency (50 Hz), the frequency is selected to be 33 Hz as power line interfering current can introduce error in the measurement through super-positioning. This sinusoidal current frequency is well below of 50 Hz and can easily be filtered of other susceptible interfering noise.

The current source is constructed in two parts, firs a RC phase-shift sinusoidal oscillator is designed to produce a voltage signal of 33 Hz, then a Howland current source is employed to convert this voltage signal to current signal. As the system uses only one frequency, the RC phase-shift oscillator is selected for its known stability in a single frequency operation. The Howland current source is selected for its known ability of keeping the output current linear over a wide variation of voltage, which is suitable for this sinusoidal current source.

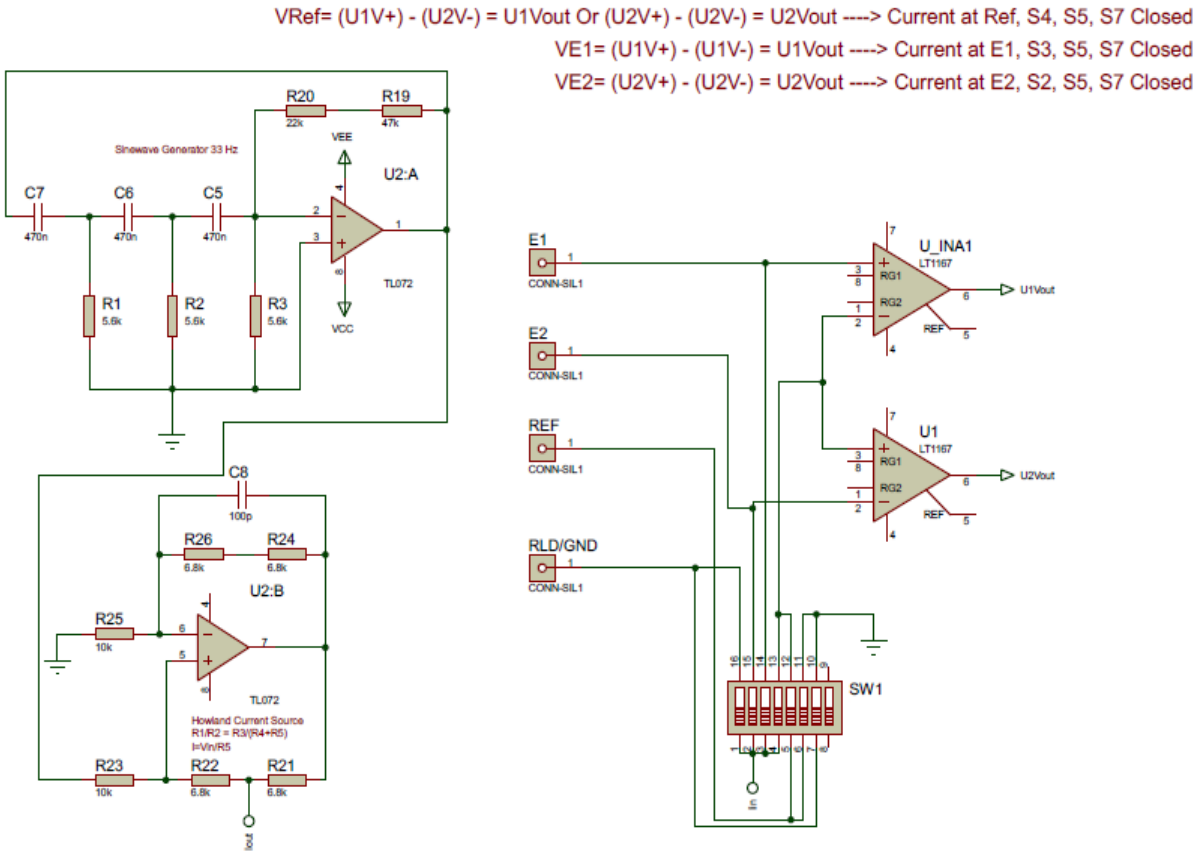

Figure 6.2: Skin-Electrode Contact Impedance Measurement System for a Multichannel Bioelectric amplifier.

The output voltages from the INA`s are digitised by a data acquisition system, then a narrow band-pass digital filter of 33 Hz is employed to cancel out all other signals. The impedance of each electrode is calculated by enabling appropriate channels of analog switch, and then the RMS values of the output signals is calculated. This RMS value is then divided by the known RMS value of the current signal which produces the contact impedance value of a particular electrode. These procedures are automated by computer software developed for the purpose.

The system is first tested and calibrated using known resistor of values from 1 kΩ to 100 kΩ with 1% tolerance, then measurement from several subjects is taken using common ECG limb electrodes and EEG cup type Ag-AgCl electrodes.

6.4 Result and Observation

The measured value of ECG limb electrode was around 20 kΩ and found to vary considerably form subject to subject. This variation is probably because of not applying rigorous skin preparation; therefore this result is well expected. The measurement of EEG cup electrode is also taken from limb but in this case skin was prepared with commercially available skin-prep material. The cup electrode measured values were 3 to 4 kΩ, these result were instantly checked with commercial EEG equipment (Carefusion Nicolet-3) and obtained similar result.

6.5 Novelty

There is always trade-off between continuous skin-electrode impedance measurement and individual measurement i.e. taking impedance measurement when bio-signal is not recording. The key trade-off factors are system complexity, bioelectric signal`s integrity, measurement efficiency etc. This proposed system uses the later choice to achieve less complex system with high efficacy. The system is light with very few components; it utilizes the instrumentation amplifiers in the bioelectric amplifier in different combinations of connections. The system can measure all the electrodes contact impedance including the common or circuit ground electrode individually. These are the novel part of the proposed system. The system is intended to use in wearable BCI system, controlled by a computer or a microcontroller, therefore, automated scheduled impedance measurement for a very short time can be as effective as continuous measurement.

Chapter 7 : Development of Miniature USB Based Data Acquisition System

7.1 Background

Computer based data acquisition system is an essential part of biomedical instrumentation and BCI systems. Most of the commercially available PC based Data Acquisition systems are of very high cost and requires specific commercial software, again at a very high cost, for data storage and analysis. Moreover, if the data is not stored in raw binary or known format, it is not possible for the user to use the data in other software of their own choice.

7.2 Problem Statement

Development of a low cost, simple and miniature USB interface based data acquisition system for BCI and biomedical application is necessary. As the system is intended for wearable system, it is required that the system should contain minimum number of parts.

The data acquisition system should have three major roles in this present work. Firstly, the acquired EEG data is required to transfer to the PC through USB. Then the data will be subjected to analysis and classification for developing a viable BCI system algorithm. Secondly, when an appropriate data classification method is selected, the data classification part of the BCI system can be ported to the on-board computer of the data acquisition system to have a standalone BCI system. The third function of the system is to provide digital control I/O for selecting channels of analog swathes for skin-electrode contact impedance measurement circuit. These digital I/O`s are also will be used for controlling other electromechanical devices according to the classified data.

7.3 Method

The hardware system is designed around a low cost 8-bit Atmel AVR ATmega8 (Atmel, 2014) microcontroller with integrated analog to digital converter (ADC). The associated circuitry needs only an isolation amplifier, which is used to achieve electrical isolation between the mains ac and bioelectrical signal source (human body) when the system is connected to PC (mains connected). This isolation is required for user safety and to reduce noise from the mains line by increasing Isolation Mode Rejection Ratio (IMRR) (Van Rijn et al., 1991b). Some optocouplers are used to

isolate digital I/O's for the same reason and a few passive components are used. This design reduced the cost and complexity very much. With reference to Figure 7.1, the analog bioelectric signal from the human body is first conditioned and transferred to the non-isolated PC side through the analogue isolation amplifier mentioned above. Then the signal is conditioned to meet the ADC input requirement. The signal is then converted to digital values using the on-board 10-bit ADC of the microcontroller. The digital data is then transferred to the PC through its USB port. Necessary USB interface (USBIF, 2014) was developed for this purpose, based on the same microcontroller.

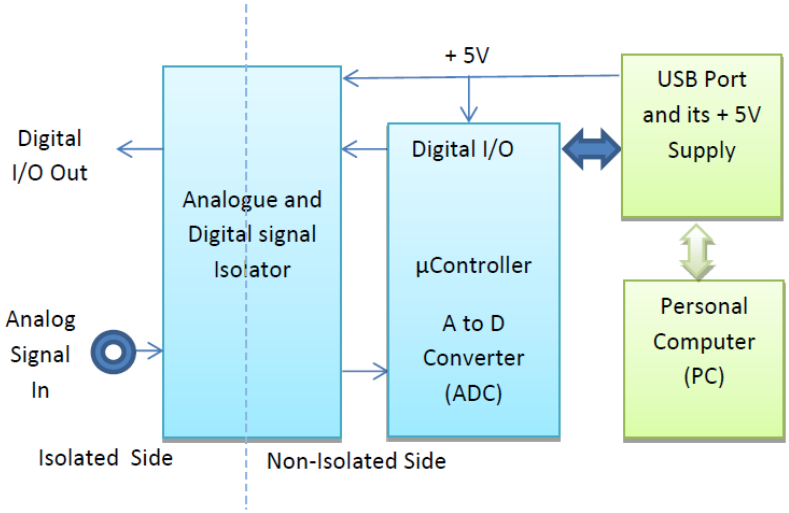

Figure 7.1: Block Diagram of Data Acquisition System

For powering the isolated circuitry in the isolated side, a medical grade isolated dc to dc converter is used; it uses the non-isolated +5 volt supply available from the USB port of the PC, and produces ±12 volt split power at the isolated side. Therefore no external battery or power supply is needed when the system is connected to PC. Figure 7.2 shows the circuit diagram of the Data Acquisition system.

The microcontroller has 10 bit successive approximation ADC module, it has two selectable internal references 5V and 2.56 V. The 2.56 V is used for this device for stability and higher voltage resolution of the bioelectric signal. After digitally converting the signal most significant 8 bits are used as the least significant two bits are more prone to noise. The 8 bits are kept also

for the reason that the byte wise data storage and transfer is more efficient. The 2.56 V reference of the ADC produces the resolution of 10 mV per bit for 8 bit conversion.

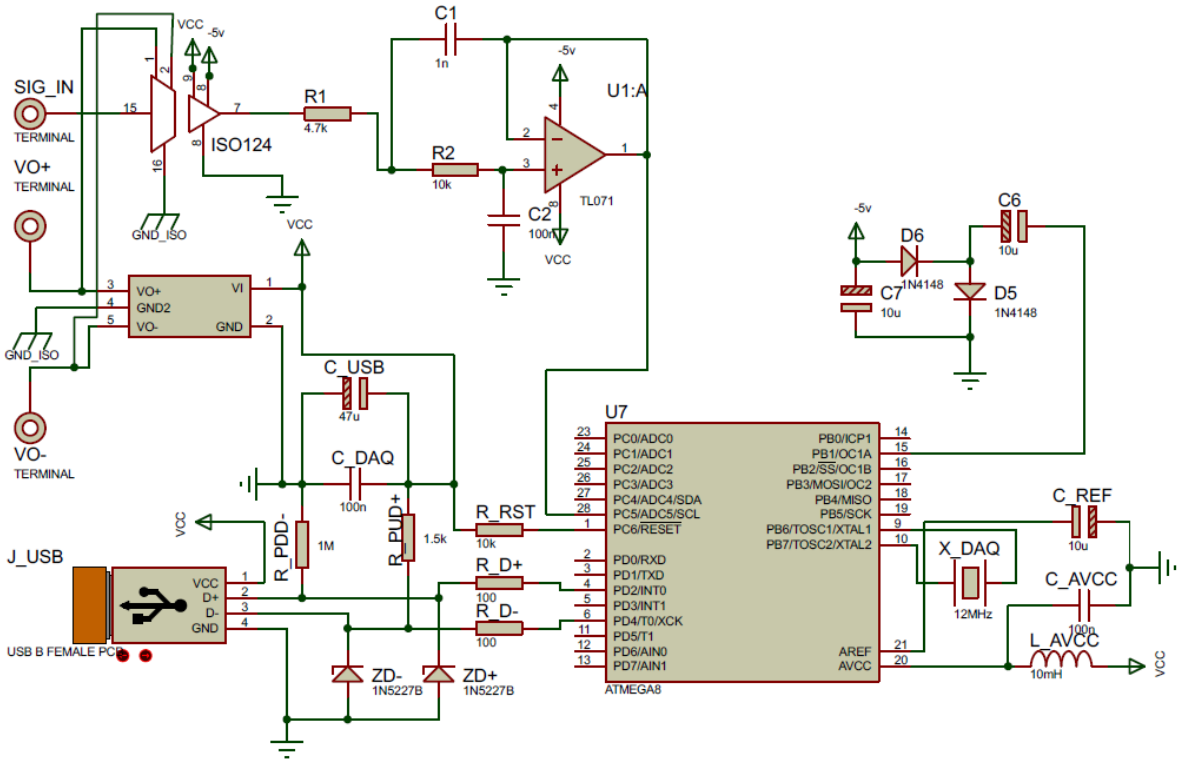

Figure 7.2: Circuit Diagram of Data Acquisition System

The device operates in two modes,

(i) *Continuous conversion and data transfer*: The sampling frequency is 800 Hz, it is selected to match the USB 1.1 periodic 'Interrupt In' timing and data transfer rate. This sampling rate is suitable for low frequency signals like ECG, EEG etc.

(ii) *Batch transfer*: The data can be sampled very fast, i.e. minimum of 13 µs per conversion (recommended minimum conversion time of the ADC module of the microcontroller) provides maximum of 76.9 KHz of sampling rate. The data is stored in a large SRAM space of 800 bytes in the microcontroller and then transferred periodically by USB 'Control In' transfer.

The Continuous conversion data is transferred by 'Interrupt In transfer' for graphical display and storage by the developed software. By specification this 'Interrupt In transfer' type has maximum of 8 bytes transfer every 10 ms. The USB host controller generates this timing and it is adopted as que for starting ADC conversion. So, at every 10 ms there are 8 bytes of data conversion takes place at equal interval of 1.25 ms (10/8 ms), resulting sample rate of 800 Hz. The 1.25 ms interval for analog data conversion is precisely generated using the 16 bit 'Timer 1' module of the microcontroller; this timing generates an interrupt to start ADC conversion at every 1.25 ms. The sampling and data transfer is done simultaneously and these are well synchronized. Thus form sampling to display has latency of 10 ms, which can be regarded as real time. The Flowchart of the Continuous mode firmware is shown in Figure 7.3.

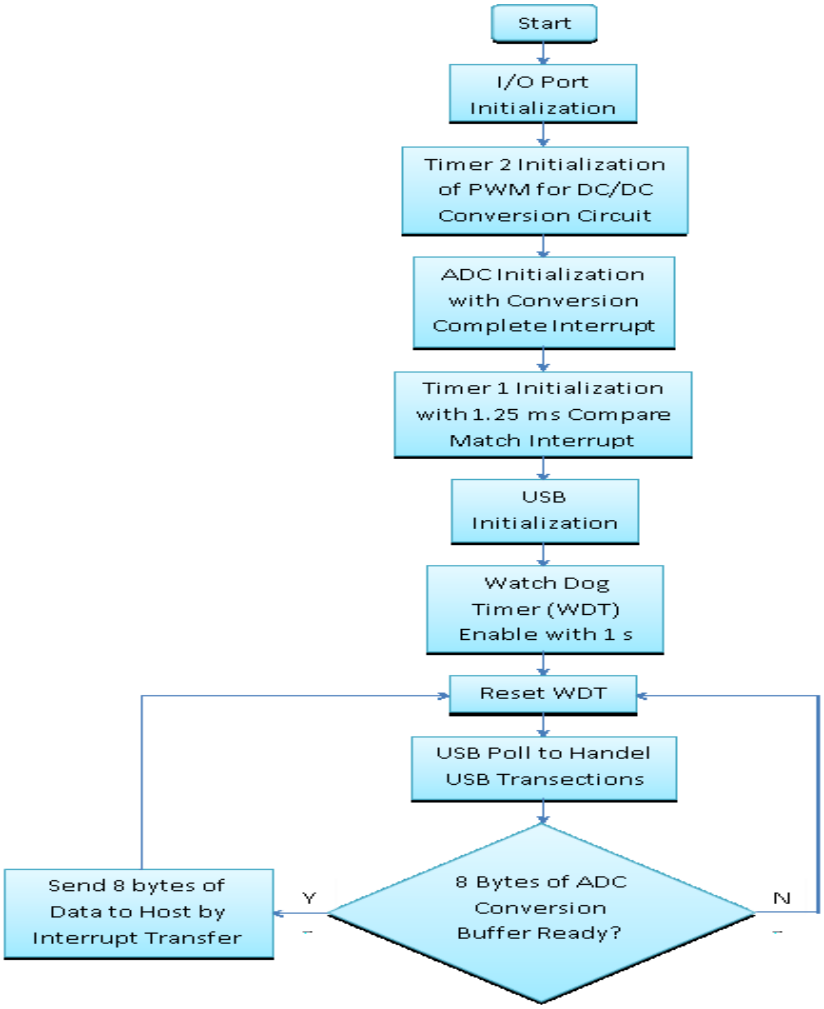

Figure 7.3: Continuous Conversion Flowchart

The Batch Transfer uses both ‘Interrupt In’ and ‘Control In’ transfer of the USB. The ‘Interrupt In’ transfer cannot provide data transfer rate more than 800 bytes/sec (max. 8 bytes per 10 ms) but has guaranteed time of 10 ms interval of each transfer. This timing is used as synchronization with PC software and start of conversion Que. The ‘Control In’ transfer can transfer large amount of data (maximum of 1.5 Mbit/sec, depending on the bus bandwidth availability) but its transfer timing is not guaranteed. This transfer is primarily specified for transferring device descriptors and other host control over USB, but it is not forbidden to use

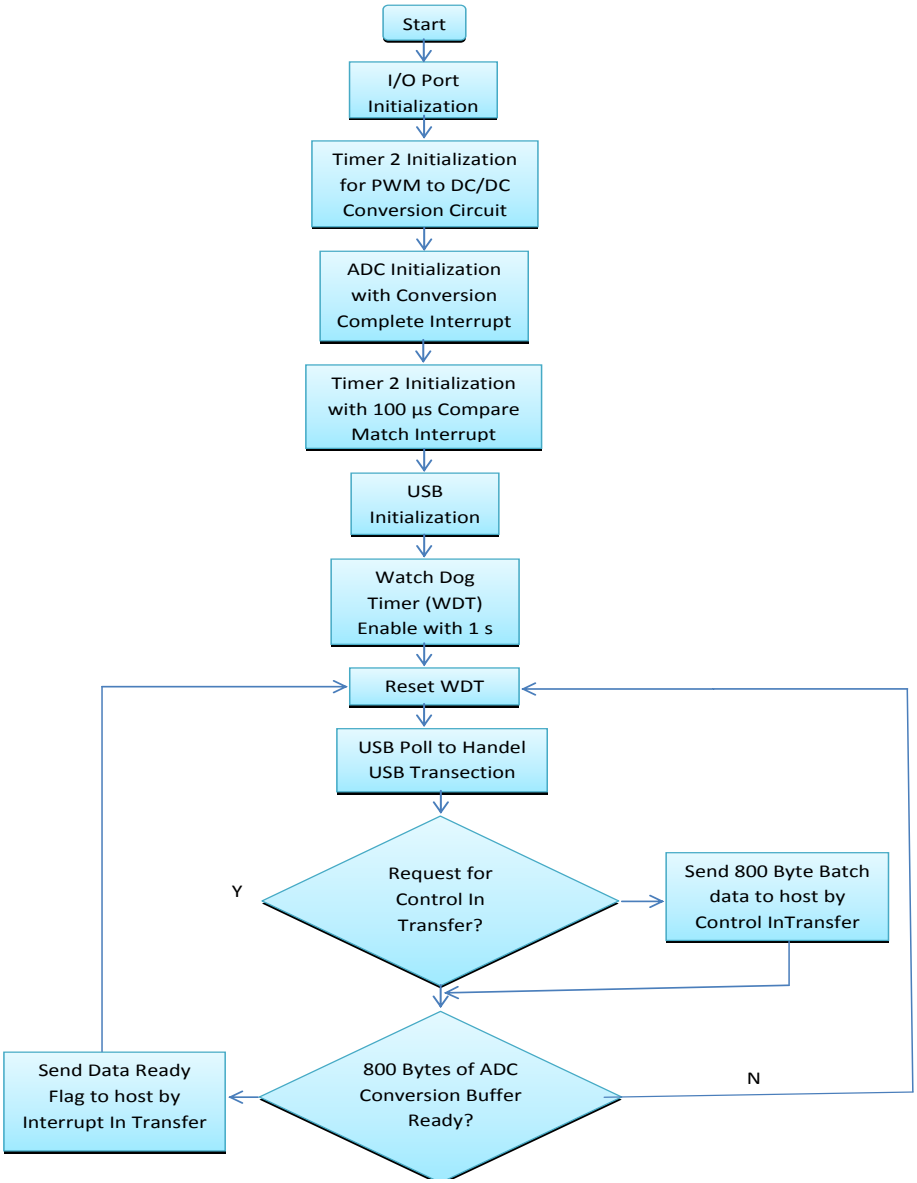

Figure 7.4: Batch Mode Conversion Flowchart

'Control In' for other data transfers in the USB specification. The ADC sampling interval is controlled in similar manner like the Continuous mode but now this interval can be as low as 13 µs. The software polls the device for acknowledge 800 bytes (this is the current microcontroller's maximum SRAM free space after other use) of batch data conversion accomplishment, every 10 ms through 'Interrupt In' transfer. If the data is available, the software initiates a 'Control In' transfer for the 800 bytes data. After transferring the batch data to PC, the 'Interrupt In' polling is used to initiate converting another batch of data.

Since the microcontroller is low cost and have no hardware USB stack, the USB library called V-USB (Objective D., 2011) of the firmware was used for implementation of USB 1.1 low speed standard protocol. The firmware for the microcontroller was developed using free GNU C compiler (WinAVR, 2014) with AVR Studio IDE (Atmel, 2014). The software is a graphical user interface which allows viewing the bioelectrical signal in selectable different time scale and can store data in raw binary format. It was developed using 'JAVA' platform considering its operating system (OS) independent feature. The open source and free development environment (IDE) 'Netbeans' (Oracle, 2014) was used for development of this software.

7.4 Results and Observations

A sinusoidal wave of 80 Hz is fed from a signal generator to the data acquisition system and resulting display on a PC produced by the developed software is shown in Figure 7.5.

The GUI of the software developed for this system has a main window that displays the graphical form of the data. It also has selectable options for the time window from 1 to 8 seconds. The software implements an 8^{th} order IIR digital notch filter with stop band cantered at 50 Hz. This notch filter can be selected to turn on and off. Another display shows the configuration statuses, like data sampling rate, vertical and horizontal scaling etc. There is also a window which displays the numerical values of the digitized data.

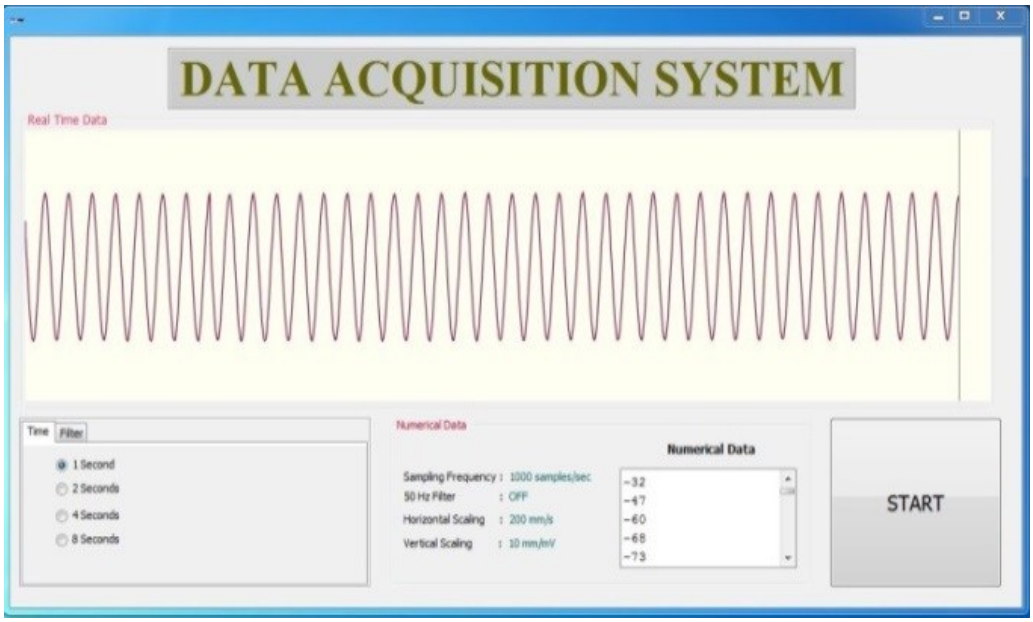

Figure 7.5: GUI software of Data Acquisition System

It may be observed that the system reproduces the signal very nicely in PC. Further measurement at different frequencies showed that for Continuous conversion mode and Batch mode, aliasing effect was seen after 150 Hz and at 12 KHz respectively. The system showed no significant phase or amplitude change up to 100 Hz and 10 KHz for Continuous conversion and Batch mode respectively. The system is being used in ECG, EMG, NCV and FIM (Focused Impedance Measurement system, developed by Rabbani et al, 1999) with excellent satisfactory results.

Most of the bioelectrical signals occur within the band width of 0 to 10 KHz; therefore this system satisfies the biomedical instrumentation requirements. The only limitation of the system is the ADC resolution, which is comparatively low, but it is acceptable for most of the application stated before. It is possible to use several ADC channel for data acquisition, since the microcontroller has 6 ADC channels and minimum conversion time of 13 µs which would be negligible time laps between multiple conversions. If it is required to have higher resolution of ADC, larger SRAM and more ADC channels, different microcontroller can be used with the same working procedure since the firmware is written in C language.

7.5 Novelty

Though, USB specifies medical device class, the HID type was chosen because most of the current PC operating system provides driver for this class, thus unnecessary complexity of PC side driver development could be avoided. In continuous conversion and transfer mode, the sampling and data transfer are done simultaneously and are well synchronized. From sampling to display the system has a latency of approximately 10 ms, which can be regarded as real time. This transfer mode is suitable for low frequency signals like ECG, EEG etc. The Batch transfer mode provides higher sample rate and it is suitable for high frequency bioelectric signals like EMG, NCV etc.

The system is small with low component count and therefore cost effective, making it suitable for standalone BCI system.

Chapter 8 : Analysis of Spatial Pattern of EEG μ-Rhythm for BCI

8.1 Background

Primary sensory motor cortex area of human brain typically shows oscillatory behaviour in EEG at a frequency of approximately 8-12 Hz when they are not processing sensory information or not producing motor output. This oscillatory signal is called μ-rhythm. It is believed that this μ-rhythm is generated due to interactions between the thalamus and the cortex (Gastaut, 1952) and reflects the synchronous firing of motor neurons in rest state i.e. no motor action or movement of body parts. The amplitude of μ-rhythm decreases or suppresses when a motor action is performed, possibly because of the normal neuronal system and the mirror neuron system "go out of sync" and interfere with each other (Oberman, et al., 2005). Several publications (Pfurtscheller et al., 2006 & 2001; Neuper et al., 2009; Hwang et al., 2009; Kübler et al., 2005) showed that the μ-rhythm activity corresponds to motor output by various different frequencies within the band of 8-12 Hz. The μ-rhythm frequencies sometimes overlap and also appear as harmonics in β band (18-25 Hz). The μ-rhythm activity corresponding to motor outputs can be distinguished by precise location of origin from sensorimotor cortex. In other words, these rhythms are directly associated with the cortical area which are responsible for brain's normal

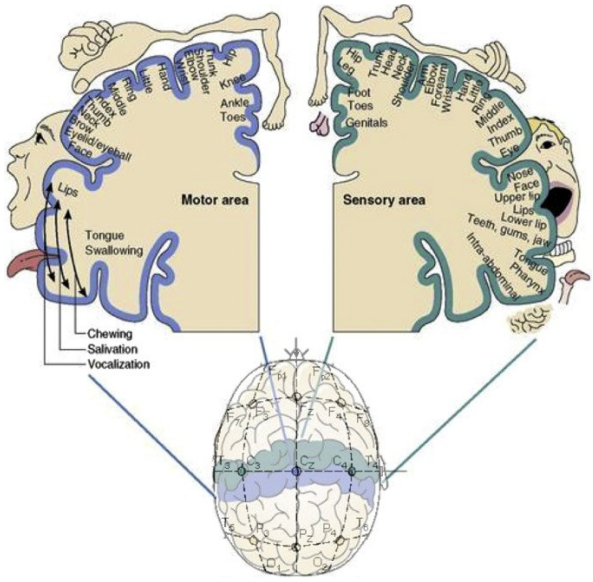

Figure 8.1: Somatotopic organization of the sensorimotor cortex (de Klerk, et al., 2015) with The international 10–20 system of EEG electrode placement.

motor actions. Figure 8.1 shows the sensorimotor cortex of human brain and typical locations (marked with typical 10-20 EEG electrode placement system) associated with motor output for various body parts (de Klerk, et al., 2015).

The mapping of human brain locations associated with different function is called cortical homunculus. Dr. Wilder Penfield and his co-investigators Edwin Boldrey and Theodore Rasmussen are considered to be the originators of the sensory and motor homunculi; there work compellingly illustrates the data at a single glance and it became most famous conceptual maps in modern neuroscience (Cazala, et al., 2015). The 'homunculus' is also described by Jasper et al., (1949).

The μ-rhythm activity can be good choice for BCI as it decreases over sensorimotor cortex with movement or intention of movement or even imagination of movement. This decrease in amplitude associated with movement is labelled as 'Event Related Desynchronization' (ERD) (Pfurtscheller, 1999) and its counterpart is 'Event Related Synchronization' (ERS) which corresponds to relaxation or pre-movement. The ERD and ERS can occur with motor imagination as well, i.e. it does not require actual movement and it can occur independent of brain's normal output for peripheral nerves and muscle (McFarland et al., 2000). Therefore, ERD can be used in BCI very effectively. Furthermore, continuous feedback from the BCI system to the user can lead to improved control over the μ-rhythm activity produced by the user, which can reinforce the performance of the BCI system.

Throughout this present work, the Motor Imaginary BCI or using imagination of movement of body parts for BCI is studied. This MI-BCI is chosen for its relevance to control neuro-prosthesis by an alternative channel other than the brains normal motor output channel. Also the MI-BCI provides the user a set of distinct mental task (i.e. imagination of movement of specific body parts) which is simple and easy to perform and can be treated as different classes for BCI. Furthermore, the μ-rhythm activity of ERD and ERS during motor imagination has adequate physiological significance, therefore these properties of μ-rhythm is expected to produce efficient, simple and easy implementation of Brain-Computer Interface.

8.2 Problem Statement

The main task of the present work is to analyse EEG signals to detect a particular task and to distinguish between different subtypes of the task. The present work performs the above through an attempt to identify whether the subject imagines movement of a hand, and to distinguish whether it is the right hand or the left hand. This is the classification that the present work will attempt to obtain and the objectives may be summarised are as follows:

i. To determine whether the chosen μ-rhythm gives a viable performance for the proposed task of MI-BCI.
ii. To locate the minimum number of brain locations, based on standard EEG electrode placement geometry, that will give an optimum result for the above task using the μ-rhythm.
iii. To determine amplitudes and frequencies of μ-rhythm that are most likely to produce more accurate results in later stage of machine learning process for automated classification

These locations, amplitudes, frequencies and other possible attributes should have maximum likelihood of belonging to a particular class of MI and should be distinguishable by a considerable amount between different classes. These attributes of μ-rhythm can be considered as features and then can be subjected to a suitable machine learner to classify the MI class.

8.3 Method

This section analyses the μ-rhythm activity during the mental task of imagined movement of Left and Right hand to find the suitable features that can be used for classification of the MI tasks. The μ-rhythm activity analysis is carried out using Matlab (MathWorks, 2005) based Offline Analysis tool of BCI2000 (Schalk et al., 2004). Firstly, through an offline analysis of continuous EEG sample data set for many channels, obtained from open source data the objectives (i) and (ii) above were achieved and are detailed below.

8.3.1 Source and type of EEG Data

Continuous EEG sample data sets were obtained from open source published data; courtesy of Romain Grandchamp, CERCO, Toulouse, France (Grandchamp, 2009). This data contains two class imaginary movements as a sequence of trials in which a subject was instructed to imagine moving either the Left hand or the Right hand. The data have event-markers or time stamps that indicate the timing and type of these instructions including the rest or relaxed conditions. These EEG data were recorded from 29 channels of the standard 10-20 electrode position system.

8.3.2 EEG Signal Pre-Processing

(i) *Temporal Filter*: Since the μ-rhythm band is 8-12 Hz, and also it can have harmonics in higher frequency bands (β band, 18-25 Hz)) an IIR filter with passband of 6-32 Hz was employed to remove all other frequencies. The rejected frequencies can be major cause of interference like 50 Hz line interference.

(ii) *Spatial filter*: A Common Average Reference (CAR) filter was used to detect the location of origin of a desired signal more precisely. A CAR filter treats one channel as the active channel while the average of signals from all other channels (in some other cases, only a few neighbouring channels) acts as a reference. Subtraction of this reference signal from the active signal effectively removes the influence or interference from neighbouring channels. This process is performed to all other channels in a similar manner, which essentially gives a spatial filtering. After performing this spatial filtering, particular amplitude and other attributes can easily be related to the specific location of the cortex during MI task i.e. imagined Left Hand or Right Hand movement.

8.3.3 Data Analysis

After performing the temporal and spatial filtering, average signal amplitude was computed for each condition i.e. Left Hand and Right Hand MI task. The EEG Amplitude is averaged for each frequency of the pass band (6-32 Hz) over a period of time or epoch of the specific mental task. There are total of 128 epochs of which 64 are the left hand and other 64 are of right hand imagined movement (There are also 64 epochs of rest state which will be used for the later part of the analysis). So, the EEG data set is now divided into two sets that corresponds to the conditions of imagined left and right hand movement and can provide the features as:

(i) Average value of EEG amplitude
(ii) That at a certain frequency
(iii) That in a certain channel

These features can describe for each location, how much the signal strength is, at which frequency and at what condition (imagined movement of left or right hand). To compute a number representing how much a feature's value tells about the condition under which it was recorded, the 'Determination Coefficient', or r^2 was used. The r^2 is the squared correlation coefficient for a bivariate distribution constructed from two sets of variables and have been used and reported in similar analysis (McFarland et al., 2000 and 1997). To compute the r^2 value for each channel and each particular frequency, there are data of 2 columns and 128 rows. Each row (x) of first column is the average amplitude of a particular epoch at the specific frequency, and the second column is the corresponding MI class i.e. left hand right hand represented by +1 and -1 respectively .These +1 and -1 representing the MI-class are just tags of the categorical variable (y). Hence, a two dimensional data set can be formed and Determination Coefficient for a particular channel and frequency can be obtained as,

$$r^2 = \frac{COV(x,y)^2}{var(x)var(y)} \tag{8.1}$$

The larger a feature`s $r^2$, the more correlation exists between a feature`s value and the condition under which it was recorded.

After performing this analysis for Left/Right Hand MI class, Individual classes are assessed with respect to rest or relax state in same manner.

8.4 Results and Discussions

The r^2 values are plotted with respect to EEG channel number and frequency in a three dimensional spectral plot, as shown in Figure 8.2. In this plot the value of r^2 increases with increased colour depth.

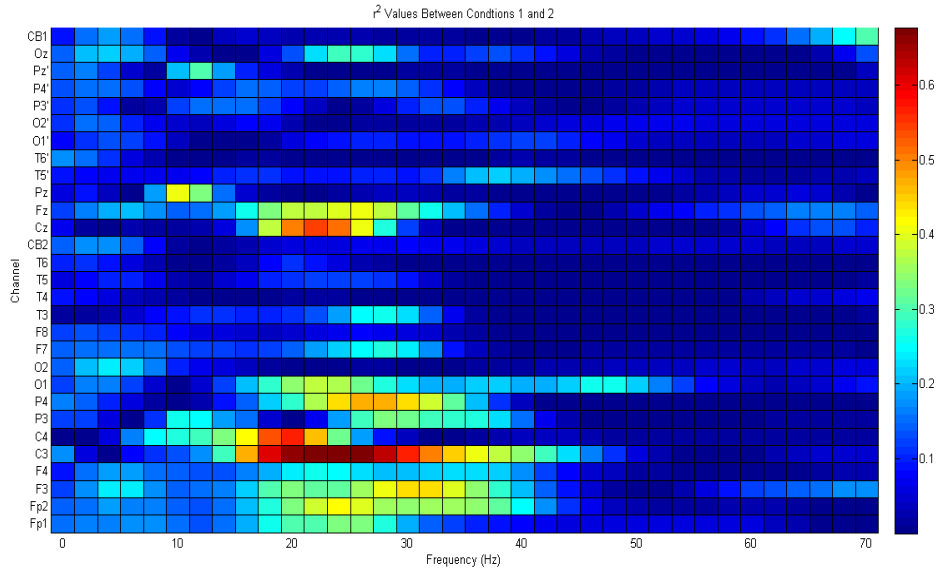

Figure 8.2: Spectral plot of r^2 values as a function of EEG channel and frequency

From this plot (Figure 8.2), it was observed there are clusters of high values of r^2(>0.6) occurred in the frequency range 12 to 30 Hz in the channel C3, C4 and Cz.

Spectral plots of amplitudes for imagined movement of left hand (red plot) and that of right hand (blue plot) for these channels and the associated r^2 values were then obtained and are presented in Figure 8.3. Figure 8.4 presents the same for the channels Fp2, F3 and Fz.

From these figures (Figure 8.3 and 8.4) it is evident that the most viable channels to distinguish the two classes (imagined movement of left and right hand) are C3 and C4, since there amplitudes are greatly separable in the frequency range of 10 to 16 Hz, even though the r^2 values are low. All other plotted channel shows little or no distinguishable properties between the two classes. This is well expected as the channel C3 and C4 are placed on the sensorimotor cortex that are responsible for motor action of hand and leg as shown in Figure 8.1.

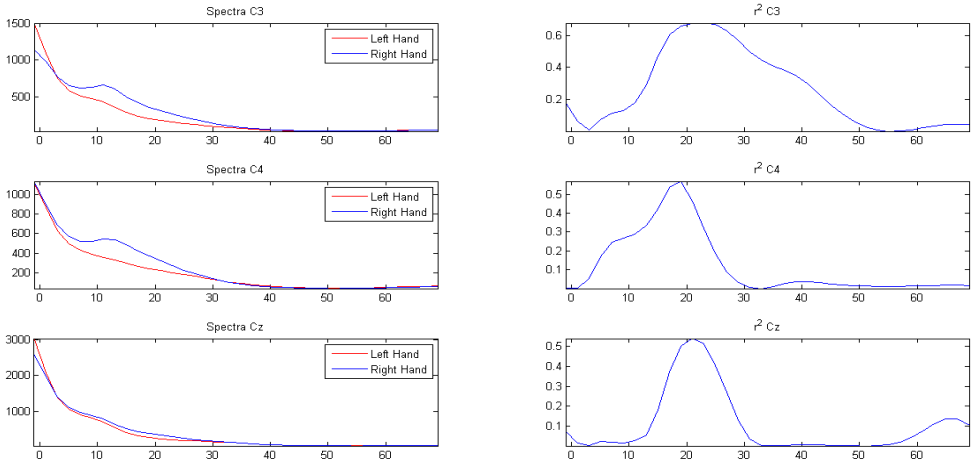

Figure 8.3: Spectral plots of Amplitude and r^2 for Channels C3, C4 and Cz

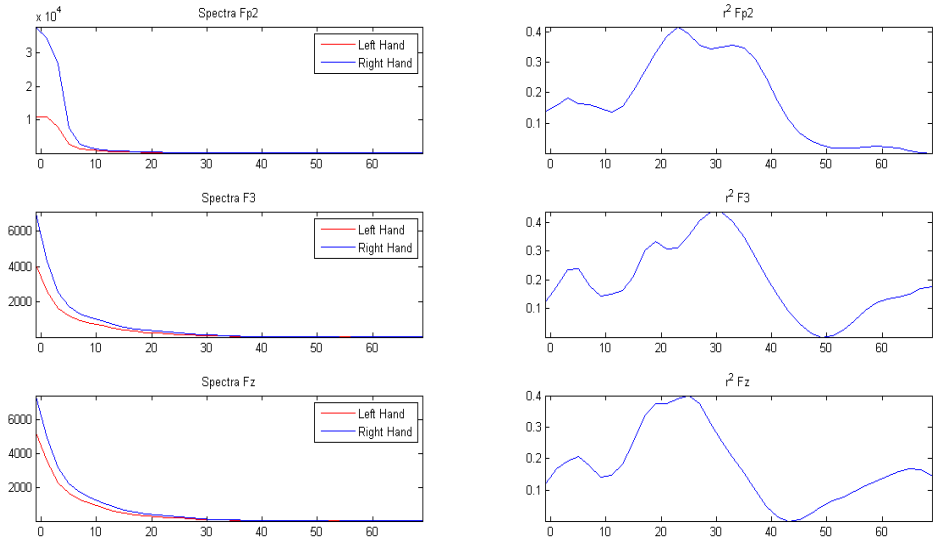

Figure 8.4: Spectral plots of Amplitude and r^2 for Channels Fp2, F3 and Fz

Next, a topographic plot of r^2 values over the scalp were plotted at 6 different frequencies of interest (10, 12, 16, 22, 30 and 32 Hz) as shown in Figure 8.5.

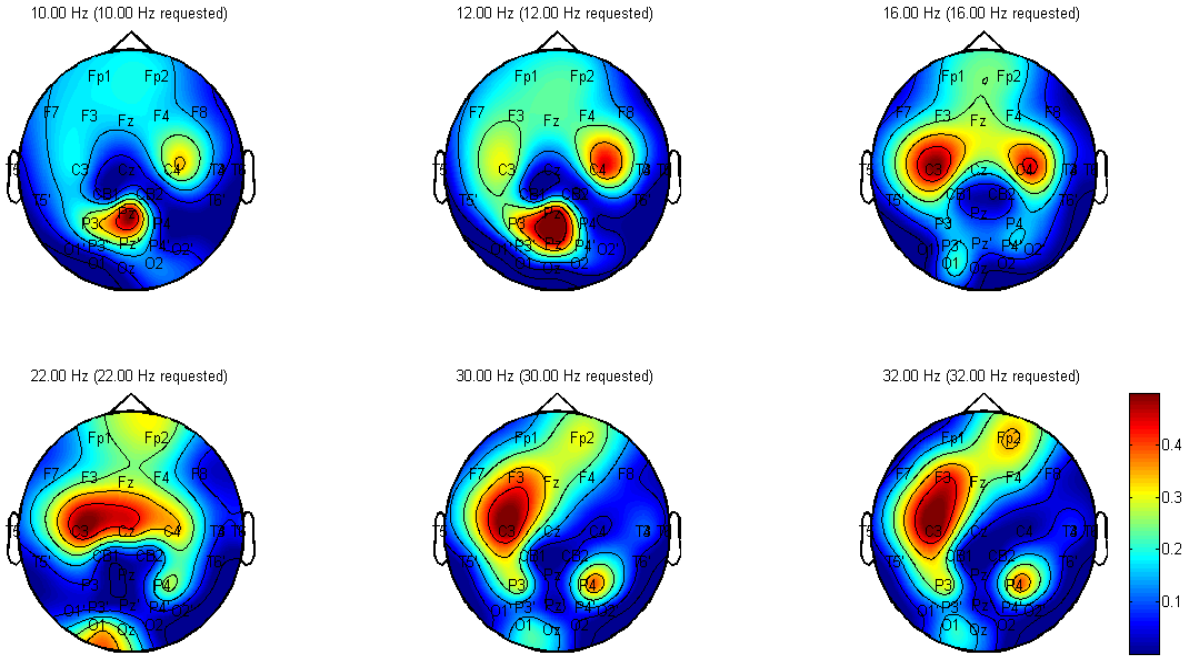

Figure 8.5: Topographic plot of r^2 at frequencies 10, 12, 16, 22, 30 and 32Hz

From the above figure it is evident that the most correlated channels to the motor imaginary classes are the C3 and C4 channels and at frequencies of 12 and16 Hz. The 16 Hz frequency is out of the μ-rhythm band, but this occurrence is probably an overlapped case and is expected as stated before. Other frequencies of interest are 10 Hz and 12 Hz, as C4 and C3 shows reasonable activity at 10 Hz and 12 Hz respectively. Other frequencies (22, 30, 32 Hz) show large r^2values, but as seen from Figure 8.3, these frequencies has less distinguishable characteristics, and therefore, not valuable features.

Now, the results of analysis of individual classes, i.e. Left Hand vs Rest state and Right Hand vs Rest state are presented below. These two analyses are carried out in the same manner but only topographical plots at frequency of interest (10 and 12 Hz) are presented at Figures 8.6 and 8.7.

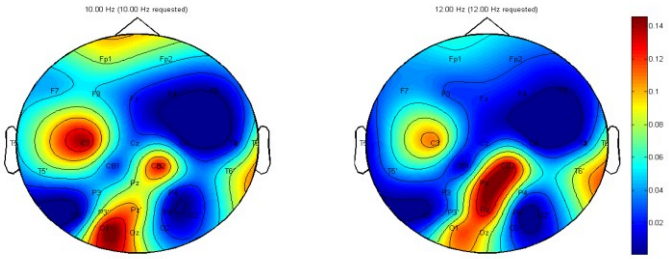

Figure 8.6: Left Hand vs Rest state, Topographic plot of r^2 at frequencies 10, 12 Hz

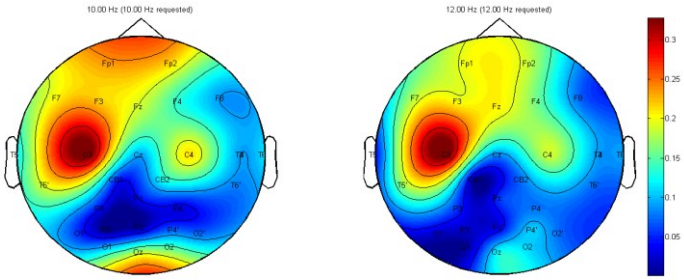

Figure 8.7: Right Hand vs Rest state, Topographic plot of r^2 at frequencies 10, 12 Hz

The above figures clearly shows contralateral activity at 12 Hz at the channel C3 and CB2 (which is very close to C4) for Left Hand and Right Hand motor imaginary movement.

8.5 Conclusions

This analysis was performed to evaluate the feasibility of using μ-rhythm attributes as features for MI-BCI. From the analyses results it can be confidently expressed that the μ-rhythm is a very strong parameter for BCI system that employs Motor Imaginary tasks. And also these analyses sorts out the feasible features as spatial locations, amplitude and frequencies that are most likely to produce higher accurate result in later stage of machine learning process for automated classification.

In this EEG data of the particular subject, it is found that the most important spatial locations are C3, C4 and CB2 and the average amplitudes at 10, 12 and 16 Hz frequencies which can be used

as viable features. The contralateral activity of μ-rhythm for Left and Right hand imaginary movement presented at Figure 8.6 and 8.7 are very interesting which is supported by the physiology of human nervous system. Along with 12 Hz frequency and topographic locations, the result supports the μ and β-rhythm activity associated with the homunculus for human motor movement.

Though this analysis is carried out with large number of electrode channels, the actual BCI system that is being developed in the present work would have very few channels, preferably two. This feature selection technique and classification of various MI states using several machine learning techniques are described in the following chapter.

Chapter 9 : Classification of Two and Three Class Motor Imaginary EEG Data

9.1 Background

The classification of EEG data for BCI requires signal processing to remove unwanted noise and interference. Then, Feature Extraction procedure is performed to find feasible features that have attributes related to the desired classes of the data. Finally, the features are used to train a machine learning method to identify the class of new data i.e. classification of new data that was not in the training set. Figure 9.1 shows the simplified block diagram of the procedure.

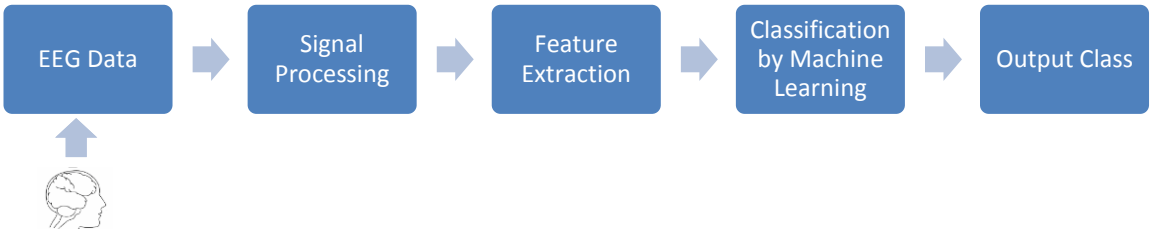

Figure 9.1: Typical EEG Data Classification Block Diagram

The μ-rhythm analysis of the previous chapter is similar to the basis of a feature extraction method called 'Common Spatial Patterns' (CSP). The CSP algorithm (Fukunaga, 1990) was first introduced to BCI applications by Graz BCI group (GRAZ BCI, 2017) which is an optimized spatial filter for discrimination of different conditions of human brain activity (Ramoser et al., 2000). This method was reported in an experiment (Guger et al., 2000) where a feedback study was conducted with a CSP-based BCI operating on a 27 channel EEG data. The feedback study contained three subjects, 6 sessions on 4 days for each of the subjects CSP is very efficient in calculating spatial filters for identifying ERD and ERS [what are these? Give the full once here in this chapter] conditions (Koles et al., 1998), and therefore is suitable to use in ERD based MI-BCI. This algorithm is very fast and robust and flexible as it is an adaptive filter which deals with the problem of inter-subject variability and produces complex but physiologically meaningful features. The CSP algorithm was successfully used in motor imaginary BCI tasks, reported in several publications (Blankertz et al., 2007; 2008), and it was also extended to multi-class BCI (Dornhege et al., 2004). Using this method, four patients with complete or partial

paralysis or paresis of their lower limbs were successfully trained to operate a variant of the Graz BCI system that uses band power features of only 2 bipolar channels placed on the position C3 and C4 (Standard 10-20 EEG electrode placement system). For This BCI, a basket game is used as feedback to a user who controls the horizontal movement of a ball which is falling vertically at a constant speed (Krausz et al., 2003). The result of this experiment is presented as Information Transfer Rate (ITR) and the participants achieved ITR between 5 to 17 bits/min. A similar methodology was successfully used with 4 patients suffering from Amyotrophic Lateral Sclerosis (ALS) (Kübler et al., 2005). This is the first study that demonstrated that the ALS patients are capable of voluntarily modulating the amplitude of their sensorimotor rhythms to control a BCI. This study resulted in accuracy between 76 to 81%.

The features from CSP algorithm is physiologically meaningful i.e. corresponding to spatial patterns of origin of sensorimotor rhythms (μ and β band). It also effectively reduces the dimension of EEG data to very low dimension of features. Therefore, a simple, light and fast machine learning techniques can be used to classify the motor imaginary states using this CSP algorithm. The common machine learning techniques that have been extensively used in BCI applications for classification are Linear Discriminant Analysis (LDA), Logistic Regression (LR), Support Vector Machine (SVM), Neural Networks (NN) (Lotte et al., 2007) etc. Among these, the LDA and SVM are linear classifiers and probably the most popular classifiers used in BCI. The LDA (Duda et al., 2001) uses hyperplanes to separate the data representing the different classes. The LR (Hosmer et al., 2013) is a nonlinear classifier which works with categorical class by transforming them to continuous values. The SVM (Burges, 1998) also uses hyperplanes like LDA but the selected hyperplane is the one that maximizes the distance from the nearest training points. NN (Bishop, 1995) is an assembly of several artificial neurons which produces nonlinear decision boundaries.

For simplicity and robustness, along with the CSP feature extraction method, the LDA, LR and SVM are used as classifiers in the present research work described in the next sections.

9.2 Problem Statement

The proposed BCI system will have low electrode count and comparatively less computational power as mentioned in the beginning. Therefore, it is important to implement an efficient EEG data classification method which uses motor imaginary sensorimotor rhythms (μ and β band). The CSP algorithm finds the spatial patterns that are most discriminative between MI classes; it requires low computational steps and produces small number of effective features. The CSP algorithm can resemble obtaining features form few viable electrode positions, therefore it is used in the present study as the feature extraction method. The main objective of this present study is to evaluate several machine learning techniques to find most promising classifier that uses a few viable features and can be used for the particular case of proposed BCI system. Also, to improve the classifier accuracy, effect of combining several classifiers in parallel will also be assessed.

9.3 Method

The EEG data of three subjects for Two and Three class offline classification were obtained from Berlin Brain-Computer Interface's BCI competition III (BBCI, 2004). This Data Set, named IIIa is provided by the Laboratory of Brain-Computer Interfaces (BCI-Lab), Graz University of Technology. The data for fourth subject is the same data described in section 8.3.1. The epoch extraction from the target marker for specific class in the data, signal processing, CSP feature extraction and machine learning methods were carried out using Matlab based tool 'BCILAB'(BCILAB, 2017).

The motor imaginary data of three subjects corresponding to Left Hand, Right Hand and Foot movement were first classified as a Two-class problem (Left/Right Hand). Three classification methods, LDA, LR and SVM, were used for this purpose. Then the Three-class (Left/Right Hand and Foot movement) motor imaginary data classification was carried out using the same classifiers. Data from the fourth subject was first classified as Two-class (Left/Right Hand) and then Three-class (Left/Right Hand and Rest state) problems using the same methods as stated above. Finally, using the forth subject`s data, a parallel classification was evaluated using the three classifiers simultaneously and getting the classification output by majority voting algorithm for the two-class problem.

9.3.1 Data Description

The data set IIIa contains cued (time stamp for each recording condition) multi-class signals. There were 4 classes: Left Hand, Right Hand, Foot & Tongue motor imaginary EEG data which were obtained from three subjects (k3b, k6b & l1b), recorded with 60 channels using the left mastoid for reference and the right mastoid as ground. There are 60 epochs per class. The EEG was sampled at 250 Hz, and was processed using a bandpass filter between 1 and 50Hz and a Notch filter at 50 Hz.

The subject sat in a relaxing chair with armrests. The task was to perform imaginary left hand, right hand, foot or tongue movements according to a cue. The order of cues was random. The experiment consists of several runs (at least 6) with 40 trials each. After trial begin (t=0), the first 2s were quiet, at t=2s an acoustic stimulus indicated the beginning of the trial, and a cross "+" is displayed; then from t=3s an arrow to the left, right, up or down was displayed for 1 s; at the same time the subject was asked to imagine a left hand, right hand, tongue or foot movement, respectively, until the cross disappeared at t=7s. Each of the 4 cues was displayed 10 times within each run in a randomized order. The timing paradigm for data acquisition is shown in Figure 9.2.

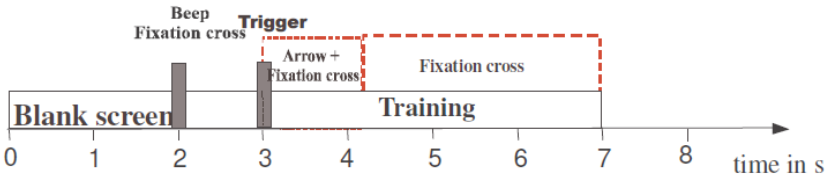

Figure 9.2: Timing of the Data Acquisition Paradigm

The data set of fourth subject was described before in section 8.3.1.

9.3.2 The CSP Algorithm

The Common Spatial Pattern (CSP) algorithm finds information (i.e., spatial filters) in two distributions of high-dimensional space. The EEG signal is first processed with a bandpass filter in the frequency domain of interest. Then the CSP algorithm maximizes variance for one class and that at the same time minimizes variance for the other class. High or low signal variance reflects a strong and a weak (attenuated) rhythmic activity, respectively.

If a raw EEG data from a single trial constructs a matrix E of elements $N \times T$, where N is the number of channels and T is the measured samples per channel, the normalized spatial covariance of the EEG can be obtained by,

$$C = \frac{EE'}{Trace(EE')} \tag{9.1}$$

Where *Trace* is the sum of diagonal elements of EE'. For each of the two distributions to be separated (For example, Left and Right Hand motor imagery), the spatial covariance $\overline{C_d} \in [l, r]$ is calculated by averaging over the trials of each group. The composite spatial covariance is given as,

$$C_c = \overline{C_l} + \overline{C_r} \tag{9.2}$$

C_c can be factored as $C_c = U_c \lambda_c U_c'$, where U_c is the eigenvector matrix and $\lambda_c$is the diagonal matrix of eigenvalues which is assumed to be sorted in descending order. The whitening transformation gives,

$$P = \sqrt{\lambda_c^{-1} U_c'} \tag{9.3}$$

Which equalizes the variances in the space spanned by U_c i.e., all eigenvalues of PC_cP' are equal to one. If $\overline{C_l}$ & $\overline{C_r}$ are transformed as,

$$S_l = P\overline{C_l}P' \quad \text{and} \quad S_r = P\overline{C_r}P' \tag{9.4}$$

If $S_l$and S_r has common eigenvectors, i.e., if,

$$S_l = B\lambda_l B' \quad \text{then} \quad S_r = B\lambda_r B' \quad \text{and} \quad \lambda_l + \lambda_r = I \tag{9.5}$$

Where I is the identity matrix. Since the sum of two corresponding eigenvalues is always one, the eigenvector with largest eigenvalue for $\overline{S_l}$ has the smallest eigenvalue for $\overline{S_r}$ and vice versa. The projection of whitened EEG onto the first and last eigenvectors in B (i.e., the eigenvectors corresponding to the largest λ_l and λ_r) will give feature vectors that are optimal for

discriminating two populations of EEG. With the projection matrix $W = (B'P)'$ the mapping of a trial E is given as,

$$Z = WE \tag{9.6}$$

The columns of W^{-1} are the common spatial patterns and can be regarded as time-invariant EEG source distribution vectors.

9.3.3 Linear Discriminant Analysis (LDA)

The Linear Discriminant Analysis separates the data of different classes by a hyperplane. For a two class classification, the class of the feature vector of the data sample is determined by which side of the hyperplane is the vector resides. The classification of more than two classes is accomplished by more than two hyperplanes.

LDA assumes the data is normally distributed and in case of the simpler version of 'Fisher`s LDA' the data is assumed to have equal covariance matrix for both class. The separating hyperplane is obtained by seeking the projection that maximizes the distance between the mean and minimizing the variance of two classes. For a multiclass BCI, the 'one versus the rest' (OVR) strategy is used which involves in separating each class from all the others. Figure 9.3 shows graphical view of LDA with simulated data sets with identical covariance matrices.

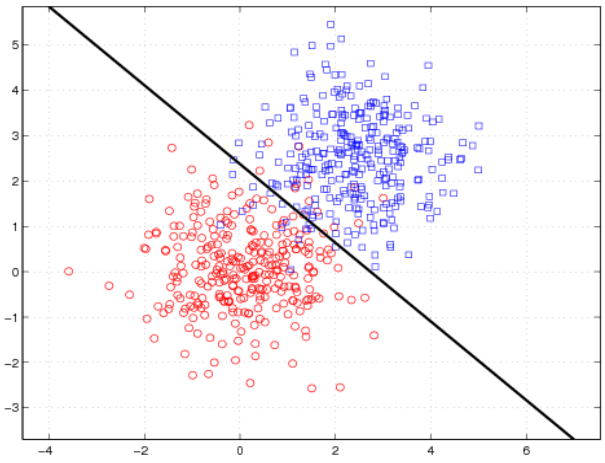

Figure 9.3: LDA with Simulated Data sets with Gaussian distribution and Identical Covariance Matrices Between two Classes

For a set of observation that constitute a feature vector set $\vec{x}$ and for each sample of observation corresponds to a known class y, then $\vec{x}$ and y creates a training set that can be applied to classify unknown observations similar or same distribution of samples where $\vec{x}$ is taken form.

LDA solves the problem by assuming that the conditional probability density functions $p(\vec{x}|y=0)$ and $p(\vec{x}|y=1)$ are both normally distributed with means and covariance parameters $(\overrightarrow{\mu_0}|\sum_0)$ and $(\overrightarrow{\mu_1}|\sum_1)$ respectively. Now, Bayes optimal solution is to predict that a sample belongs to second class if the log of the likelihood ratio is bellow some threshold T, that is,

$$(\vec{x}-\overrightarrow{\mu_0})^T\sum_0^{-1}(\vec{x}-\overrightarrow{\mu_0})+ln|\sum_0|-(\vec{x}-\overrightarrow{\mu_1})^T\sum_1^{-1}(\vec{x}-\overrightarrow{\mu_1})+ln|\sum_1|>T \tag{9.7}$$

Equation 9.7 is called Quadric Discriminant Analysis (QDA). To simplify more, the LDA, makes further assumptions that the class covariances are identical i.e., $\sum_0=\sum_1=\sum$ (Homoscedasticity Assumption), and also covariances have full rank. So, the decision criterion in Equation 9.7 becomes,

$$\vec{w}\cdot\vec{x}>c \tag{9.8}$$

Where c is some threshold constant given by,

$$\frac{1}{2}(T-\mu_0^T\sum_0^{-1}\mu_0+\mu_1^T\sum_1^{-1}\mu_1) \tag{9.9}$$

And,

$$\vec{w}=\sum^{-1}(\mu_0-\mu_1) \tag{9.10}$$

So, the criterion of an input $\vec{x}$ being in a class y is purely a function of this linear combination of the known observations.

9.3.4 Logistic Regression (LR)

Logistic regression is a natural extension of the ideas behind linear regression and linear discriminant analysis. LR is basically classifies categorical binary dependent variable, i.e. it can take only two values, "0" and "1" represent outcomes such as pass/fail, win/lose etc. For

multiclass problem ‘one versus the rest’ (OVR) strategy (as mentioned in LDA section) can be applied.

The core of the LR method is ‘Logistic Function’, also called the ‘Sigmoid Function’ is an S-shaped curve that can take any real-valued number t, ($t \in R$) and map it into a value between 0 and 1, but not exactly at those limits. This function is given as,

$$\sigma(t) = \frac{1}{1+e^{-t}} \tag{9.11}$$

Where a graph of the logistic function is shown in Figure 9.4.

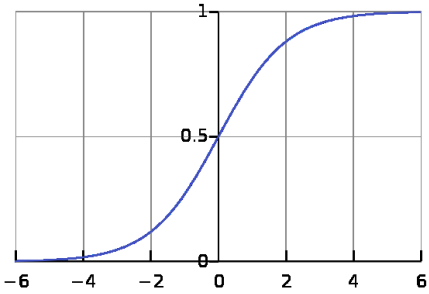

Figure 9.4: The standard logistic function where σ(t)∈(0,1) for all t

If t is a linear function of a single explanatory variable, it can be expressed as,

$$t = \beta_0 + \beta_1 x \tag{9.12}$$

Where β_0 is the bias or intercept term and $\beta_1$is the coefficient for the single input value x. Therefore each value of the input data from any feature set $\vec{x}$, has an associated β coefficient (a constant real value) that must be learned by the training data. So, the logistic function can now be written as:

$$F(x) = \frac{1}{1+e^{-(\beta_0+\beta_1 x)}} \tag{9.13}$$

The $F(x)$ is interpreted as probability of the dependent variable equals a case, given some linear combination of the predictors. For a output class y ($y \in (0,1)$), the LR can be understood by finding coefficients that best fit:

$$y = \begin{cases} 1 & \beta_0 + \beta_1 x + \varepsilon > 0 \\ 0 & else \end{cases} \quad (9.14)$$

The coefficients (β_i) of the logistic regression algorithm must be estimated from training data set and this is usually accomplished by using Maximum-Likelihood Estimation (Scholz, 1985) method. This maximum-likelihood estimation process is different form the linear regression and uses an iterative process to find the coefficients that result in the highest probability of the class that is known in the training set. In other words, a search procedure seeks values for the coefficients that minimize the error in the probabilities predicted by the model to those in the data, i.e., it is a minimization algorithm which is used to optimize the best values for the coefficients for training data. This process begins with a tentative solution, revises it slightly to see if it can be improved. This repetition of the revision continues until no more improvement can be made, at which point the process is said to have converged.

In some cases the maximum-likelihood estimation method may not converge. Non-convergence of a model indicates that the coefficients are not meaningful.

9.3.5 Support Vector Machine (SVM)

The Support Vector Machine uses a discriminant hyperplane which is selected on the basis of maximizing margins from the nearest training points. The maximizing of margin results in increased generalization capabilities of the classifier (Burges, 1998; Bennett et al., 2000). It also uses a regularization parameter C that permits accommodation of outliers and allows errors on

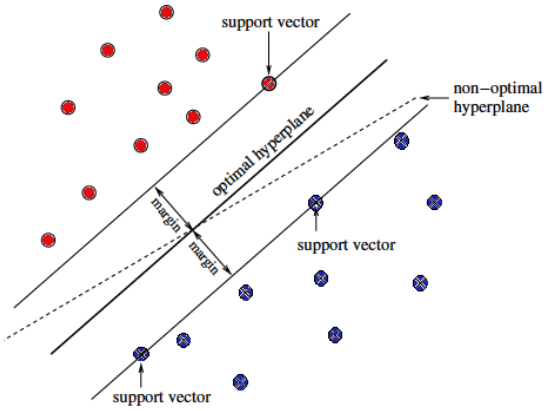

Figure 9.5: SVM finds the optimal hyperplane

the training set. The SVM is also insensitive to overtraining (Jain et al., 2000). SVM that performs classification using linear decision boundaries is known as linear SVM. Figure 9.5 shows the support vectors that are used to find an optimal hyperplane that has maximum margin.

It is possible to produce non-linear boundaries using the kernel function $K(x_i, x_j)$, which maps the data to another space where the data can be separated by linear boundaries, generally of much higher dimensionality. The kernel generally used in BCI research is the Gaussian or Radial Basis Function (RBF) kernel:

$$K(x_i, x_j) = e^{\left(\frac{-\|x_i - x_j\|^2}{2\sigma^2}\right)} \tag{9.15}$$

The SVM that uses the kernel function and has non-linear boundaries is known as Gaussian SVM or RBF SVM. The use of kernel function to separate the input data in higher dimension features space is shown in figure 9.6.

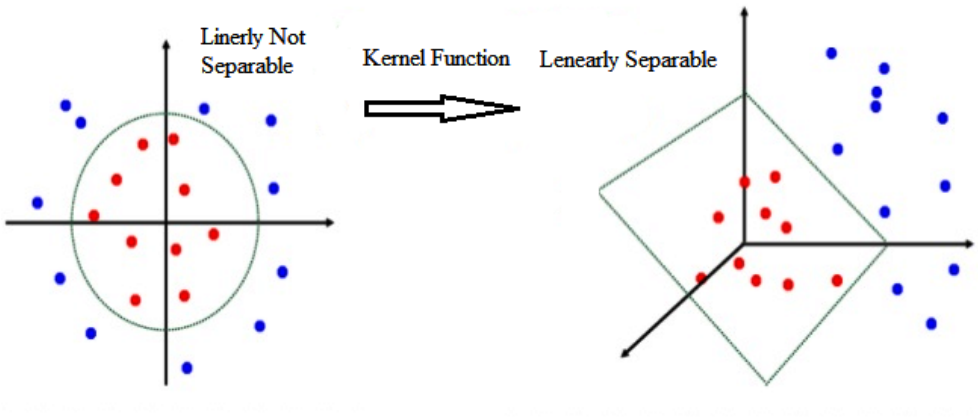

Figure 9.6: Gaussian or RBF SVM finds Optimal Hyperplane for Nonlinearly Separable Data by Kernel Mapping

For a training set x_i of N samples, each associated with a class $y \in (+1, -1)$ the standard SVM solution is derived from the following optimizing problem:

$$\min_{w,b,\xi} \frac{1}{2} w^T w + c \sum_{i=1}^{N} \xi_i$$

This is subject to,

$$y_i(w^T\phi(x_i) + b) \geq 1 - \xi_i$$

$$\&,\ \xi_i \geq 0$$

Where w is the normal vector and b is the bias of the separation hyperplane. When $\phi(x) = x$ SVM is a linear classifier, otherwise, if $\phi(x)$ maps x to a higher dimensional space, the SVM is termed nonlinear.

When the training data cannot be separated without error, the slack variable $\xi_i \geq 0$ and regularization parameter C is introduced. Therefore a training sample is allowed to be a small distance ξ_i on the wrong side of the hyperplane without violating the stated constraint. With the advantages of simpler constraints, the optimization problem becomes,

$$\min_{\alpha} \frac{1}{2}\alpha^T Q\alpha - e^T\alpha$$

This is subject to,

$$0 \leq \alpha_i \leq C\ ,\quad i = 1,2, \ldots \ldots . N$$

$$\&,\ \ y^T\alpha = 0$$

Where e is the vector of all ones, $Q$is an $N \times N$ positive semidefinite matrix, given by,

$$Q_{i,j} = y_i y_i K(x_i, x_j) \tag{9.16}$$

And $K(x_i, x_j) = \phi_i^T\phi_j$ is the kernel function. The decision function is then,

$$F(x) = sgn(y_i\alpha_i K(x_i, x_j) + b) \tag{9.17}$$

Since the performance of the SVM classifier depends on the regularization parameter C, choice of an appropriate value of C is an essential part of the SVM classification method.

9.3.6 Majority Voting Algorithm

The Majority Voting (Jain et al., 2000) classification technique involves several classifiers. Each of the classifier`s input is presented with same feature vector corresponding to a particular class. Then the output classes are finally chosen on majority basis. Because of its simplicity and efficiency majority voting is the most popular way of combining classifiers in BCI research (Lotte et al., 2007).

9.3.7 Cross-validation

To evaluate the performances of classifiers used in this study, a 10-fold cross-validation with one leave out method is used (Rodriguez, et al., 2010). There were 30 epochs for each class (total of 60 epochs for two class and 90 epochs for three class classification) of motor imaginary for each subject in the data set. The epochs are randomly partitioned into 10 equal size subsamples. Of the 10 subsamples, a single subsample is retained as the validation data for testing the model, and the remaining 9 subsamples are used as training data. The cross-validation process is then repeated 10 times (the folds), with each of the 10 subsamples used exactly once as the validation data. The 10 results from the folds are then averaged to produce a single estimation. The advantage of this method is that all observations are used for both training and validation, and each observation is used for validation exactly once.

9.4 Results and Observations

The results of Two (Left/Right Hand) and Three (Left/Right Hand/Foot) class motor imaginary offline classification of subject with ID: **'k3b'** is given in Table 9.1, 9.2 and 9.3:

Table 9.1: Classification accuracy for LDA of subject 'k3b'

Classifier	**MI Class**	**Subject ID: 'k3b' (%)**	
Liner Discriminant Analysis (LDA)	Two Class Left Hand and Right Hand	True positive	95.5
		True negative	98.3
		False positive	1.7
		False negative	4.5
		Error rate	3.3
	Three Class: Left Hand, Right Hand and Foot	Accuracy	96.3
		Error rate	3.7

Table 9.2: Classification accuracy for LR of subject 'k3b'

Classifier	**MI Class**	**Subject ID: 'k3b' (%)**	
Logistic Regression (LR)	Two Class Left Hand and Right Hand	True positive	98.0
		True negative	96.3
		False positive	3.7
		False negative	2.0
		Error rate	3.3
	Three Class: Left Hand, Right Hand and Foot	Accuracy	93.2
		Error rate	6.8

Table 9.3: Classification accuracy for SVM of subject 'k3b'

Classifier	**MI Class**	**Subject ID: 'k3b' (%)**	
Support Vector Machine (SVM)	Two Class Left Hand and Right Hand	True positive	97.5
		True negative	90.3
		False positive	9.7
		False negative	2.5
		Error rate	6.7
	Three Class: Left Hand, Right Hand and Foot	Accuracy	92.5
		Error rate	7.5

All the classifier performed very well with over all accuracy more than 90%. However the LDA and LR outperformed SVM.

The results of Two (Left/Right Hand) and Three (Left/Right Hand/Foot) class motor imaginary offline classification of subject with ID: 'k6b' is given in table 9.4, 9.5 and 9.6:

Table 9.4: Classification accuracy for LDA of subject 'k6b'

Classifier	**MI Class**	**Subject ID: 'k6b' (%)**	
Liner Discriminant Analysis (LDA)	Two Class Left Hand and Right Hand	True positive	69.0
		True negative	24.2
		False positive	75.8
		False negative	31.0
		Error rate	55.0
	Three Class: Left Hand, Right Hand and Foot	Accuracy	45.6
		Error rate	54.4

Table 9.5: Classification accuracy for LR of subject 'k6b'

Classifier	**MI Class**	**Subject ID: 'k6b' (%)**	
Logistic Regression (LR)	Two Class Left Hand and Right Hand	True positive	65.7
		True negative	24.2
		False positive	75.8
		False negative	34.3
		Error rate	56.7
	Three Class: Left Hand, Right Hand and Foot	Accuracy	47.8
		Error rate	52.2

Table 9.6: Classification accuracy for SVM of subject 'k6b'

Classifier	**MI Class**	**Subject ID: 'k6b' (%)**	
Support Vector Machine (SVM)	Two Class Left Hand and Right Hand	True positive	55.3
		True negative	31.7
		False positive	68.3
		False negative	44.7
		Error rate	61.7
	Three Class: Left Hand, Right Hand and Foot	Accuracy	37.8
		Error rate	62.2

None of the classifier produced a good results, the error rate is rather larger than the accuracy of the classifiers. This may resulted because of large artefacts in the data or the subject showed minimal variation in ERD or ERS.

The results of Two (Left/Right Hand) and Three (Left/Right Hand/Foot) class motor imaginary offline classification of subject with ID: 'l1b' is given in Table 9.7, 9.8 and 9.9:

Table 9.7: Classification accuracy for LDA of subject 'l1b'

Classifier	**MI Class**	**Subject ID: 'l1b' (%)**	
Liner Discriminant Analysis (LDA)	Two Class Left Hand and Right Hand	True positive	91.7
		True negative	92.5
		False positive	7.5
		False negative	8.3
		Error rate	8.3
	Three Class: Left Hand, Right Hand and Foot	Accuracy	84.4
		Error rate	15.6

Table 9.8: Classification accuracy for LR of subject 'l1b'

Classifier	**MI Class**	**Subject ID: 'l1b' (%)**	
Logistic Regression (LR)	Two Class Left Hand and Right Hand	True positive	88.3
		True negative	89.2
		False positive	10.8
		False negative	11.7
		Error rate	11.7
	Three Class: Left Hand, Right Hand and Foot	Accuracy	81.1
		Error rate	18.9

Table 9.9: Classification accuracy for SVM of subject 'l1b'

Classifier	**MI Class**	**Subject ID: 'l1b' (%)**	
Support Vector Machine (SVM)	Two Class Left Hand and Right Hand	True positive	88.3
		True negative	85.8
		False positive	14.2
		False negative	11.7
		Error rate	13.3
	Three Class: Left Hand, Right Hand and Foot	Accuracy	78.9
		Error rate	21.1

All of the classifier performed well and LDA has the highest accuracy.

The results of Two (Left/Right Hand) and Three (Left/Right Hand/Rest) class motor imaginary offline classification of subject with ID: 'DanSR02' is given in Table 9.10, 9.11 and 9.12, also the results of majority voting algorithm is presented in section (iv).

Table 9.10: Classification accuracy for LDA of subject 'DanSR02'

Classifier	**MI Class**	**Subject ID: 'DanSR02' (%)**	
Liner Discriminant Analysis (LDA)	Two Class Left Hand and Right Hand	True positive	78.0
		True negative	86.0
		False positive	14.0
		False negative	22.0
		Error rate	18.8
	Three Class: Left Hand, Right Hand and Rest	Accuracy	78.7
		Error rate	21.3

Table 9.11: Classification accuracy for LR of subject 'DanSR02'

Classifier	**MI Class**	**Subject ID: 'DanSR02' (%)**	
Logistic Regression (LR)	Two Class Left Hand and Right Hand	True positive	84.1
		True negative	84.3
		False positive	15.7
		False negative	15.9
		Error rate	16.5
	Three Class: Left Hand, Right Hand and Rest	Accuracy	82.6
		Error rate	17.4

Table 9.12: Classification accuracy for SVM of subject 'DanSR02'

Classifier	**MI Class**	**Subject ID: 'DanSR02' (%)**	
Support Vector Machine (SVM)	Two Class Left Hand and Right Hand	True positive	79.7
		True negative	82.9
		False positive	17.1
		False negative	20.3
		Error rate	19.7
	Three Class: Left Hand, Right Hand and Rest	Accuracy	79.3
		Error rate	20.7

The average error for Two class problem for subject 'DanSR02'from all three classifier is = 18.33 %. The majority voting algorithm resulted in an error of = 9.4%, which is a clear significant reduction in misclassification.

All the classifier performed fairly well and LR has the highest accuracy rate.

9.5 Conclusions

For all cases of classification (except for subject 'k6b') the Linear Discriminant classifier (LDA) performed excellent classification. The Logistic Regression (LR) performance is very close to LDA. The Support Vector Machine performed fairly well, but this method is complex and takes a substantial amount of time to train and also suffers from low speed of execution.

The LDA classification technique has very low computational requirement, simple to use and generally provides efficient classification. Therefore LDA is suitable for a BCI system which has few feature vector and low computational power. Therefore, this classification method can be used with the developed BCI system.

The majority voting algorithm produced excellent result; this technique can be applied to problems that have low accuracy for classifiers, provided that the BCI system has no computational constraints.

Chapter 10 : Evaluation of the Developed BCI system through An ERD Based Single Trial Online Motor Imaginary Classification Using Only Two Electrodes

10.1 Background

The previous chapters describe how μ and β rhythm from the sensorimotor cortex can be utilized to accomplish a functional Brain-Computer Interface. The Event Related Desynchronization (ERD) is suppression of μ and β rhythm during motor movement or imagination of movement (Koles et al., 1998). It has been showed in several publications that the ERD can be employed to distinguish between motor imaginary tasks of limb movement for BCI purpose as described in section 9.1. An adaptive spatial filter can be achieved by applying the so called 'Common Spatial Pattern' (CSP) algorithm (Guger et al., 2000), which finds the maximum variation in EEG sensorimotor rhythm attributes at spatial positions of the scalp that correlates the ERD for different classes of motor imaginary tasks. Then, with the features from CSP, a machine learning method can be applied to classify the motor imaginary task for BCI.

The online classification i.e. asynchronous real time EEG data classification for BCI is somewhat different from offline or synchronous classification. It is difficult to identify the beginning of each mental task in asynchronous part (Lotte et al, 2007). There are several reports of online experiment of BCI using ERD and employing different approaches for feature extraction and classification. Obermaier et al. (2001) used Hidden Markov Model classifier for online classification of ERD based single trail EEG data during motor imagination of Left or Right hand movement. This experiment used four recording electrodes positioned near posterior and interior of C3 and C4 location. This study resulted in average accuracy of 81.4%. In another report actual movement of left and right index finger was real time classified using logistic regression classifiers. For features, power-frequency spectrum obtained by FFT from the electrodes placed at C3 and C4 and a few neighboring position were used (Lehtonen et al., 2008). This study reports to have accuracy of 80%.

As was mentioned before, a BCI system for neuro-prosthesis and communication needs to be simple, with low complexity, wearable and easily manageable. Therefore, for a EEG based BCI system with low number of electrode attached to the user`s scalp is desired. Guger et al. (2001) showed that it is possible to use Adaptive Auto Regressive (AAR) parameters resulting from two bipolar electrodes at the sensorimotor cortex (C3 and C4, in standard 10-20 EEG electrode placement) to classify motor imaginary tasks. Classification accuracy between 70% and 95% was obtained in this study. Also It has been reported that 4 patients with complete or partial paralysis or paresis of their lower limbs were trained to operate a CSP based BCI that uses band power features of only 2 bipolar channels (Krausz et al., 2003); this study resulted at information transfer rate between 5 to 17 bits/min. A similar methodology (using only two recording electrode) was successfully used with 4 patients suffering from Amyotrophic Lateral Sclerosis (ALS) (Kübler et al., 2005). This study resulted in accuracy between 76% and 81%.

Thus, along with the physiological evidence of 'homunculus' model (Jasper et al., 1949), it can be assumed that only two bipolar electrode that are positioned at the sensorimotor cortex which are responsible for hand movement (C3 and C4) may be sufficient for an effective BCI system. Moreover, since the sensorimotor rhythms (μ and β band) that constitutes ERD are natural, single trial training should suffice to find the subject specific features that can be used for online classification of the motor imaginary task. Also, the system should be operative with the users who did not have any previous experience of using any kind of BCI system.

The frequencies corresponding to μ and β rhythm varies person to person, but always in distinct bands, i.e. 8 to 12 Hz for μ and 18 to 25 Hz for β. So, the assumption can be extended to the fact that, if the band power of these two rhythms from the two electrodes (C3 and C4) is used as features, it should be possible to distinguish ERD's that represent the particular motor imaginary task.

10.2 Problem Statement

The objective of this present study is to use ERD corresponding to sensorimotor rhythms for online classification of EEG data of motor imaginary tasks. The system should use only two recording electrode place at the motor cortex. The study will implement and evaluate an online BCI system, developed as a part of the present work, which uses a single trial to extract ERD attributes as features and employs classifiers of light computational requirement. Using these methodologies a BCI experiment will be carried out on inexperienced subjects.

This study will assess the overall developed BCI system of this present research work. The EEG hardware and the software for BCI that had been developed will be employed in this online classification of motor imaginary task.

10.3 Method

Three subjects were asked to perform a two-class motor imaginary task, Left Hand and Right Hand imagined movement, and the data were classified online. The EEG data was first band pass filtered from 8 to 30 Hz. Since there is only two electrodes, no spatial filtering was carried out, only the frequencies and amplitudes of the ERD that are most discriminant for the particular subject and for the associated class were investigated and used as features. A simple Linear Discriminant Analysis was used as a classifier which gave the class probabilities as the outputs. A graphical user interface was designed to input various circuit parameters and to show relevant outcomes, described in a little more detail in the ‘software’ section below.

10.3.1 Hardware

The two channel EEG device that has been developed in the present work and described before from Chapters 2 to 8 was used to record the EEG data. For data acquisition, a device from National Instruments (‘cDAQ9171’, National Instruments, 2017) was used instead of the developed miniature USB based data acquisition system. This was done to avoid complexity at the research phase where hardware and software may require quick changes. The EEG signal was sampled at 1024 Hz. To ensure user safety and noise reduction, the analog front end was electrically isolated by means of isolation amplifier (ISO126) for signal and a medical grade DC to DC converter for power. The data acquisition device is on the non-isolated PC side and it also

uses USB interface to connect with the PC. It needs to be mentioned that the ground point referred to in Chapters 2 to 8 for the patient connected parts of the EEG are not the same as the ground of the mains connected part. Therefore, in a combined system, the ground of the isolated part is usually referred to as the 'Neutral' or the 'Common' point.

10.3.2 Software

The Data acquisition, Graphical User Interface (GUI) and Computational algorithms of the BCI system was developed using LabVIEW professional development system (LabVIEW, 2017) and Matlab (MathWroks, 2005). The GUI contains two EEG trace-viewing window for 3 seconds (the time scale is changeable), four numerical inputs to configure upper and lower cut-off frequencies of two IIR digital bandpass filter of the 16^{th} order for the two channels, two real time FFT window which performs on every 0.5 seconds of data and two vertical indication bars which represents the probability of the class of Left and Right Hand imagined movement. The vertical indications serves as a measure of classification accuracy and as well as feedback to the user.

10.3.3 Subjects

Three research students from the Department of Biomedical Physics and Technology volunteered for this study. All of the subjects are in the age group of 25 to 35 years, male and Right handed. The subjects did not have any previous experience regarding BCI and EEG recordings. The subjects were informed about the study, explained of their task and an oral consent was taken from each of them.

10.3.4 Practical Measurement

The subject was seated in an armchair and two EEG electrodes were attached on the scalp at positions C3 and C4 respectively. The Ground and Reference Electrodes were attached at right and left mastoids respectively. The subject was asked to relax for several minutes. Then a soft voiced que was presented to the subject to imagine either a Left Hand or a Right Hand movement. The data was then divided into 3 second epochs for training purpose. The training data was then used for subsequent online classification through the same voiced cue.

The data was analyzed and the resulting probabilities of the output class were presented on the vertical indication bar for every 1.5 second epochs. For every cued class, 10 results were

recorded for every session and 5 sessions were performed. The accuracy of the classification of these 10 trials (for each session) were calculated and results from 5 sessions were averaged.

10.4 Result and Observations

The screenshot of the GUI of the BCI system is shown in Figure 10.1, in which the subject was asked to close his eyes. Considerable appearance of Alpha band frequency is visible, which validates the EEG data quality of the developed system. The presence of Alpha oscillation at C3 and C4 is probably due to the fact that these positions are close to the occipital lobe of the brain which is responsible for visual processing.

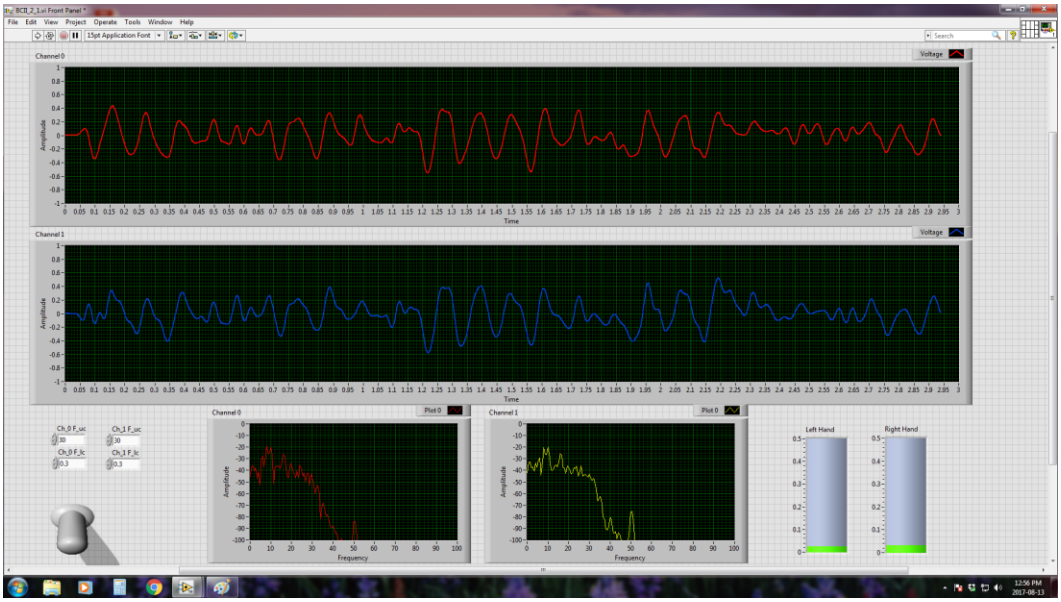

Figure 10.1: Alpha Rhythm at Both Channels During Eyes Closed of Subject 1

The Screenshots of the GUI during Left hand and Right Hand motor imaginary task and Rest state for subject 1 is shown in Figure 10.2, 10.3 and 10.4 respectively.

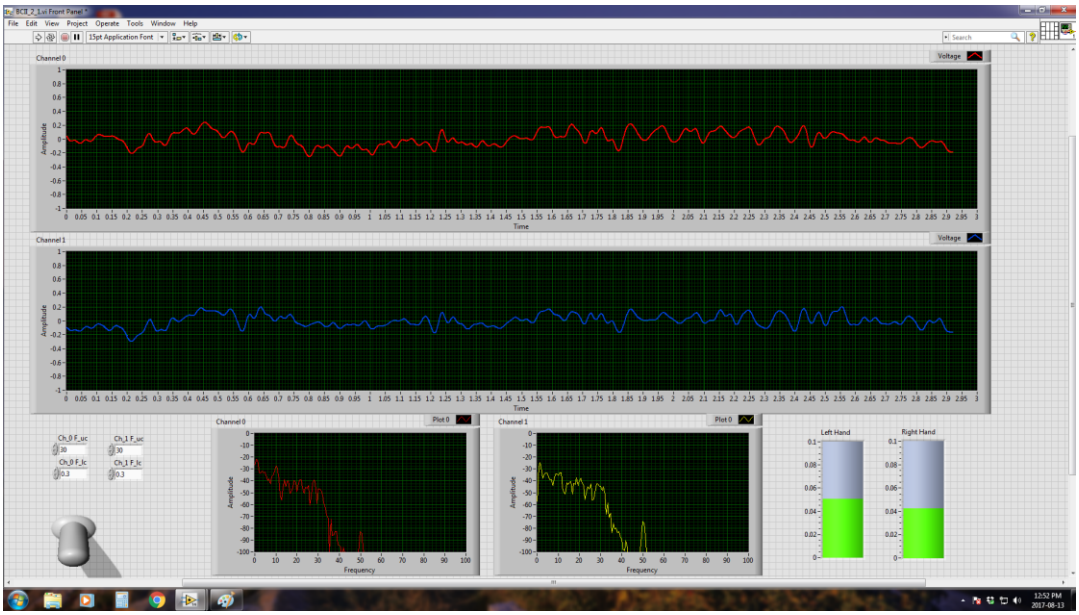

Figure 10.2: Output during Left Hand Imaginary Movement of Subject 1

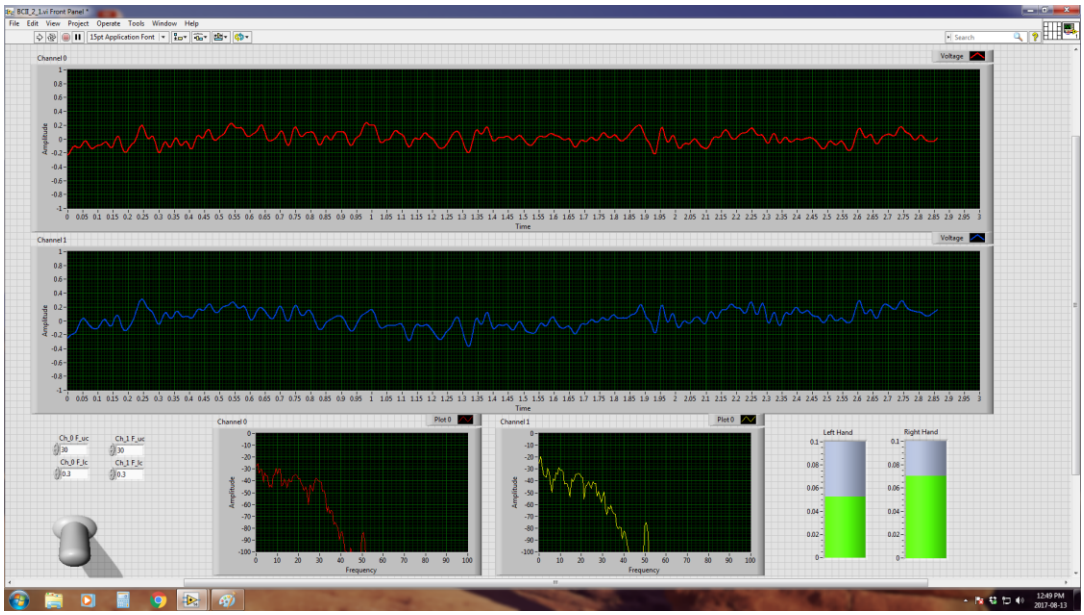

Figure 10.3: Output during Right Hand Imaginary Movement of Subject 1

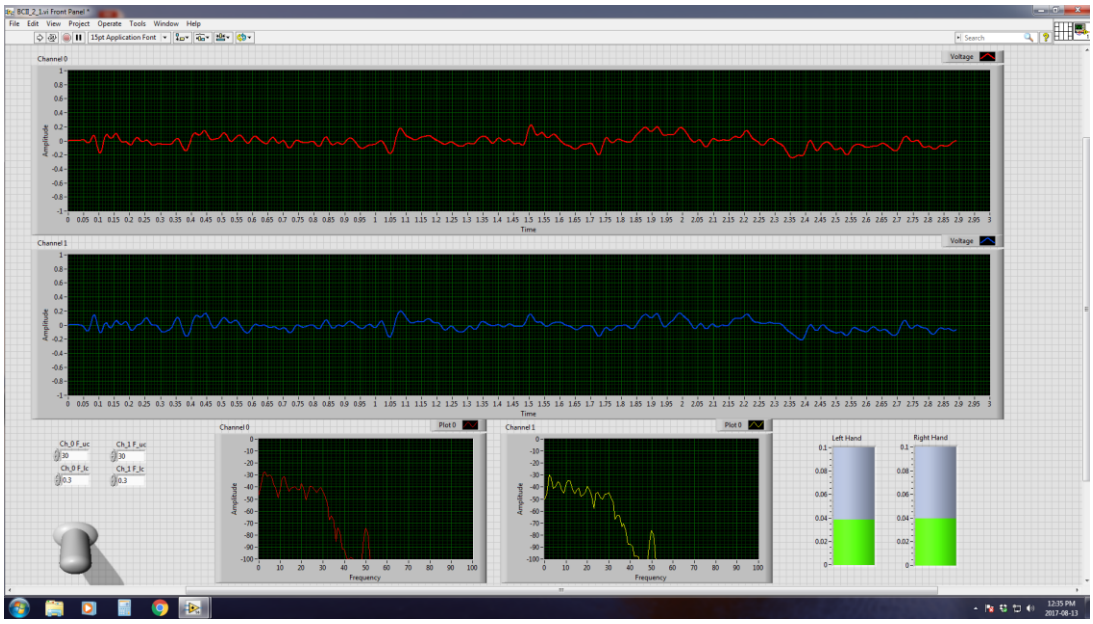

Figure 10.4: Output during Rest of Subject 1

For the online classification, the first and third subject performed well with reasonably good accuracy. The second subject could not show any realistic output associated with the task. The accuracy of the classification is presented in Table 10.1.

Table 10.1: Online classification accuracy of three subjects

Subject	Left Hand %	Right Hand %	Average Accuracy %
1	70	100	85
2	50	60	55
3	70	90	80

10.5 Conclusion

The EEG recording of the developed system is excellent and stable, which is verified by the appearance and disappearance of Alpha waves of EEG for the three subjects with the eyes closed and open respectively. The movement artifacts are observed to be very small probably due to the fact that the electrode positions are far from the usual moving muscles. The EEG system has integral electrode impedance measurement system; it displays four numerical values for the impedance of two active EEG electrodes and that of the ground and reference electrodes. However, the graphical view of these results is not presented here.

The online classification method of motor imaginary EEG data presented in this study are extremely simplified, where only two recording channel and very few features are used with inexperienced subjects. However, the study performed reasonable positive output on single trial training. In this study two of the subjects had average accuracies of more than 80% which is similar to that obtained by other studies, even with a larger number of electrodes, as described in section 10.1. The second subject who was unable to produce any reasonable result reported that he was unable to imagine his hand movement. Similar failures with particular subjects have also been reported by other workers. This could be due to individual psychological attributes and needs further investigation.

The success of the simple software developed in the present work requiring a minimum of electrodes and computational power shows that this is a promising method that can be practically used for the developed BCI system.

Chapter 11 : Feasibility of Employing EOG in Combination with EEG Based BCI for Control of a wheelchair

11.1 Background

Electrooculography (EOG) is the recording trace of electrical potential that is produced across the cornea and retina due to eyeball movement. The potential arises due to the action potentials from the muscles that are contracted during eyeball movement (Brown et al., 2006; Birndorf et al., 1973). The EOG signal typically has an amplitude of 1 to 2 mV and has a single peak wave shape with an average time span of 300 to 400 ms. The signal is usually recorded from electrodes placed on the face surrounding the eyes, mainly at the forehead, temple and just below the eyes. Figure 11.1 shows the electrode placement and corresponding output measurement system for left-right (horizontal) and up-down (vertical) movement of the eyeball.

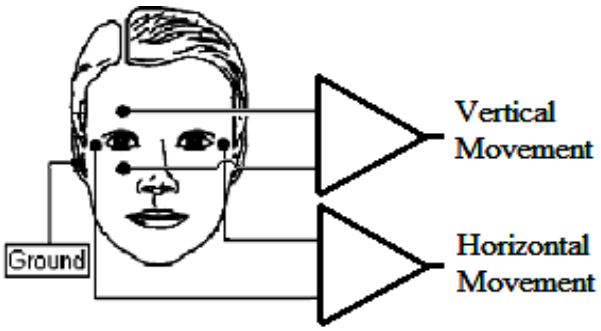

Figure 11.1: EOG Recording System

The EOG signals from these different electrodes have very distinct wave shapes for left, right, up and down movement of the eyeball. These wave shapes are easily distinguishable and used for Human-Machine Interface (HMI). In several publications, the EOG has been reported for onscreen keyboard controls and for robot control (Usakli et al., 2010a and 2010b; Kumar et al., 2002; Kim et al., 2007). Barea et al. (2002) reported an EOG based electric wheelchair control. Since unintentional eye movement can result in unwanted control of machine, these HMI systems relying on only EOG are not fully reliable.

11.2 Problem Statement & Objectives

As mentioned above, reliability of only EOG based systems have a serious drawback, due to unintentional eye movements. On the other hand, the EEG based BCI system is never 100% accurate, therefore control of wheelchair by only BCI can result in unwanted movement. Therefore, both systems, used individually, are not fully reliable and may even result in disastrous consequences. On the other hand, a combination of these two different maneuvers of a person may give a better reliability since it is less probable that two such maneuvers will occur simultaneously. Therefore, it would be interesting to investigate whether combining these two methods improves the outcome of the desired control.

The objective of this study is to produce improved and reliable wheelchair control combining classification results (Class probabilities) of EEG motor imaginary BCI and detectable classes of eyeball movement though EOG. This should not be sensitive to movement of the eyes or in the motor imaginary EEG that are not related to the desire to control the movement of a wheelchair. Here only predicted classes of Left Hand/Right Hand imagined movement and horizontal Left/Right eyeball movement is studied with different weightage to each. If a particular combination of these states improves the overall output than the individual EEG based BCI, other combination of states or classes can be applied to control a wheelchair.

11.3 Method

The motor imaginary EEG data is taken form a published source (Grandchamp, 2009) described in section 8.3.1 but from a different subject. The EOG data is taken from a previous research work performed at the Department of Biomedical Physics, University of Dhaka, (Atique et al., 2016).

For the EOG, outputs for only the left-right control (horizontal) were used. The Left and Right side (horizontal) movement of eyeball produces opposite EOG signal outputs, shown in figure 11.2 and 11.3 respectively. This is expected from the placement of the two electrodes on the two sides of the face as shown in Figure 11.1.

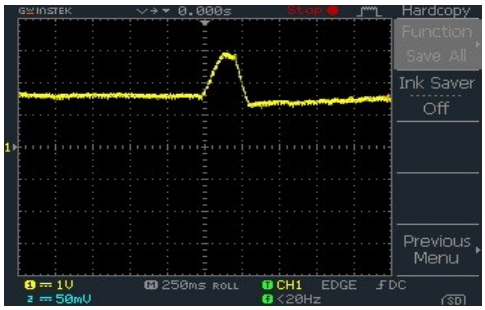

Figure 11.2: EOG Signal for Left Sided eyeball Movement

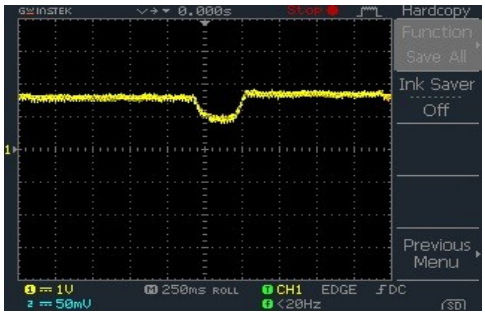

Figure 11.3: EOG Signal for Right Sided eyeball Movement

Since the EOG signals from these to eyeball movement produces signal of opposite polarities, these are identified with almost 100% accuracy simply using a discriminant type classification. Therefore, the classes representing intentions for Left and Right movement by EOG usually have no misclassification rate.

The EEG data is classified using the CSP algorithm for feature extraction and Linear Discriminant Analysis classifier in the same manner described in section 9.3.

Different combination of the two classification modalities may result in different magnitudes of improvement. Therefore, the combinations were made with several different weightages. The predicted class probabilities were added percentage wise to have a combined class probability. Different combinations of weighted probabilities were used and the results were compared to improve the insight.

11.4 Results and Observations

Results of different weighted probability combinations are given in Table 11.1.

Table 11.1: Results of combination of EEG and EOG probabilities

Weight of the BCI Probability %	Weight of the EOG Probability %	Number of wrong prediction among 128 samples	Misclassification Rate (Error) %	Accuracy %
100	0	13	10.2	89.8
70	30	7	5.5	94.5
60	40	4	3.1	96.9
50	50	0	0	100.0

11.5 Conclusion

It is well known that detectability of EOG alone is almost 100% accurate. The reason of not using it alone is its reliability in control applications, due to movement of the eyes for other purposes. Again, BCI can also lead to inadvertent signals if the user imagines of moving the hands with other intentions. However, probability of having both these maneuvers together for other purposes than the desired control would be very small. Therefore, a combination of EOG and BCI, even though the latter is less accurate, may lead to a greater reliability in terms of avoidance of undesired control signals.

From the above table it appears that a combination of BCI and EOG in the weightage ratios of 60:40 or 50:50 appears to be the best for a reliable and accurate control.

Chapter 12 : Conclusion

The objective of this research work is to develop a functional BCI system indigenously, meeting the criteria of having low component count, of being light weight, power efficient, user safe, small sized, wearable and comfortable. The BCI system is intended to be of low cost which will be used for controlling prosthesis, communication module and wheelchair to provide day to day functionality of physically challenged people of the low resource countries (LRC) of the world. Such systems are under development in many other laboratories of the world and the technology has not matured yet. Besides, most of these developments are taking place in the economically advanced countries (EAC) and when the systems will be ready for commercialization, they will be prohibitively expensive for the users-in-need in the LRCs. There are two reasons for this, Firstly, the developers in the EACs usually go for very complex systems providing a host of facilities, many of which may not be needed by an average user. Secondly, the wages of research personnel differ widely in these two regions of the world which contributes greatly to a high cost if developed in an EAC. Therefore, there is a great need for such equipment and systems to be developed within the LRCs keeping their own situations in consideration.

Therefore, the present work tackles the problem from scratch, from the basic design of an appropriate EEG circuitry to the development of an appropriate BCI technique, all considering the above mentioned requirements.

A BCI system usually consists of EEG recording hardware and data analysis or classification software. Both of these have been developed during this work and evaluated. The bioelectric amplifier of the EEG hardware is optimized in terms of number of amplifying stages and bandpass filtering and the choice of a low cost but high quality instrumentation amplifier. Careful design of the Sallen-Key second order filters at the amplifier gain stages resulted in very stable active filters with high attenuation (total of 4^{th} order) at the stopbands, minimum phase distortions and having quick settling time. Beside the very high gain (100 dB) of the developed bioelectric amplifier, the performance is excellent with stable output with no ringing or self-oscillation. The output shows very low noise and very high overall Common Mode Rejection Ratio (CMRR ~115 DB). These features make it very much appropriate for EEG recording. The

bioelectric amplifier has been constructed for two channels only, based on the need for simplicity, and the outcome of the requirement study carried out in this work for a cost effective BCI system. It is possible to extend the channels to higher numbers, if necessary, by just simply adding more components of single channel section following the architecture of the design.

A novel AC coupling method has been developed and implemented, which allows higher gain at the first stage instrumentation amplifier (INA) without compromising the input impedance and CMRR. The AC coupling at the input stage also enforces user safety by capacitive isolation. This innovation may find use in all bioelectric amplifiers.

To reduce interference and noise and as well as user protection a novel improved Driven Right Leg (DRL) circuit has been designed and constructed. This DRL circuit is free from DC saturation and therefore very high gain can be applied which in turn substantially reduces the effective skin-electrode contact impedance at the reference electrode or ground. Thus it minimizes the common mode voltage.

A novel MOSFET and JFET based self-biased low-noise two wired active electrode system has been developed. This active electrode effectively removes the problem of skin-electrode mismatch and the mains borne 50Hz interference produced by long input leads. It essentially reduces the common mode to differential mode conversion due to 'Potential divider effect'. This active electrode is also AC coupled to the subject. Due to the special architecture developed, the RC components do not required to be exactly matched.

A skin-electrode contact impedance measurement circuit has been developed. Unlike similar other measuring systems; this one is able to calculate the ground and reference electrode contact impedances too, which is essential for noise free EEG recording.

A USB based simple data acquisition system has been developed for the BCI system which is suitable for data acquisition during training phase and can also be used as standalone signal processing, data classification and control unit for the wearable BCI system.

To determine a suitable EEG signal analysis and data classification method that can be used with minimum number of electrode or channels (in this case only two), spatial pattern of μ-rhythm

was analyzed from motor imaginary EEG data obtained from published sources. This analysis shows that the μ and β rhythm bands highly correlate to the motor imaginary hand movement. Then a similar method called CSP was used to extract features from EEG data of several subjects preforming motor imaginary task, and then various machine learning techniques were used to find most efficient classifier. The simpler classifier called Linear Discriminant Analysis (LDA) was found to be the most efficient. This implies the important fact that low computational methods like LDA can be effectively used in standalone BCI system. It was also found that combination of several classifies producing output by majority voting results in higher accuracy. Finally, an online classification of motor imaginary movement of left and right hand is carried out using the methods of offline classification and using only two recording electrodes placed at C3 and C4 position. Three volunteers participated in the study and two of them achieved more than 80% accuracy in single trail based study. One of them did not achieve any practical output, and informed that he is having difficulties imagining hand movement.

Finally, a combination of BCI with Electro OculoGram (EOG) with different weightage showed that a ratio of 50:50 gave the best accuracy, 100%, together with reliability against unrelated movements of the eye or imagining movements.

These observations suggest that it is sufficient to use only two electrodes at the sensorimotor cortex along with the developed EEG hardware to construct a functional BCI system.

Thus the present thesis has shown that it is possible to develop a high quality EEG circuitry for BCI using low cost ICs and other components, suitable for a LRC. Although such devices for BCI are in existence, the technology is still not fully developed. In this direction, several innovations have been made in the EEG circuit hardware which will help the LRCs as well as the EACs. Together with the hardware innovations, the present work also showed that only two EEG electrodes at appropriate points of the scalp is enough to give a very satisfactory output for BCI for which simple software has been developed that will be helpful in low resource countries of the world.

References

Almasi, J. J., & Schmitt, O. H. (1970). *Systemic and random variations of ECG electrode system impedance*. Annals of the New York Academy of Sciences, 170(1), 509-519.

Ang, K. K., Chin, Z. Y., Wang, C., Guan, C., & Zhang, H. (2012). *Filter bank common spatial pattern algorithm on BCI competition IV datasets 2a and 2b*. Frontiers in neuroscience, 6.

Atique, M. M. U., Rakib, S. H., & Siddique-e-Rabbani, K. (2016). *An electrooculogram based control system*. In Informatics, Electronics and Vision (ICIEV), 2016 5th International Conference on (pp. 809-812). IEEE.

Atmel Corporation (2014). Retrieved March 10,2014, Form: http://www.atmel.com

Barea, R., Boquete, L., Mazo, M., & López, E. (2002). *System for assisted mobility using eye movements based on electrooculography*. IEEE transactions on neural systems and rehabilitation engineering, 10(4), 209-218.

BBCI. (2004) Retrieved August 9, 2017, from http://www.bbci.de/competition/iii/

BCILAB. (2017) Retrieved August 9, 2017, from https://sccn.ucsd.edu/wiki/BCILAB

Bennett, K. P., & Campbell, C. (2000). *Support vector machines: hype or hallelujah?*. Acm Sigkdd Explorations Newsletter, 2(2), 1-13.

BioSemi, B. V. (2011). *BioSemi ActiveTwo EEG system.* Amsterdam: BioSemi, Retrieved July 5, 2017, from: https://www.biosemi.com/active_electrode.htm

Biosignal.at. (2011). *The Annual BCI Research Award 2014 – The Winners*.. Retrieved 19 December, 2016, from http://www.biosignal.at/bci-award/winners.php

Birndorf, L. A., & Dawson, W. W. (1973). *A normal electrooculogram in a patient with a typical vitelliform macular lesion*. Investigative Ophthalmology & Visual Science, 12(11), 830-833.

Bishop, C. M. (1995). *Neural networks for pattern recognition*. Oxford university press.

Blankertz, B., Dornhege, G., Krauledat, M., Müller, K. R., & Curio, G. (2007). *The non-invasive Berlin brain–computer interface: fast acquisition of effective performance in untrained subjects*. NeuroImage, 37(2), 539-550.

Blankertz, B., Dornhege, G., Schafer, C., Krepki, R., Kohlmorgen, J., Muller, K. R., & Curio, G. (2003). *Boosting bit rates and error detection for the classification of fast-paced motor commands based on single-trial EEG analysis*. IEEE Transactions on Neural Systems and Rehabilitation Engineering, 11(2), 127-131.

Blankertz, B., Tomioka, R., Lemm, S., Kawanabe, M., & Muller, K. R. (2008). *Optimizing spatial filters for robust EEG single-trial analysis.* IEEE Signal processing magazine, 25(1), 41-56.

Bozinovski, S.(1990). *Mobile robot trajectory control: From fixed rails to direct bioelectric control*. O. Kayniak (ed.) Proc. IEEE Workshop on Intelligent Motion Control, p. 63-67.

Bozinovski, S., Sestakov, M., Bozinovska, L. (1988). *Using EEG alpha rhythm to control a mobile robot*. Harris, G. & Walker C. (eds.), Proc IEEE Annual Conference on Medical and Biological Society, New Orleans, p. 1515-1516.

Brown, B. H.(1999). *Medical Physics and Biomedical Engineering*. Sheffield, UK: IOP Publishing Ltd.

Brown, M., Marmor, M., Zrenner, E., Brigell, M., & Bach, M. (2006). *ISCEV standard for clinical electro-oculography (EOG)*. Documenta ophthalmologica, 113(3), 205-212.

Burges, C. J. (1998). *A tutorial on support vector machines for pattern recognition*. Data mining and knowledge discovery, 2(2), 121-167.

Cazala, F., Vienney, N., & Stoléru, S. (2015). *The cortical sensory representation of genitalia in women and men: a systematic review*. Socioaffective neuroscience & psychology, 5(1), 26428.

Cincotti, F., Scipione, A., Tiniperi, A., Mattia, D., Marciani, M. G., Mill´an J del, R., Salinari, S., Bianchi, L. and Babiloni, F. (2003). *Comparison of different feature classifiers for brain computer interfaces.* Proc. 1st Int. IEEE EMBS Conf. on Neural Engineering

de Klerk, C. C., Johnson, M. H., & Southgate, V. (2015). *An EEG study on the somatotopic organisation of sensorimotor cortex activation during action execution and observation in infancy*. Developmental cognitive neuroscience, 15, 1-10.

Degen, T., & Jackel, H. (2006). *A pseudodifferential amplifier for bioelectric events with DC-offset compensation using two-wired amplifying electrodes*. IEEE transactions on biomedical engineering, 53(2), 300-310.

Degen, T., & Jäckel, H. (2008). *Continuous Monitoring of Electrode--Skin Impedance Mismatch During Bioelectric Recordings*. IEEE Transactions on Biomedical Engineering, 55(6), 1711-1715.

Degen, T., Torrent, S., & Jackel, H. (2007). *Low-noise two-wired buffer electrodes for bioelectric amplifiers*. IEEE transactions on biomedical engineering, 54(7), 1328-1332.

Devlin, P. H., Mark, R. G., & Ketchum, J. W. (1984). *Detection electrode motion noise in ecg signals by monitoring electrode impedance*. Computers in Cardiology, 51-56.

Dobrev, D. P., Neycheva, T., & Mudrov, N. (2008). *Bootstrapped two-electrode biosignal amplifier*. Medical & biological engineering & computing, 46(6), 613-619.

Donchin, E., Spencer, K. M., Wijesinghe, R. (2000). *The Mental Prosthesis: Assessing the Speed of a P300-Based Brain–Computer Interface*. IEEE Transactions on Rehabilitation Engineering. 8 (2): 174–179. doi:10.1109/86.847808.

Duda R O, Hart P E and Stork D G (2001), *Pattern Recognition*, 2nd edn, New York: Wiley-Interscience.

Farwell, L. A., & Donchin, E. (1988). *Talking off the top of your head: toward a mental prosthesis utilizing event-related brain potentials*. Electroencephalography and clinical Neurophysiology, 70(6), 510-523.

Fernandez, M., & Pallas-Areny, R. (1997). *A simple active electrode for power line interference reduction in high resolution biopotential measurements*. In Engineering in Medicine and Biology Society, 1996. Bridging Disciplines for Biomedicine. Proceedings of the 18th Annual International Conference of the IEEE (Vol. 1, pp. 97-98). IEEE.

Fukunaga, K. (1990). *Introduction to statistical pattern recognition*. 2nd edition. Academic Press, Boston.

Gastaut, H. (1952). *Electrocorticographic study of the reactivity of rolandic rhythm*. Revue neurologique, 87(2), 176-182.

Geddes, L. A. (1972). *Electrodes and the measurement ofbioelectric events*. Chicester: Interscience.

Grandchamp, R., & Delorme, A. (2009, November). *NeuroTRIP: a framework for bridging between open source software. Application to training a brain machine interface. In Signal-Image Technology & Internet-Based Systems (SITIS)*, 2009 Fifth International Conference on (pp. 451-457). IEEE.

GRAZ BCI. (2017) Retrieved August 9, 2017, from https://www.tugraz.at/institute/ine/home/

Grimbergen, C. A., VanRijn, A. M., & Peper, A. (1992, October). *A method for the measurement of the properties of individual electrode-skin interfaces and the implications of the electrode properties for preamplifier design*. In Engineering in Medicine and Biology Society, 1992 14th Annual International Conference of the IEEE (Vol. 6, pp. 2382-2383). IEEE.

Grimnes, S. (1983). Impedance measurement of individual skin surface electrodes. Medical and Biological Engineering and Computing, 21(6), 750-755.

Guger, C., Ramoser, H., & Pfurtscheller, G. (2000). *Real-time EEG analysis with subject-specific spatial patterns for a brain-computer interface (BCI)*. IEEE transactions on rehabilitation engineering, 8(4), 447-456.

Guger, C., Schlogl, A., Neuper, C., Walterspacher, D., Strein, T., & Pfurtscheller, G. (2001). Rapid prototyping of an EEG-based brain-computer interface (BCI). IEEE Transactions on Neural Systems and Rehabilitation Engineering, 9(1), 49-58.

Gulati, Tanuj., Won, Seok Joon., Ramanathan, Dhakshin S., Wong, Chelsea C., Bodepudi, Anitha., Swanson, Raymond A., Ganguly, Karunesh. (2015). *Robust Neuroprosthetic Control from the Stroke Perilesional Cortex*. The Journal of Neuroscience. 35 (22): 8653–8661. PMID 26041930. doi:10.1523/JNEUROSCI.5007-14.2015.

Hamilton, P. S., Curley, M. G., Aimi, R. M., & Sae-Hau, C. (2000). *Comparison of methods for adaptive removal of motion artifact*. In Computers in Cardiology 2000 (pp. 383-386). IEEE.

Hann, M. (2010). *Analog Fundamentals of the ECG Signal Chain*. a Texas Instruments technical presentation.\

Horst Van Der, M. J., Van Rijn, A. M., Peper, A., & Grimbergen, C. A. (1998). *High frequency interference effects in amplifiers for biopotential recordings*. In Engineering in Medicine and Biology Society, 1998. Proceedings of the 20th Annual International Conference of the IEEE (Vol. 6, pp. 3309-3312). IEEE.

Hosmer Jr, D. W., Lemeshow, S., & Sturdivant, R. X. (2013). *Applied logistic regression* (Vol. 398). John Wiley & Sons.

Huhta, J. C., & Webster, J. G. (1973). *60-Hz interference in electrocardiography*. IEEE Transactions on Biomedical Engineering, (2), 91-101.

Hwang, H. J., Kwon, K., & Im, C. H. (2009). *Neurofeedback-based motor imagery training for brain–computer interface (BCI)*. Journal of neuroscience methods, 179(1), 150-156.

Jain, A. K., Duin, R. P. W., & Mao, J. (2000). *Statistical pattern recognition: A review*. IEEE Transactions on pattern analysis and machine intelligence, 22(1), 4-37.

Jasper, H., & Penfield, W. (1949). *Electrocorticograms in man: effect of voluntary movement upon the electrical activity of the precentral gyrus*. European Archives of Psychiatry and Clinical Neuroscience, 183(1), 163-174.

Kim, Y., Doh, N. L., Youm, Y., & Chung, W. K. (2007). Robust discrimination method of the electrooculogram signals for human-computer interaction controlling mobile robot. Intelligent Automation & Soft Computing, 13(3), 319-336.

Ko, W. H. (1998, October). *Active electrodes for EEG and evoked potential*. In Engineering in Medicine and Biology Society, 1998. Proceedings of the 20th Annual International Conference of the IEEE (Vol. 4, pp. 2221-2224). IEEE.

Koles, Z.J., Soong, A.C.K., (1998). *EEG source localization: implementing the spatio-temporal decomposition approach*. Electroencephalogr. Clin. Neurophysiol. 107, 343–352.

Krausz, G., Scherer, R., Korisek, G., Pfurtscheller, G., (2003). *Critical decision-speed and information transfer in the "Graz Brain–Computer Interface*. Appl. Psychophysiol. Biofeedback 28 (3), 233–240.

Krucoff, Max O., Rahimpour, Shervin., Slutzky, Marc W., Edgerton, V. Reggie., & Turner, Dennis A. (2016). Enhancing Nervous System Recovery through Neurobiologics, Neural Interface Training, and Neurorehabilitation. *Neuroprosthetics. 10: 584. PMC 5186786 Freely accessible. PMID 28082858. doi:10.3389/fnins.2016.00584.*

Kübler, A., Nijboer, F., Mellinger, J., Vaughan, T.M., Pawelzik, H., Schalk, G., McFarland, D.J., Birbaumer, N., Wolpaw, J.R., (2005). *Patients with ALS can use sensorimotor rhythms to operate a brain–computer interface*. Neurology 64 (10), 1775–1777.

Kugelstadt, T. (2008). *Active filter design techniques*. Op amps for everyone: design reference, 271-281.

Kumar, D., & Poole, E. (2002). Classification of EOG for human computer interface. In Engineering in Medicine and Biology, 2002. 24th Annual Conference and the Annual Fall Meeting of the Biomedical Engineering Society EMBS/BMES Conference, 2002. Proceedings of the Second Joint (Vol. 1, pp. 64-67). IEEE.

LabVIEW, NI. (2017) Retrieved August 15, 2017, from http://sine.ni.com/nips/cds/view/p/lang/en/nid/212669

Lehtonen, J., Jylanki, P., Kauhanen, L., & Sams, M. (2008). *Online classification of single EEG trials during finger movements*. IEEE Transactions on Biomedical Engineering, 55(2), 713-720.

Lotte, F., Congedo, M., Lécuyer, A., Lamarche, F., & Arnaldi, B. (2007). *A review of classification algorithms for EEG-based brain–computer interfaces.* Journal of neural engineering, 4(2), R1.

MathWorks, Inc. (2005). *MATLAB: the language of technical computing. Desktop tools and development environment*, version 7 (Vol. 9). MathWorks.

McFarland, D. J., McCane, L. M., David, S. V., & Wolpaw, J. R. (1997). *Spatial filter selection for EEG-based communication*. Electroencephalography and clinical Neurophysiology, 103(3), 386-394.

McFarland, D. J., Miner, L. A., Vaughan, T. M., & Wolpaw, J. R. (2000). *Mu and beta rhythm topographies during motor imagery and actual movements*. Brain topography, 12(3), 177-186.

Metting VanRijn, A. C., Kuiper, A. P., Dankers, T. E., & Grimbergen, C. A. (1996, October). *Low-cost active electrode improves the resolution in biopotential recordings*. In Engineering in Medicine and Biology Society, 1996. Bridging Disciplines for Biomedicine. Proceedings of the 18th Annual International Conference of the IEEE (Vol. 1, pp. 101-102). IEEE.

National Instruments. (2017) Retrieved August 15, 2017, from http://www.ni.com/documentation/en/compactdaq-chassis/latest/cdaq-9171/specs/

Neuper, C., Scherer, R., Wriessnegger, S., & Pfurtscheller, G. (2009). *Motor imagery and action observation: modulation of sensorimotor brain rhythms during mental control of a brain–computer interface*. Clinical neurophysiology, 120(2), 239-247.

Nijboer, F., Sellers, E. W., Mellinger, J., et al.(2008). *A P300-based brain–computer interface for people with amyotrophic lateral sclerosis*. Clin Neurophysiol. 119: 1909–1916. PMC 2853977 Freely accessible. PMID 18571984. doi:10.1016/j.clinph.2008.03.034.

Nishimura, S., Tomita, Y., & Horiuchi, T. (1992). *Clinical application of an active electrode using an operational amplifier*. IEEE Transactions on Biomedical Engineering, 39(10), 1096-1099.

Obermaier, B., Guger, C., Neuper, C., & Pfurtscheller, G. (2001). *Hidden Markov models for online classification of single trial EEG data*. Pattern recognition letters, 22(12), 1299-1309.

Oberman, L. M., Hubbard, E. M., McCleery, J. P., Altschuler, E. L., Ramachandran, V. S., & Pineda, J. A. (2005). *EEG evidence for mirror neuron dysfunction in autism spectrum disorders*. Cognitive brain research, 24(2), 190-198.

Objective Development Gmbh (2011). Virtual USB port for AVR microcontrollers. Retrieved August 15, 2011, Form: http://www.obdev.at/products/vusb/index.html

Oracle Corporation (2014). NetBeans IDE, Retrieved March 10, 2014, Form: www.netbeans.org

Pacela, A. F. (1967). *Collecting the body's signals* (Biopotential detection, recording and design noting electrocardiogram and electroencephalogram use to monitor weightlessness in manned space programs). Electronics, 40, 103-112.

Padmadinata, F. Z., Veerhoek, J. J., Van Dijk, G. J. A., & Huijsing, J. H. (1990). *Microelectronic skin electrode*. Sensors and Actuators B: Chemical, 1(1-6), 491-494.

Pallas, R., & Areny, J. G. (1999). *Webster, Analog Signal Processing*. New York: Wiley, 1999.

Pallas-Areny, R., & Webster, J. G. (1990). *Composite instrumentation amplifier for biopotentials*. Annals of biomedical engineering, 18(3), 251-262.

Pallás-Areny, R., & Webster, J. G. (1991). *Common mode rejection ratio in differential amplifiers.* IEEE Transactions on Instrumentation and Measurement, 40(4), 669-676.

Pallás-Areny, R., & Webster, J. G. (1993). *AC Instrumentation Amplifier for Bioimpedance Measurements*. IEEE Transactions on Biomedical Engineering, 40(8), 831.

Pfurtscheller, G. (1989). *Functional topography during sensorimotor activation studied with event-related desynchronization mapping*. Journal of Clinical Neurophysiology, 6(1), 75-84.

Pfurtscheller, G. (1999). *EEG event-related desynchronization (ERD) and event-related sybchronization (ERS)*. Electroencephalography: Basic principals, clinical applications and related fields, 958-967.

Pfurtscheller, G., & Neuper, C. (2001). *Motor imagery and direct brain-computer communication*. Proceedings of the IEEE, 89(7), 1123-1134.

Pfurtscheller, G., Brunner, C., Schlögl, A., & Da Silva, F. L. (2006). *Mu rhythm (de) synchronization and EEG single-trial classification of different motor imagery tasks*. NeuroImage, 31(1), 153-159.

Pfurtscheller, G., Neuper, C., Guger, C., Harkam, W. A. H. W., Ramoser, H., Schlogl, A., & Pregenzer, M. A. P. M. (2000). *Current trends in Graz brain-computer interface (BCI) research*. IEEE Transactions on Rehabilitation Engineering, 8(2), 216-219.

Piccione, F., Giorgi, F., Tonin, P., et al. (2006). *P300-based brain computer interface: Reliability and performance in healthy and paralysed participants*. Clin Neurophysio. 117 (3): 531–537. PMID 16458069. doi:10.1016/j.clinph.2005.07.024.

Rabbani K S, Abir A R, Bodiuzzaman A K M., 2011. *Design and Development of a Low Cost Personal Computer based ECG Monitor*. Bangladesh Journal of Medical Physics 2011; 4(1).

Rabbani KS, Sarker M, Akond MH, Akter T, 1999. *Focused impedance measurement (FIM): A new technique with improved zone localization*, Ann. N. Y. Acad. Sci. 873 408-420

Ramoser, H., Muller-Gerking, J., & Pfurtscheller, G. (2000). *Optimal spatial filtering of single trial EEG during imagined hand movement*. IEEE transactions on rehabilitation engineering, 8(4), 441-446.

Rodriguez, J. D., Perez, A., & Lozano, J. A. (2010). Sensitivity analysis of k-fold cross validation in prediction error estimation. IEEE transactions on pattern analysis and machine intelligence, 32(3), 569-575.

Sallen, R. P., & Key, E. L. (1955). *A practical method of designing RC active filters*. IRE Transactions on Circuit Theory, 2(1), 74-85.

Schalk, G., McFarland, D. J., Hinterberger, T., Birbaumer, N., & Wolpaw, J. R. (2004). *BCI2000: a general-purpose brain-computer interface (BCI) system. IEEE Transactions on biomedical engineering*, 51(6), 1034-1043.

Schalk, G., Miller, KJ., Anderson, NR., Wilson, JA., Smyth, MD., Ojemann, JG., Moran, DW., Wolpaw, JR., Leuthardt, EC. (2008). *Two-dimensional movement control using electrocorticographic signals in humans*. Journal of Neural Engineering.

Scherer, R., Muller, G. R., Neuper, C., Graimann, B., & Pfurtscheller, G. (2004). *An asynchronously controlled EEG-based virtual keyboard: improvement of the spelling rate*. IEEE Transactions on Biomedical Engineering, 51(6), 979-984.

Scholz, F. W. (1985). *Maximum likelihood estimation. Encyclopedia of statistical sciences*. John Wiley & Sons.

Searle, A., & Kirkup, L. (2000). *A direct comparison of wet, dry and insulating bioelectric recording electrodes*. Physiological measurement, 21(2), 271.

Serruya, MD, & Donoghue JP. (2003). *Chapter III: Design Principles of a Neuromotor Prosthetic Device in Neuroprosthetics: Theory and Practice*, Imperial College Press.

Spach, M. S., Barr, R. C., Havstad, J. W., & Long, E. C. (1966). *Skin-electrode impedance and its effect on recording cardiac potentials*. Circulation, 34(4), 649-656.

Spinelli, E. M., & Mayosky, M. A. (2000). *AC coupled three op-amp biopotential amplifier with active DC suppression*. IEEE transactions on biomedical engineering, 47(12), 1616-1619.

Spinelli, E. M., Mayosky, M. Á., & Pallás-Areny, R. (2006). *A practical approach to electrode-skin impedance unbalance measurement*. IEEE transactions on biomedical engineering, 53(7), 1451-1453.

Spinelli, E. M., Pallàs-Areny, R., & Mayosky, M. A. (2003). *AC-coupled front-end for biopotential measurements*. IEEE transactions on biomedical engineering, 50(3), 391-395.

Stitt, R. M. (1990). *AC coupling instrumentation and difference amplifiers.* Application Report…sboa003.

Usakli, A. B., & Gurkan, S. (2010a). Design of a novel efficient human–computer interface: an electrooculagram based virtual keyboard. IEEE Transactions on Instrumentation and Measurement, 59(8), 2099-2108.

Usakli, A. B., Gurkan, S., Aloise, F., Vecchiato, G., & Babiloni, F. (2010b). On the use of electrooculogram for efficient human computer interfaces. Computational intelligence and neuroscience, 2010, 1.

USBIF (2014). Universal Serial Bus Implementation Forum. Retrieved Jan 14, 2014 Form: http://www.usb.org

Van Rijn, A. M., Peper, A., & Grimbergen, C. A. (1990). *High-quality recording of bioelectric events*. Medical and Biological Engineering and Computing, 28(5), 389-397.

Van Rijn, A. M., Peper, A., & Grimbergen, C. A. (1991a). *High-quality recording of bioelectric events. part 2. lownoise, low-power multichannel amplifier design*, Medical & Biological Engineering & Computing, vol. 29, no. 4, pp. 433–440

Van Rijn, A. M., Peper, A., & Grimbergen, C. A. (1991b). *The isolation mode rejection ratio in bioelectric amplifiers*. IEEE transactions on biomedical engineering, 38(11), 1154-1157.

Webster, J. G. (1998). *Medical Instrumentation, Application and Design*. John Wiley and Sons, 3rd edition.

Wikipedia. (2017, June 22). Retrieved July 4, 2017, from https://en.wikipedia.org/wiki/Electroencephalography

Wikipedia. (2017, June 28). Retrieved July 5, 2017, from https://en.wikipedia.org/wiki/Brain%E2%80%93computer_interface#Non-invasive_BCIs

WinAVR (2014). Retrieved March 10, 2014, Form: http://www.webring.org/l/rd?ring=avr;id=59;url=http%3A%2F%2Fwinavr%2Esourceforge%2Enet%2F

Winter, B. B., & Webster, J. G. (1983). *Driven-right-leg circuit design*. IEEE Transactions on Biomedical Engineering, (1), 62-66.

Wolpaw, J. R., Birbaumer, N., McFarland, D. J., Pfurtscheller, G., & Vaughan, T. M. (2002). *Brain–computer interfaces for communication and control*. Clinical neurophysiology, 113(6), 767-791.

Yanagisawa, Takafumi. (2011). *Electrocorticograpic Control of Prosthetic Arm in Paralyzed Patients*. American Neurological Association. doi:10.1002/ana.22613.

Appendix 1

Circuit Diagram for a single channel of the EEG Hardware:

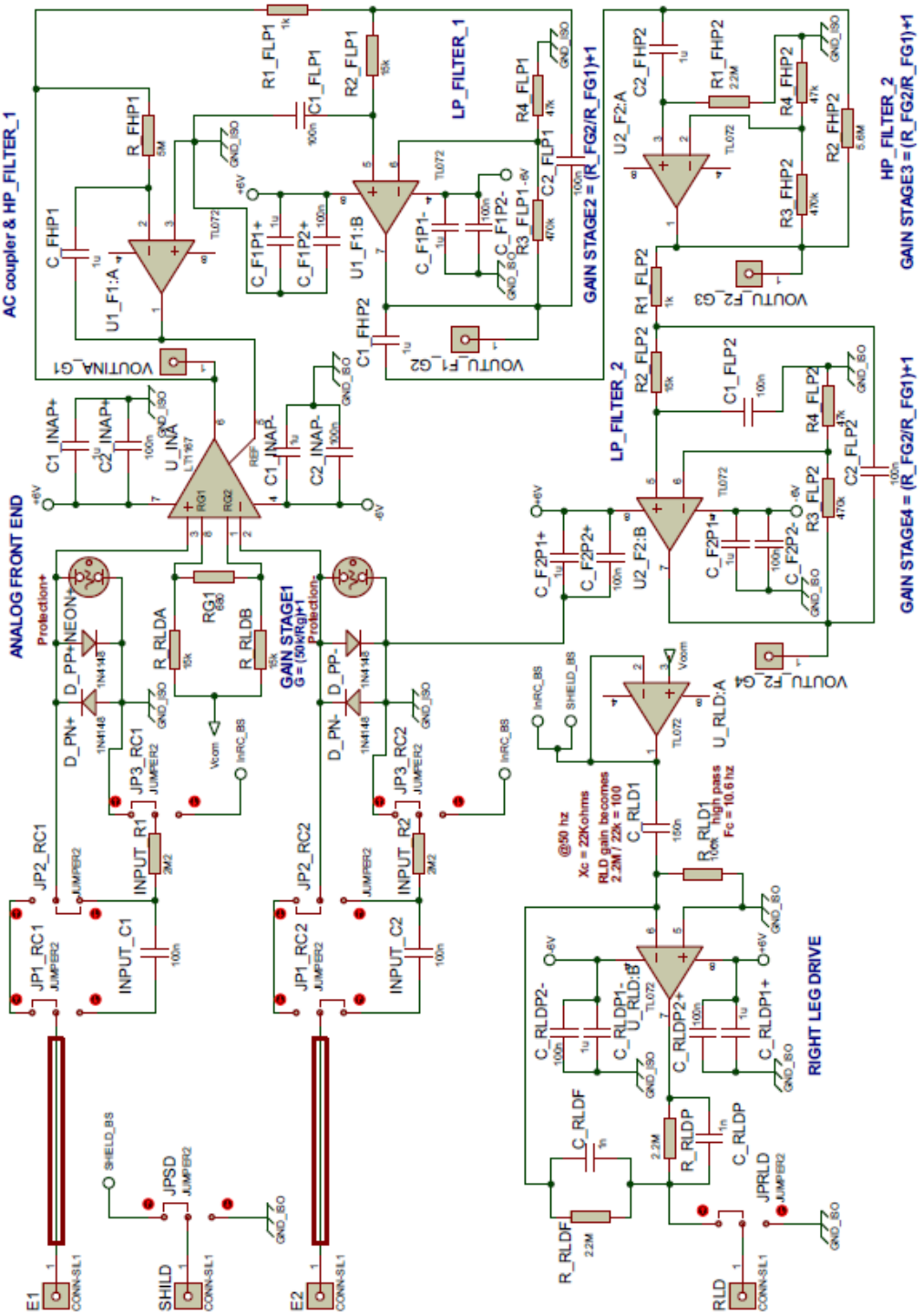

Appendix 2

LabVIEW Module Diagram of BCI System: